

International Journal of Modern Physics E
 © World Scientific Publishing Company

HADRONS IN STRONGLY INTERACTING MATTER

STEFAN LEUPOLD^a, VOLKER METAG^b AND ULRICH MOSEL^a
 stefan.leupold@theo.physik.uni-giessen.de

a: Institut fuer Theoretische Physik

b: II. Physikalisches Institut

Universitaet Giessen, Giessen, D-35392, Germany

We review the current status of theories and experiments aiming at an understanding and a determination of the properties of light vector and scalar mesons inside strongly interacting hadronic matter. Starting from a discussion of the relevant symmetries of QCD and their connection with the hadronic description through QCD sum rules we then discuss hadronic models used to calculate the in-medium self-energies of hadrons and their spectral functions. The difficulties to link these calculated properties to actual observables are emphasized. Finally, we review in detail all the running experiments searching for in-medium changes of vector and scalar mesons, both with relativistic heavy-ion reactions as well as with elementary reactions on (cold) nuclei. Inconsistencies among experimental results are discussed. While almost all experiments observe a considerable broadening of vector mesons inside the nuclear medium, no evidence for mass changes is observed in the majority of the experiments.

Contents

1	Introduction	2
2	Symmetries of QCD, Hadron Properties, and QCD Sum Rules	5
2.1	Symmetry pattern of QCD	5
2.1.1	Center symmetry	5
2.1.2	Chiral symmetry	6
2.1.3	Order parameters of chiral symmetry breaking	7
2.1.4	In-medium changes of the symmetry pattern	9
2.1.5	In-medium changes of the order parameters	10
2.2	Hadronic and current-current correlation functions	13
2.2.1	Hadronic correlation functions	13
2.2.2	Current-current correlation functions	14
2.2.3	Connections to chiral symmetry	15
2.2.4	In-medium changes of correlation functions	16
2.3	QCD sum rules and in-medium changes of hadron properties	18
2.3.1	Generic structure of QCD sum rules	18
2.3.2	QCD condensates of dimension 4	20
2.3.3	QCD condensates of higher dimensions	21

2 *S. Leupold, U. Mosel, V. Metag*

2.3.4	Consequences for the spectral distribution	24
3	Hadronic Models	26
3.1	ρ meson	30
3.1.1	ρ meson in cold matter	30
3.1.2	ρ meson at finite temperatures	33
3.2	ω meson	34
3.3	ϕ meson	37
3.4	Scalar-meson (σ) production on nuclei	37
4	Hadronic Spectral Functions and Observables	38
4.1	Non-equilibrium effects	38
4.2	Nuclear transparency	38
4.3	Influence of branching ratios	39
4.4	Observability of collisional broadening	40
4.5	Final-state interactions	43
5	Experimental Approaches and Results	44
5.1	Experimental challenges	46
5.2	Pioneering Experiments	48
5.3	In-medium properties of the ρ meson	49
5.3.1	Heavy-ion experiments	49
5.3.2	Nuclear reactions with elementary probes	55
5.4	In-medium properties of the ω meson	60
5.4.1	Heavy-ion reactions	60
5.4.2	Nuclear reactions with elementary probes	61
5.5	In-medium properties of the ϕ meson	64
5.6	Ongoing dielectron spectroscopy experiments	66
5.6.1	Vector-meson production at RHIC	66
5.6.2	Dilepton emission in the 1 AGeV range	68
5.7	Summary of vector-meson experiments	69
5.8	2π correlations in nuclei: the σ meson	70
6	Conclusions	72
7	Acknowledgments	74

1. Introduction

It is nowadays commonly accepted that hadrons, the strongly interacting particles, are composite objects made out of quarks and gluons. In principle, the dynamics of the latter is governed by Quantum Chromodynamics (QCD). In practice, the non-perturbative sector of QCD which covers the formation of hadrons out of quarks and gluons is still not fully understood, in particular on the quantitative level.

In vacuum, a single hadron has specific properties like its mass and life time. It is rather suggestive that the properties of a composite object are modified once it is placed in a piece of matter (e.g., a nucleus) or in a heat bath (e.g., a fireball emerging in a relativistic heavy-ion collision). At least if the density of the system is so high that the size of the composite object is comparable to the average distance between the constituents of the system, then the intrinsic structure of the composite object starts to play a role. Obviously one probes in that way more and more the fundamental degrees of freedom, i.e. the quarks and gluons.

This interplay between hadrons on the one hand and quarks and gluons on the other hand has identified the in-medium changes of hadrons as one of the key aspects in understanding the non-perturbative sector of QCD. Consequently, the necessary studies are both fascinating and demanding. Two issues become important here: First, to make qualitative and quantitative predictions concerning the change of properties of a given hadron, and second, to figure out how to measure these changes in a situation where the detectors are, of course, outside of the dense strongly interacting system. For the latter issue the finite life time of the considered hadron becomes important. Only if the decay happens inside of the strongly interacting matter one can hope to see an in-medium modification of the properties of the hadron. In addition, it is most advantageous to produce in this decay final state particles which leave the strongly interacting system without further interactions. In that way one can make sure that the information about the in-medium modifications reaches the detectors without distortion. Otherwise one needs a good understanding of the final-state interactions (see the corresponding discussion in Sect. 4.5 below).

These considerations highlight the role of dileptons as good candidates for final-state particles. Emerging from an electromagnetic process they can directly couple to hadrons which have the quantum numbers of a photon. The hadrons which satisfy this condition are the vector mesons which will be the main focus of the present review. The fact that vector mesons provide interesting candidates concerning the observation of in-medium modifications has already been stressed in the early eighties of the last century.¹ The field has been further stimulated in the early nineties by spectacular predictions for drastic in-medium modifications — most notably dropping masses, as obtained from a scaling conjecture² and from QCD sum rule considerations³. It should be stressed, however, that in particular for light vector mesons earlier calculations based on a quark model did not yield significant mass shifts.⁴

Besides possible mass changes also modifications of the life times of nucleons and pions in a thermal bath have been addressed from a hadronic point of view in Ref. 5 using the low-density expansion and chiral perturbation theory. The results indicate significant widths but little mass modifications. Subsequently, the scope has been widened by studying also other hadrons and by considering more generally the spectral shape of a given hadron. Such questions can be tackled more easily from a hadronic point of view since a change of the life time is due to modifications of the hadronic decay channels (Pauli blocking, Fermi motion, ...) and

the appearance of additional processes, in particular “collisional broadening” due to hadron-hadron scattering events.⁶ In quark models a reliable description of such decay and scattering processes is notoriously difficult. Nowadays it is common practice to use hadronic many-body calculations with different degrees of sophistication to calculate hadronic in-medium spectra. Nonetheless, the connection to quark-based approaches like quark models or in particular QCD sum rules remains important to bring in the aspects of the fundamental degrees of freedom hidden inside the hadronic composite objects.

A very recent review⁷, similar in spirit to the present one, covered a very broad range of in-medium effects with an emphasis on a discussion of the various experiments. Here — in contrast — we concentrate on the light vector and scalar mesons. Other recent reviews include Refs. 8, 9, 10 which all deal with particular aspects of this topic, but are mostly limited to the discussion of in-medium effects in heavy-ion collisions while we discuss experiments both with heavy-ion and with elementary probes, mainly photons.

It is the purpose of the present work to review the current status of the physics of in-medium modifications of hadrons both from the theoretical and the experimental side. We will cover the range from fundamental QCD-based considerations via hadronic models and the identification of observables finally to the actual observations. We, therefore, start in Sect. 2 with a discussion of the relevant symmetries of Quantum Chromodynamics (QCD) and then link them to observable properties of hadrons via the QCD sum rule method. One main result of this discussion is that QCD sum rules can constrain hadronic in-medium properties, but they cannot unambiguously predict them.

The following Sect. 3, therefore, outlines the methods used to calculate hadronic in-medium properties using “conventional” hadronic interactions. We point out that the nucleon-resonance excitations play a dominant role in determining the in-medium properties of vector mesons through their coupling to the meson-nucleon final states. This is the same physics as that determining the Delta-hole model that was so successful in explaining the properties of pions and Delta excitations in nuclei (for a review see Ref. 11).

A relatively short Sect. 4 then deals with the connection between the calculated spectral functions and actual observables. Since the in-medium properties of a meson have to be inferred from measurements of its decay products, the latter should reach the detector with as little distortion by the medium as possible. From this point of view ideal probes are dileptons (e^+e^- or $\mu^+\mu^-$) which, however, suffer from the small electromagnetic coupling constants. On the other hand, hadronic final states can get distorted by the surrounding nuclear medium; in this case a realistic, state-of-the-art treatment of the final-state interactions is mandatory.

In Sect. 5 we finally discuss at some length the various experiments searching for in-medium properties of scalar and vector mesons. Here we discuss in detail experimental methods, limitations and successes of both heavy-ion collisions and nuclear reactions with elementary probes. Consistencies and discrepancies between different

experimental results are evaluated. The importance of detector acceptances for the comparison of experimental data and for the sensitivity to theoretical predictions is emphasized. We find that the results from ultra-relativistic heavy-ion collisions are compatible with those from photon-induced reactions: both classes of experiments show a significant broadening of vector mesons in the medium, but — so far — no mass shift has been established. We provide an outlook on expected results from presently running and planned future experiments.

Finally our conclusions are presented in Sect. 6.

2. Symmetries of QCD, Hadron Properties, and QCD Sum Rules

In the present section we review our current understanding of the symmetry pattern of QCD and the expected changes in a strongly interacting medium, the connection to the in-medium properties of hadrons, and the bridge between hadrons and QCD condensates based on QCD sum rules.

2.1. Symmetry pattern of QCD

Quantum chromodynamics (QCD), the by now accepted theory of the strong interaction,¹² has two faces: At high enough energies one can observe quarks and gluons as active degrees of freedom, e.g. in deep inelastic scattering and in jet production. The quarks and gluons also constitute the elementary building blocks which enter the QCD Lagrangian. On the other hand, it is not possible to isolate single quarks and gluons. Instead, at low energies one observes hadrons which are understood as composite objects formed by the elementary building blocks. The quarks and gluons are *confined* within hadrons.

2.1.1. Center symmetry

Confinement is related to the approximate center symmetry of QCD.^{13,14} A non-abelian gauge group governs the theoretical description of the interaction between quarks and gluons. If one restricts the Lagrangian to static quarks, the QCD action possesses a symmetry with respect to the center of this non-abelian gauge group. For a system at finite temperature T one can introduce the Polyakov loop¹⁵

$$L(\vec{x}) = \text{Tr} \mathcal{T} \exp \left[i \int_0^{1/T} dt A_0(t, \vec{x}) \right] \quad (1)$$

where the “time” integral concerns a Euclidean time,^a \mathcal{T} denotes time ordering of the exponential, A_0 is the gluon field and Tr denotes the trace over the color indices.

^aOne makes use here of the formal similarity between a time evolution operator $\exp(iHt)$ and a finite-temperature density operator $\exp(-H/T)$.¹⁶

6 *S. Leupold, U. Mosel, V. Metag*

In general, the Polyakov loop is not invariant with respect to the center symmetry. Under a center transformation an additional phase is obtained,

$$L \rightarrow e^{2\pi i n/3} L \quad \text{with} \quad n \in \{1, 2, 3\}. \quad (2)$$

One can show that the thermal expectation value of the Polyakov loop is related to the free energy F of a single static quark,¹⁵

$$\langle L \rangle = \exp(-F/T). \quad (3)$$

This aspect connects the center symmetry to confinement: If the expectation value of L vanishes, the phase in (2) does not matter. Both the QCD action and the system are center symmetric. In this case the free energy of a single quark is infinite. In other words, one needs an infinite amount of energy to isolate a static quark from the rest of the system, i.e. quarks are confined. In particular such a statement concerns the system with vanishing temperature, the vacuum: If the center symmetry is also realized for the ground state, the vacuum, and not only for the QCD action, then the energy of a single isolated quark is infinitely large. This would yield an explanation for the confinement mechanism. In reality, however, i.e. for non-static quarks, things are more complicated. The center symmetry is explicitly broken by the finite, i.e. non-infinite, quark masses. It is not so obvious how good the static-quark approximation actually is. Phenomenologically, one observes the following: If one tries to tear away a single quark from the rest of a hadron, it does not become more and more expensive in energy. Instead, the hadron splits into two or several hadrons as soon as there is enough energy for the additional hadron(s) to be generated. In that way confinement is dynamically realized. Nonetheless, the center symmetry provides qualitative insight and is an important aspect for theoretical descriptions within lattice QCD.¹⁷ For further details we refer to the literature.¹⁸

2.1.2. *Chiral symmetry*

In the following we discuss in some depth a second approximate symmetry which significantly influences the low-energy face of QCD. For massless quarks, QCD exhibits a chiral symmetry:^{19,20} The interaction is the same for left- and right-handed quarks and for different flavors. In reality, the masses of up and down quarks are very small as compared to typical hadronic scales.²¹ Also the mass of the strange quark is moderately small. In the following, we mainly restrict our discussion to the two lightest flavors.^b For the hadronic world it is more convenient to understand the combined left- and right-handed flavor symmetries as an invariance with respect to

^bWhen we come to our main subject of in-medium modifications we often concentrate on cold nuclear matter or nuclei as the strongly interacting medium. Here a flavor symmetry including strange quarks is anyway heavily broken explicitly by the medium which contains nucleons but no strange baryons.

vector and axial-vector flavor transformations.^c For two flavors the vector symmetry is just the isospin symmetry which leads to the appearance of isospin multiplets in the hadronic spectrum. In contrast, there are no (approximately) degenerate single-hadron states which correspond to the axial-vector symmetry. This symmetry would demand the existence of “chiral multiplets” where the members of one multiplet possess different parity. However, there are, e.g., no known hadrons with negative parity and the mass of the nucleon or with positive parity and the mass of the pion or ρ meson.²¹ One explains this finding by the conjecture that chiral symmetry is spontaneously broken — on top of the explicit breaking by the finite quark masses. In other words, the vacuum of QCD is in the symmetric Wigner-Weyl phase concerning the vector flavor symmetry and in the symmetry-broken Nambu-Goldstone phase concerning the axial-vector flavor symmetry. Formally:

$$Q_V^a |0\rangle = 0, \quad Q_A^a |0\rangle \neq 0, \quad (4)$$

with the QCD vacuum $|0\rangle$, the isospin charge

$$Q_V^a := \int d^3x j_V^{0a}(x), \quad (5)$$

the axial isospin charge

$$Q_A^a := \int d^3x j_A^{0a}(x), \quad (6)$$

and the corresponding currents

$$j_V^{\mu a} := \bar{q} \gamma^\mu \tau^a q, \quad j_A^{\mu a} := \bar{q} \gamma^\mu \gamma_5 \tau^a q, \quad (7)$$

defined in terms of the quark fields $q = (u, d)$ and the isospin^d matrices τ^a .

A spontaneously broken symmetry implies the existence of massless modes, the Nambu-Goldstone bosons. However, chiral symmetry is not only spontaneously, but also explicitly broken. The light-quark masses are non-vanishing, but small compared to hadronic scales.²¹ As a consequence the Nambu-Goldstone bosons need not be exactly massless, but should be light compared to all other excitations. Indeed, the pions satisfy this requirement²¹ and are consequently interpreted as the Nambu-Goldstone bosons of the spontaneously broken chiral symmetry of QCD.

2.1.3. Order parameters of chiral symmetry breaking

A phase with a broken symmetry can be characterized by an order parameter. Typically one can find several order parameters which might differ in their usefulness in practice. Due to the two faces of QCD one can introduce order parameters at

^cWe do not discuss here the axial non flavor-changing $U_A(1)$ transformations. They constitute a symmetry of the classical QCD Lagrangian, but not of the quantum field theory emerging from it. For a discussion of this $U_A(1)$ anomaly we refer to Ref. 12.

^dA generalization to more than two flavors is straightforward.

the quark-gluon and at the hadronic level. A much celebrated order parameter at the fundamental level is the (two-)quark condensate²²

$$\frac{1}{2} \langle 0 | \bar{q}q | 0 \rangle = \frac{1}{2} (\langle 0 | \bar{u}u | 0 \rangle + \langle 0 | \bar{d}d | 0 \rangle) \approx \langle 0 | \bar{u}u | 0 \rangle \approx \langle 0 | \bar{d}d | 0 \rangle \neq 0. \quad (8)$$

Below we introduce also other condensates which characterize the QCD vacuum. Only some of them are related to the chiral symmetry of QCD. It is easy to show that the operator $\bar{q}q$ which appears in (8) is not invariant with respect to chiral — to be specific — axial-vector flavor transformations. Thus, the quark condensate can only be non-vanishing, if the chiral symmetry is spontaneously broken.

On the hadronic level an appropriate order parameter is the pion-decay constant $f_\pi \approx 92$ MeV. More generally, this decay constant is defined for a pseudoscalar state (ps) with momentum k and isospin characterized by the index b in the following way:

$$\langle 0 | j_A^{\mu a} | \text{ps}^b(k) \rangle = i k^\mu f_{\text{ps}} \delta^{ab}, \quad (9)$$

with the axial-vector current defined in (7) above. In QCD one finds the partial conservation of the axial-vector current (PCAC):

$$\partial_\mu j_A^{\mu a} = i \bar{q} \{ \mathcal{M}, \tau^a \} \gamma_5 q. \quad (10)$$

Here the curly brackets denote the anticommutator and the quark-mass matrix is given by

$$\mathcal{M} = \begin{pmatrix} m_u & 0 \\ 0 & m_d \end{pmatrix}. \quad (11)$$

Using (9) and (10) it is easy to see that the combination $M_{\text{ps}}^2 f_{\text{ps}}$ is proportional to the quark masses, i.e. vanishes in the chiral limit:

$$M_{\text{ps}}^2 f_{\text{ps}} = 0 \quad \text{for } \mathcal{M} \rightarrow 0. \quad (12)$$

This relation holds irrespective whether the chiral symmetry is broken or not. However, which of the two quantities M_{ps} or f_{ps} actually vanishes depends on the phase. If there is no massless pseudoscalar state in the spectrum, the decay constants of all pseudoscalar states vanish — this is the Wigner-Weyl phase, i.e. the chirally restored phase. On the other hand, in the chirally broken Nambu-Goldstone phase, there must be a massless pseudoscalar state (in the chiral limit), the pion. Here, the corresponding decay constant, f_π , does not vanish. Consequently, the pion-decay constant is an order parameter of chiral symmetry breaking.

As a consequence of PCAC, the two order parameters identified so far are actually related by the Gell-Mann–Oakes–Renner relation:²²

$$f_\pi^2 M_\pi^2 \approx -\bar{m}_q \langle 0 | \bar{q}q | 0 \rangle \approx -2 \bar{m}_q \langle 0 | \bar{u}u | 0 \rangle \approx -2 \bar{m}_q \langle 0 | \bar{d}d | 0 \rangle, \quad (13)$$

which holds up to corrections of higher powers in the quark masses. Here \bar{m}_q denotes an averaged quark mass.

	vacuum	high temperature
chiral symmetry	broken	restored
order parameters: two-quark condensate, pion-decay constant	non-vanishing	vanishing
consequences	existence of Nambu-Goldstone bosons, non-degenerate spectra of chiral partners	no Nambu-Goldstone bosons, degenerate spectra of chiral partners
center symmetry	unbroken	broken
order parameter: Polyakov loop	vanishing	non-vanishing
consequence	confinement	deconfinement

Table 1. Symmetry pattern of QCD.

2.1.4. *In-medium changes of the symmetry pattern*

For a symmetry which is spontaneously broken in the vacuum, one typically finds that it becomes restored at some finite temperature. More generally, we expect changes in the symmetry pattern of QCD, if the vacuum is replaced by strongly interacting matter. Corresponding to the exact conservation laws for energy and baryon number we characterize such a medium in the following discussion by temperature and baryo-chemical potential. For large temperatures the typical momenta and therefore also the typical momentum exchanges in reactions are large. Consequently, quarks and gluons should become relevant degrees of freedom. Indeed, lattice-QCD calculations suggest that for temperatures larger than about 200 MeV a quark-gluon plasma (QGP) is formed.^{17,23} We recall that in the vacuum the center symmetry is realized (confinement), while the chiral symmetry is spontaneously broken (non-degenerate chiral multiplets, “massless” pions). At high temperatures, i.e. in the QGP, this picture is reversed:¹⁷ The center symmetry becomes spontaneously broken leading to deconfinement. Chiral symmetry is restored. Correlation functions (cf. Sect. 2.2 below) related by chiral transformations become degenerate. Due to deconfinement they might not necessarily contain quasi-particle structures any more (cf. Ref. 24 and Sect. 2.2 below). The situation is summarized in Table 1.

So far, lattice-QCD calculations are restricted to small baryo-chemical potentials. Therefore, at low temperatures, but large baryo-chemical potentials it is more speculative which properties the system has and how the symmetry pattern changes. Qualitatively, one can also expect here that with increasing density the momentum transfers become larger, involving quarks as active degrees of freedom. The role of real gluons is suppressed at low temperatures. They do play a role, however,

as exchange particles. The quarks form a Fermi sea. Their interaction is largely suppressed by Pauli-blocking effects. Consequently, the most interesting processes happen close to the Fermi surface. Here, an attractive interaction leads to an instability which drives the system in a (color) superconducting phase.^{25,26} For further considerations, one has to become more quantitative. At least for asymptotically high chemical potentials one can reliably use QCD perturbation theory to determine the interaction between quarks near the Fermi surface. The dominant attractive interaction leads to a special kind of color superconductivity, the so-called color-flavor locking (CFL) phase involving up, down and strange quarks on equal footing.²⁷ Here, chiral symmetry is also spontaneously broken, albeit quantitatively the breaking is smaller than in vacuum. Interestingly, the excitations in that particular phase resemble the QCD vacuum excitations, i.e. the hadrons. Therefore, it has been speculated that no real phase transition is required, if there is a direct transition from the low-density hadronic to the high-density CFL state.²⁸ However, there are also alternative scenarios, since it is not clear down to which densities the perturbative QCD calculations can be trusted. There might be other color superconducting phases in between the hadronic and the CFL matter. In particular, in a two-flavor color superconducting phase, chiral symmetry would be restored. Recently, the existence of a quarkyonic phase has been suggested.²⁹ There, the excitations are of hadron type, i.e. quarks are confined, but chiral symmetry is restored. In any case, it is suggested that chiral symmetry breaking becomes lifted or at least significantly weakened in a dense strongly interacting medium, no matter whether high (energy) density is achieved by large temperatures or large chemical potentials or both.

2.1.5. *In-medium changes of the order parameters*

Already at low densities one finds a drop of the order parameters of chiral symmetry breaking. If the density is low enough, one can neglect the interactions between the medium constituents. The order parameter can be regarded as a probe which interacts independently with the states which form the medium. We discuss two special cases for which one can make exact, model independent statements: (i) A baryon-free low-temperature system described by a gas of pions and (ii) cold nuclear matter described by a Fermi sphere of nucleons. For the first system it is assumed that the temperature is so low that no other particles are significantly populated^e and that the pions do not interact. Actually the latter assumption can be dropped since the interaction between the pions can be systematically included using chiral perturbation theory.³⁰ For the second system we assume that the temperature is exactly zero and that the baryo-chemical potential, i.e. the Fermi energy, is lower than the mass of the first excited baryon. Thus, the system contains only nucleons. Their interaction can be neglected for not too large densities.

^eNote that the pions are the lightest degrees of freedom due to their Goldstone-boson character.

We discuss the change of the two-quark condensate and of the pion-decay constant: The in-medium two-quark condensate is just given by $\langle \Omega | \bar{q}q | \Omega \rangle$ with the state $|\Omega\rangle$ characterizing the in-medium system. The in-medium generalization of the pion-decay constant defined for the vacuum case in (9) requires some care, since the medium introduces an additional Lorentz vector. Following Ref. 31 we use for the definition the zeroth component of the axial-vector current, since it is directly related to the charge (6) which in turn governs the chiral transformations:

$$\langle \Omega | j_A^0 | \pi^b(k) \rangle = i k^0 \delta^{ab} f_\pi^{\text{med}}. \quad (14)$$

For a pion gas described by chiral perturbation theory the change of the two-quark condensate has been evaluated in Ref. 30 up to three loops.^f The result in lowest order in the pion density (i.e. neglecting interactions) is

$$\frac{\langle \Omega | \bar{q}q | \Omega \rangle_{\text{pionic med.}}}{\langle 0 | \bar{q}q | 0 \rangle} = 1 - \frac{\rho_\pi}{f_\pi^2}, \quad (15)$$

with the scalar pion density

$$\rho_\pi = 3 \int \frac{d^3k}{(2\pi)^3} \frac{1}{2E_k} \frac{1}{e^{E_k/T} - 1} \xrightarrow{M_\pi \rightarrow 0} \frac{1}{8} T^2, \quad (16)$$

the temperature T and the pion energy $E_k = \sqrt{\vec{k}^2 + M_\pi^2}$.

The leading-order change of the pion-decay constant with temperature is given by:^{32,33}

$$f_\pi^{\text{pionic med.}} = f_\pi \left(1 - \frac{2\rho_\pi}{3f_\pi^2} \right). \quad (17)$$

Naively, one might conclude from the Gell-Mann–Oakes–Renner relation (13) that the square of the pion-decay constant could scale with the two-quark condensate. As can be seen from (15,17) this is not the case. f_π^2 drops faster by a factor 4/3 for low densities. At the same time the in-medium pion mass increases such that at the temperatures considered in Ref. 32 the Gell-Mann–Oakes–Renner relation (13) still holds.

Cold nuclear matter is characterized by its density

$$\rho_N = 4 \int \frac{d^3k}{(2\pi)^3} \Theta(k_F - |\vec{k}|) \quad (18)$$

with the Fermi momentum $k_F = \sqrt{\mu^2 - m_N^2}$ and baryo-chemical potential μ . For the in-medium change of the two-quark condensate one obtains³⁴

$$\frac{\langle \Omega | \bar{q}q | \Omega \rangle_{\text{nucl. med.}}}{\langle 0 | \bar{q}q | 0 \rangle} = 1 - \frac{\rho_s m_N \sigma_N}{f_\pi^2 M_\pi^2} \approx 1 - \frac{1}{3} \frac{\rho_N}{\rho_0} \quad (19)$$

^f “One-loop” corresponds to non-interacting pions.

12 *S. Leupold, U. Mosel, V. Metag*

with ρ_0 denoting nuclear saturation density and with the scalar nucleon density

$$\rho_s = 4 \int \frac{d^3k}{(2\pi)^3} \frac{1}{\sqrt{\vec{k}^2 + m_N^2}} \Theta(k_F - |\vec{k}|) \approx \frac{\rho_N}{m_N}, \quad (20)$$

where the last relation holds for small enough densities. The nucleon sigma term,

$$\sigma_N = \bar{m}_q \frac{dm_N}{d\bar{m}_q} \approx 45 \text{ MeV}, \quad (21)$$

which appears in (19) can be obtained within the framework of chiral perturbation theory from low-energy πN scattering.³⁵

For cold nuclear matter the leading-order change of the pion-decay constant is related model independently to some low-energy constants of pion-nucleon scattering. Graphically this is depicted in Fig. 1. We stress that the additional processes depicted in the lower part of Fig. 1 are just the scattering of a pion on a nucleon from the medium into a weak current and a nucleon, i.e. standard hadronic effects which can be determined model independently within chiral perturbation theory. The change of the pion-decay constant has been calculated, e.g., in Ref. 31 with the numerical result:

$$f_\pi^{\text{nucl. med.}} = f_\pi \left(1 - \frac{\rho_N}{\rho_0} (0.26 \pm 0.04) \right). \quad (22)$$

Again, we observe that the square of the pion-decay constant drops faster than the quark condensate (cf. also Ref. 36).

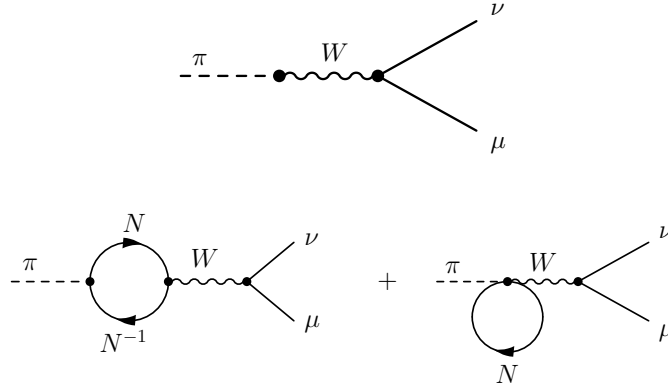


Fig. 1. Pion decay into muon and neutrino in vacuum (top) and in a nucleonic medium (bottom). See main text for details.

We conclude that already in a hadronic medium the order parameters of chiral symmetry breaking start to drop. It is important to stress that at least this onset of chiral restoration is caused by standard hadronic interactions. It is the main

purpose of Fig. 1 to illustrate that point. The corresponding statement holds also for the finite-temperature effect in (17). Hence chiral restoration does not happen on top of ordinary hadronic effects. At least at low densities it is the presence of the hadronic medium constituents which is responsible for the onset of changes of the symmetry pattern of QCD.

2.2. Hadronic and current-current correlation functions

Before we discuss further consequences of symmetry changes on hadronic properties we introduce a proper framework which is suitable to characterize hadrons and to make contact with QCD. The central objects are correlation functions. Corresponding to the two faces of QCD we introduce hadronic and current-current correlation functions. The currents which enter the latter are formed from quark (and, if necessary, gluon) fields.

2.2.1. Hadronic correlation functions

We start with the description of a single hadron in the hadronic language. We concentrate on mesons in the following, but the extension to baryons is straightforward. It is convenient to introduce a field $h(x)$ with the quantum numbers of the hadron under consideration. The properties of the meson can be obtained from the retarded hadronic correlation function or propagator D_{ret} .[§] Schematically, i.e. suppressing all other quantum numbers besides the space-time information, one has

$$D_{\text{ret}}(q) = i \int d^4x e^{iqx} \Theta(x_0) \langle \Omega | [h(x), h(0)] | \Omega \rangle. \quad (23)$$

We recall that Ω characterizes the in-medium system. The retarded correlator is analytic in the upper half of the complex energy plane. It satisfies a dispersion relation

$$D_{\text{ret}}(q) = \int_{-\infty}^{+\infty} dk_0 \frac{\mathcal{A}(k_0, \vec{q})}{q_0 - k_0 + i\epsilon}, \quad (24)$$

where we have introduced the spectral function

$$\mathcal{A} = -\frac{1}{\pi} \text{Im} D_{\text{ret}}. \quad (25)$$

It is essentially given by the Fourier transform of the commutator $[h(x), h(0)]$.

The important message from (24) is that all information is contained in the spectral function. A single hadron appears as a quasi-particle peak in the spectral function. From the peak position and the peak width one can obtain mass and life

[§]In vacuum one might use the time-ordered correlator as well. In a medium the appropriate object to characterize *one* state is the retarded correlator. The time-ordered object contains information about the state *and* about its population.³⁷

time of the hadron. This extraction is fairly unambiguous as long as the life time is long, i.e. the width is small (as compared to the mass). For large widths it is insufficient to characterize the hadron by mass and life time. The whole spectral shape becomes important. A large width implies that there are other (hadronic) states which couple strongly to the considered hadron. These other states can also interact without exciting this hadron described by h . This causes a physical background which interferes on the amplitude level with the resonant amplitude. Actually the hadron field h can be redefined such that part of the background is included. In other words, background can be shifted back and forth and the choice of the field $h(x)$ to characterize the hadron of interest is not unique (see, e.g., Ref. 38 concerning vector mesons). Therefore, strictly speaking, the spectral function changes if a different field is chosen (see also, e.g., Ref. 39). Again, this is of no concern as long as the hadron is a quasi-particle state, i.e. if the width is sufficiently small. From a theoretical point of view there is no problem with the mentioned ambiguities. The spectral function provides a tool to calculate observable quantities. The latter, of course, are independent of the chosen field.

In a medium the spectral function can become more complicated. In many hadronic models one typically finds significant increases of the widths of hadrons. In addition, several models predict additional structures in the spectral functions caused by many-body effects like resonance-hole excitations.^{40,41,42,43,44,45,46}

2.2.2. Current-current correlation functions

We now turn to the description of a hadron and its properties in the quark-gluon language. Here, one introduces a current with the quantum numbers of the hadron of interest.⁴⁷ As an example we discuss the ρ^0 meson. A generalization to other hadrons is straightforward. A quark current with the quantum numbers of the ρ^0 is given by^{48,49}

$$j^\mu = \frac{1}{2} (\bar{u}\gamma^\mu u - \bar{d}\gamma^\mu d) . \quad (26)$$

We note in passing that this is one of the symmetry currents appearing in (7). In complete analogy to the formalism described in (23,24) one introduces the (retarded) current-current correlation function

$$\Pi_{\text{ret}}^{\mu\nu}(q) = i \int d^4x e^{iqx} \Theta(x_0) \langle \Omega | [j^\mu(x), j^\nu(0)] | \Omega \rangle . \quad (27)$$

A dispersion relation similar to (24) can be formulated. In other words, all information is contained in $\text{Im}\Pi_{\text{ret}}$ which is called “spectral distribution”.^h All hadronic

^hWe do not use the phrase “spectral function” in the present section, to avoid mixing up hadronic and current correlators. Note that in a free-field theory the spectral function satisfies a normalization condition whereas the spectral distribution does not.

objects which have the quantum numbers specified by the current enter this spectral distribution. Typically there are several hadrons with the same quantum numbers. For example, there are excited mesons with the quantum numbers of the ρ^0 at about 1450 MeV and 1700 MeV.²¹ A given current couples to several hadrons (and of course also to hadronic many-body states with the appropriate quantum numbers). Hence, one can only obtain information about a single hadron from the corresponding current-current correlator, i.e. the spectral distribution, if it is sufficiently far away from the other excitations with the same quantum numbers. In a strongly interacting medium many-body excitations become more important. The same effects which change the spectral function of a single hadron, of course, also influence the corresponding spectral distribution. Peaks which appear in the vacuum spectral distribution typically become broader. They also can get shifted. Additional structures might show up.

For special currents the spectral distribution of the current-current correlator is directly accessible by experiment: The currents

$$j_{\text{el}}^\mu = \frac{2}{3} \bar{u} \gamma^\mu u - \frac{1}{3} \bar{d} \gamma^\mu d + \dots = \underbrace{\frac{1}{2} (\bar{u} \gamma^\mu u - \bar{d} \gamma^\mu d)}_{\text{isospin 1}} + \underbrace{\frac{1}{6} (\bar{u} \gamma^\mu u + \bar{d} \gamma^\mu d)}_{\text{isospin 0}} + \dots \quad (28)$$

and $j_{\text{weak}}^{\mu a} = j_V^{\mu a} - j_A^{\mu a}$ are involved in the electromagnetic or weak interaction, respectively. Here the dots denote the contributions of other quark flavors and the currents defined in (7) come into play again. Electron-positron annihilation and τ -decay processes are used to obtain the corresponding spectral distributions in the vacuum. The dilepton production from a strongly interacting medium is a frequently used tool to study potential in-medium changes of hadrons (better to say, of the quark currents).¹⁰

Also in lattice QCD the central object to study hadronic properties are the current-current correlators. There one does not study the Fourier transform of the current-current correlator like in (27), but directly the object in coordinate space. One is restricted to space-like distances, since time-like distances would lead to path integrals where the integrands are not positive definite. Such integrals cannot be computed with Monte-Carlo methods. Consequently the full spectral distribution is not directly accessible by lattice-QCD calculations (see also Ref. 50, 51 for the use of the maximum-entropy method). Typically one is restricted to the lowest (or lowest few) excitations in the respective channel.⁵² Another theoretical approach which uses the current-current correlation functions is the QCD sum rule method which is introduced in Sect. 2.3 below.

2.2.3. Connections to chiral symmetry

Concerning chiral symmetry breaking and its restoration, the current-current correlators play an interesting role. By a chiral transformation a given current can mix with or fully transform into a current with different quantum numbers and in

particular opposite parity. This “chiral partner” current would contain the same spectral distribution as the current one started out with, if chiral symmetry was not spontaneously broken.ⁱ In turn, an observed difference between such two spectral distributions signals chiral symmetry breaking. The additional observation of a reduction of this difference in a medium would signal chiral symmetry restoration. The best explored pair of currents in that respect — for the vacuum — are the charged vector and axial-vector currents given in (7): Studying the decay $\tau^+ \rightarrow \nu_\tau + \text{hadrons}$, one probes the $V - A$ current combination $\bar{d}\gamma^\mu u - \bar{d}\gamma^\mu \gamma_5 u$. Due to G parity the vector part of this combination couples to an even number of pions whereas the axial-vector part couples to an odd number. Consequently, one has direct experimental access separately on $\bar{d}\gamma^\mu u$ and $\bar{d}\gamma^\mu \gamma_5 u$. But a chiral transformation can turn the current $\bar{d}\gamma^\mu u$ into the current $\bar{d}\gamma^\mu \gamma_5 u$. As can be seen from the τ -decay data the spectral distributions contained in $\bar{d}\gamma^\mu u$ and $\bar{d}\gamma^\mu \gamma_5 u$ are very different⁵³ which is a clear sign of chiral symmetry breaking. Unfortunately, τ decays are not so easily accessible for in-medium situations. But from a theoretical point of view it is an interesting task to study the in-medium behavior of the difference between the spectral distributions of $\bar{d}\gamma^\mu u$ and $\bar{d}\gamma^\mu \gamma_5 u$ or more general of the currents given in (7). At least the neutral vector current enters the electromagnetic current (28) — together with the isospin-0 part — and is therefore also experimentally accessible for in-medium situations from dilepton production. In this review we will frequently come back to dilepton production below.

A final remark is in order, concerning the spectral distributions of chiral partner currents and the interplay between currents and single hadrons: Note that not only a given quark current couples to different hadrons, but also a given hadron couples to different currents. This leads to ambiguities concerning the chiral partner of a given hadron. For example, besides the quark current (26) which has the quantum numbers of the ρ^0 there is also the current $\tilde{j}^\mu = \partial_\nu (\bar{q} \sigma^{\mu\nu} \tau^3 q)$ with the same quantum numbers. A chiral transformation mixes (26), e.g., with $\bar{d}\gamma^\mu \gamma_5 u$ which has the quantum numbers of the (positively charged) a_1 meson. On the other hand, \tilde{j}^μ is mixed with $\partial_\nu (\bar{d} \sigma^{\mu\nu} \gamma_5 u)$ which has the quantum numbers of the (positively charged) b_1 meson. This ambiguity exists for a given hadron.⁵⁴ For a given quark current there is, of course, no ambiguity. The latter are the ones which are explored, e.g., in vacuum in τ decays and in electron-positron annihilation.

2.2.4. *In-medium changes of correlation functions*

We have discussed in Sect. 2.1 that a change in the symmetry pattern of QCD is expected, if the vacuum is replaced by dense strongly interacting matter. Presumably this change does not happen suddenly at the transition point, but shows precursor effects. Hence, we expect that hadronic properties change already in a hadronic surrounding. On the other hand, not every in-medium change might be related to

ⁱOf course, this statement holds up to effects from explicit symmetry breaking.

symmetries. More generally, due to the two-face appearance of QCD, one can have two different points of view on in-medium modifications of hadrons, a quark-gluon and a hadronic one: From a purely hadronic point of view, the change of properties of a hadronic probe in strongly interacting matter is caused by the interactions of the probe with the hadrons which form this medium. On the other hand, in the QCD language a hadron is an excitation of the QCD vacuum. In turn, the vacuum is characterized by condensates. As can be seen, e.g., from (15,19), the condensates change in a strongly interacting medium. One might say that the underlying vacuum is modified and consequently the properties of the hadronic excitations of the changed vacuum are also modified.

It is clearly an exciting task to predict and experimentally confirm hadronic in-medium changes caused by the modified vacuum structure. However, one may wonder whether the two different points of view formulated above are not just different languages for the same physics. At least qualitatively standard hadronic effects are in line with the expectation from chiral restoration and deconfinement: As we have discussed in Sect. 2.1.5, already the presence of the hadronic medium constituents — even if they do not interact with each other — leads to a drop of the chiral order parameters. Also an onset of deconfinement can be observed in the correlation functions with hadronic quantum numbers: As we have already discussed, in vacuum these correlation functions contain quasi-particle structures, i.e. the hadrons with the corresponding quantum numbers. In contrast, in a deconfined system, the correlation functions contain a rather structureless quark-antiquark or three-quark continuum. Hence one expects that structures are washed out.⁵⁵ Indeed, hadronic many-body calculations predict increasing widths for hadronic states and also experimentally this seems to be confirmed (see below). However, to really figure out up to which point a hadronic description makes sense, more quantitative calculations are necessary. In particular, as already pointed out, QCD predicts that the correlators of currents which are connected by chiral transformations (“chiral partners”) become degenerate in a chirally restored system. Hence, one task is to figure out to which extent purely hadronic descriptions show an onset of degeneracy for the spectra of chiral partner currents.²⁴

Alternatives to standard hadronic many-body models are provided by approaches which involve quarks in one or the other way, e.g., quark models or approaches involving QCD condensates. They seem to offer a more microscopic view on the symmetry changes. One should be aware, however, that it is not so easy to translate the results of such quark-type models to hadronic observables. In particular, there are models which predict dropping masses for some or all hadrons (except for Nambu-Goldstone bosons), e.g., the famous Brown-Rho scaling conjecture.² On the other hand, there are quark models which include the phenomenon of chiral restoration and do not predict a change of the vector-meson masses (for an early application of a generalized Nambu–Jona-Lasinio model⁵⁶ see Ref. 4). If the hadronic spectra get much broader, it is not so clear in the first place what a dropping mass actually means (cf., e.g., Ref. 36). But not only the quark language has its limita-

tions: At least close to the transition to a new state of matter (QGP or quarkyonic matter or color superconducting matter) the hadronic setup might become rather uneconomical, if not inappropriate, since the relevant degrees of freedom on the other side of the transition are missing and since hadronic n -body scatterings with n large might become more and more important. As a conservative approach one should at least try to figure out how far one comes with an interpretation of the experimental results based on a standard hadronic description. Obviously, much more work on the theory side is needed to reconcile quark and hadronic models and to base them deeper on QCD. One connection between hadronic properties and QCD condensates is provided by the QCD sum rule method to which we turn next.

2.3. *QCD sum rules and in-medium changes of hadron properties*

We have seen so far that hadronic properties and their potential in-medium changes are encoded in correlation functions. However, neither the hadronic nor the current-current correlators are easily calculable in the non-perturbative regime of QCD one is interested in. On the other hand, the non-perturbative features of QCD are also characterized by the non-vanishing condensates. In a strongly interacting system also the QCD condensates change their values. We will see in the following that at least to some extent these in-medium modifications of condensates can be evaluated. In addition, the current-current correlation functions can be connected to the QCD condensates by the QCD sum rule method. This imposes constraints on possible in-medium changes of hadronic properties. We will find that these constraints are actually not strong enough that unique conclusions can be drawn for a single hadronic property, like the mass or life time of a given hadron. However, non-trivial correlations can be obtained. We will also comment on the interrelations between hadron properties, condensates and chiral symmetry.

2.3.1. *Generic structure of QCD sum rules*

Originally QCD sum rules were introduced for the vacuum^{48,49} but later on generalized to in-medium situations.⁵⁷ In particular the work of Hatsuda and Lee³ which points towards drastic in-medium changes of ρ and ω mesons has triggered a lot of activities both on the experimental and on the theory side.

To show how QCD sum rules work we consider again the ρ^0 as an example. As a strongly interacting medium we take cold nuclear matter characterized by a baryo-chemical potential μ . All connected quantities have already been introduced in the paragraph of Eq. (18). We concentrate on a meson at rest with respect to the nuclear medium. This is most appropriate since in a realistic situation where the medium has only a finite spatial extension (e.g. a nucleus), one would be interested in a probe which stays in the medium as long as possible. Note that we use the case of a ρ^0 at rest in cold nuclear matter as an illustrative and important example. However, the qualitative conclusions which we draw apply also to other hadrons

and to other in-medium situations. In the following we will frequently also comment on the case of finite temperature.

The sum rule method starts with the current-current correlation function defined in (27). Instead of the Lorentz tensor $\Pi^{\mu\nu}$ it is more convenient to study the scalar and dimensionless quantity $R = -\Pi_\mu^\mu/(3q^2)$. We note in passing that for a probe which was not at rest, more care would be needed on that stage. In vacuum the imaginary part of R is directly linked to the ratio of cross sections for $e^+e^- \rightarrow$ hadrons and $e^+e^- \rightarrow \mu^+\mu^-$, respectively.^{48,49}

There is a regime where the quarks and gluons become the relevant entities, namely at large energies/momenta. There, the correlator R can be evaluated using QCD perturbation theory. The purely perturbative result can be improved by the inclusion of expectation values of local operators, the condensates. The technical tool here is the operator product expansion (OPE) which works in the regime of large space-like momenta.⁵⁸ On the other hand, the whole information expressed by the current-current correlation function (27) or equivalently by R is contained in its spectral distribution, i.e. the values of its imaginary part along the real energy axis.^j The spectral distribution in turn contains all the hadrons which couple to the considered current. Therefore two expressions for the same quantity can be matched for large space-like momenta: one obtained from the OPE and one from a dispersion integral. Schematically (ignoring, e.g., possible subtractions) one finds

$$\int_0^\infty \frac{ds}{\pi} \frac{\text{Im} R^{\text{HAD}}(s)}{s + Q^2} = R^{\text{OPE}}(Q^2) \quad (29)$$

where we have made explicit by the superscripts where the respective information is supposed to come from. This dispersion relation corresponds to the one given in (24). In addition, we have introduced $Q^2 = -q^2 \gg 0$ for large space-like momenta, and we have rearranged the energy integration using the fact that the considered meson is its own antiparticle.

On the left-hand side of (29) the information about all hadrons with the quantum numbers of the considered current enters. The integral covers arbitrarily large energies \sqrt{s} . On the other hand, one is particularly interested in the low-energy regime, where distinct hadronic resonances have been identified. Technically one can enhance the importance of the low-energy part by a Borel transformation.^{48,49} While the high-energy part is only power suppressed by $(s + Q^2)^{-1}$ in (29), the Borel transformation achieves an exponential suppression. For a ρ meson in cold

^jNote that the space-like momenta where the OPE works can be achieved by imaginary values for the energy. This is appropriate since we assume that the studied probe is at rest with respect to the medium, i.e. that its three-momentum vanishes.

20 *S. Leupold, U. Mosel, V. Metag*

\bar{m}_q	$\langle 0 \bar{u}u 0\rangle$	$\langle 0 \frac{\alpha_s}{\pi}G^2 0\rangle$	α_s	a_2	a_4
6 MeV	$-(240 \text{ MeV})^3$	$(330 \text{ MeV})^4$	0.36	0.9	0.12

Table 2. Actual values for the ingredients of the operator product expansion. Numbers taken from Refs. 60, 61.

nuclear matter the QCD (Borel) sum rule reads^{3,59,60}

$$\begin{aligned}
\frac{1}{\pi M^2} \int_0^\infty ds \text{Im} R^{\text{HAD}}(s) e^{-s/M^2} &= \frac{1}{8\pi^2} \left(1 + \frac{\alpha_s}{\pi} \right) \\
&+ \frac{1}{M^4} \left(\bar{m}_q \langle \Omega|\bar{u}u|\Omega \rangle + \frac{1}{24} \langle \Omega|\frac{\alpha_s}{\pi}G^2|\Omega \rangle + \frac{1}{4} m_N a_2 \rho_N \right) \\
&+ \frac{1}{M^6} \left(-\frac{56}{81} \pi \alpha_s \langle \Omega|\mathcal{O}_4^V|\Omega \rangle - \frac{5}{24} m_N^3 a_4 \rho_N \right) \\
&+ \mathcal{O}(1/M^8).
\end{aligned} \tag{30}$$

Here M is the Borel mass which takes the role of the large space-like momentum variable $\sqrt{Q^2}$ after Borel transformation. On the left-hand side of (30) one sees the already announced exponential suppression of large- s contributions. One can expect that the integral is most sensitive to the low-energy part of the spectral distribution. On the OPE side, the right-hand side of (30), an expansion in inverse powers of the Borel mass M appears. It originates from the OPE which is an expansion in $1/Q^2$. The leading term is the result from QCD perturbation theory. α_s is the running coupling of QCD. Simply for dimensional reasons the contributions from QCD condensates are suppressed by powers of the Borel mass M . In the following, we discuss the terms appearing on the right-hand side of (30) one by one, focusing on three aspects: First, of course, we define their meaning, second we discuss their numerical importance and third we comment on their possible connection to chiral symmetry breaking and restoration. Actual values for the terms appearing in (30) are provided in Table 2.

2.3.2. QCD condensates of dimension 4

The first term which multiplies $1/M^4$ in (30) is the already introduced two-quark condensate. Its density dependence in leading order of the nucleon density ρ_N is given in (19). The non-vanishing of the two-quark condensate signals chiral symmetry breaking. However, its numerical influence on the sum rule is small in vacuum and also at finite nuclear densities.

One of the terms numerically important in vacuum is the gluon condensate $\langle \Omega|\frac{\alpha_s}{\pi}G^2|\Omega \rangle$. Together with the four-quark condensates, discussed below, the gluon condensate determines the vacuum properties of the ρ meson.^{48,49} The medium dependence of the gluon condensate for finite baryon densities but also for finite temperatures can be obtained from the trace anomaly.^{3,62} It turns out that this

density dependence is very weak. Hence while the gluon condensate is important for the vacuum properties, it is not responsible for strong in-medium changes — at least not for low densities. The gluon condensate is invariant with respect to chiral transformations. Thus, there is no direct connection between chiral symmetry breaking and the non-vanishing of the gluon condensate.

The last term which multiplies $1/M^4$ only shows up in the presence of a medium.^{3,62} It originates from the non-scalar twist-2 condensate $\langle \Omega | \bar{q} (\gamma_0 D_0 - \frac{1}{4} \gamma_\mu D^\mu) q | \Omega \rangle$. This condensate can be evaluated for the two in-medium situations discussed in Sect. 2.1.5, i.e. a pion gas (finite temperature) or a nucleon Fermi sphere (cold nuclear matter). In (30) we had specified the in-medium situation to the latter case. The value for a_2 can be obtained from the parton distributions determined by deep-inelastic scattering reactions. Hence, there is not much uncertainty about the size of this term. It turns out that the numerical contribution of this term is large. Since the corresponding condensate is chirally invariant, it points towards an in-medium modification which is not intimately connected to chiral symmetry. A numerical evaluation is presented in Fig. 2, left panels. The lines start out on the left-hand side from the vacuum value. If one adds *only* the a_2 term one obtains the lines with the label “only a_2 ”. Obviously, the influence of the a_2 term is quite large. Further details are given below after the four-quark condensates have been introduced.

2.3.3. QCD condensates of higher dimensions

The first term accompanied by $1/M^6$ contains a special combination of four-quark condensates:

$$\begin{aligned} \langle \Omega | \mathcal{O}_4^V | \Omega \rangle &= \frac{81}{224} \langle \Omega | (\bar{u} \gamma_\mu \gamma_5 \lambda^c u - \bar{d} \gamma_\mu \gamma_5 \lambda^c d)^2 | \Omega \rangle \\ &+ \frac{9}{112} \langle \Omega | (\bar{u} \gamma_\mu \lambda^c u + \bar{d} \gamma_\mu \lambda^c d) \sum_{\psi=u,d,s} \bar{\psi} \gamma^\mu \lambda^c \psi | \Omega \rangle, \end{aligned} \quad (31)$$

with color matrices λ^c . The size of four-quark condensates, even in vacuum, is still under debate. Originally it was assumed that in the vacuum, $\Omega = 0$, the four-quark condensate can be approximately factorized:^{48,49}

$$\langle \Omega | \mathcal{O}_4^V | \Omega \rangle \stackrel{?}{\approx} \langle \Omega | \bar{u} u | \Omega \rangle^2. \quad (32)$$

Indeed, in the limit of a large number of colors this factorization can be justified both for vacuum and for finite nuclear densities (but not for finite temperatures).⁶³ If one chooses the size of the four-quark condensates such that their order of magnitude is given by (32), one obtains a decent description of the vacuum properties of the ρ meson. A factor of two change in this size does not influence the ρ -meson properties in a drastic way. Thus the vacuum sum rule is not extremely sensitive to the detailed values of the four-quark condensates, provided the order of magnitude is correct. The change of the four-quark condensate with density and the a_2 term discussed

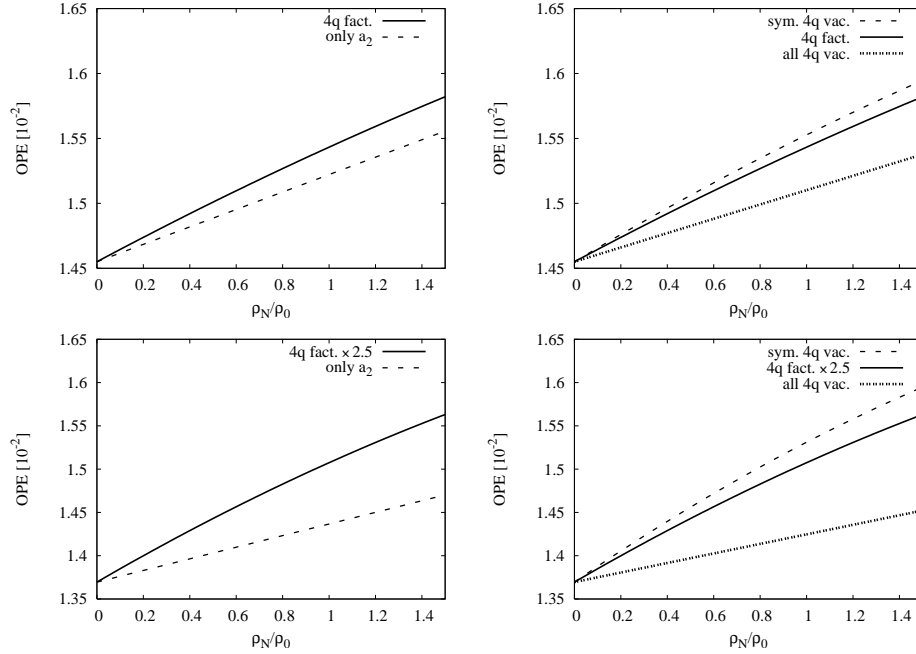


Fig. 2. The right-hand side of (30) as a function of the nuclear density for a generic value of the Borel mass, $M = 0.8 \text{ GeV}$, and for different assumptions concerning the four-quark condensates. *Top left:* Factorization (32) is assumed for all four-quark condensates. The upper line shows the full in-medium result. The lower line is obtained using vacuum values for all OPE contributions except for the a_2 term. *Top right:* For all lines vacuum factorization is assumed for all four-quark condensates. The highest (lowest) line is obtained using the respective vacuum value also for the chirally symmetric (all) in-medium four-quark condensates. For the middle line factorization is assumed for all four-quark condensates. From top to bottom these are the cases (iii), (i), and (ii) discussed in the main text. *Bottom:* Same as top panels, but instead of factorization an additional factor of 2.5 is multiplied to obtain four-quark condensates from the square of the two-quark condensate.

above have the most influence on the changes of the OPE side of (30). We will come back to that point below.

Concerning chiral symmetry, relation (32) — if true for finite densities — seems to suggest that four-quark condensates drop together with the two-quark condensate and, in particular, that the four-quark condensates vanish for a chirally restored system. On the other hand, the second term on the right-hand side of (31) is chirally symmetric. Hence, there is no strict reason why this quantity should vanish at chiral restoration. Things are different for the first term on the right-hand side of (31). This term changes under chiral transformations. Thus, there is an influence of chiral symmetry breaking and maybe restoration on the OPE side and therefore on the current-current correlator induced by specific four-quark condensates. However,

the quantitative evaluation is not straightforward. To explore the uncertainties one might study the following extreme points of view: (i) The four-quark condensates change at finite density according to (32,19). (ii) None of the four-quark condensates given in (31) changes in the medium. (iii) The chirally invariant second part of the right hand side of (31) does not change in the medium while the first term changes according to the factorization assumption. These possibilities are explored in Fig. 2. In addition, we have studied the consequences of larger values for the four-quark condensates as compared to the factorization result. For the other condensates we take typical values from the literature,⁶⁰ see also Table 2. Obviously, the variation due to the uncertainties in the four-quark condensates is significant. Nonetheless, in all explored cases there is a sizeable in-medium change of the OPE side. It is interesting to observe that case (iii) discussed above always leads to the largest deviation from the vacuum (respective top line in the right panels of Fig. 2). On the other hand, this case rests on a rather conservative assumption: It is plausible that at least the four-quark condensate which is not chirally symmetric changes similar to the two-quark condensate.

For a finite-temperature system instead of a cold nuclear system one can use PCAC relations to reduce all in-medium expectation values of four-quark operators to vacuum condensates. This leads to the much celebrated Dey-Eletsy-Ioffe mixing formula.⁶⁴ It rests on the assumption that the momenta of the pions, which form the finite-temperature system, can be neglected. For the OPE side this is a reasonable assumption as momenta of the order of the temperature are soft compared to the hard OPE expansion parameter (Q^2 or M^2). We note in passing, however, that the mixing formula is sometimes also used for the spectral side where for typical values of the temperature on the order of 100 MeV it yields misleading results like the appearance of the a_1 -meson peak in the vector channel. A kinematically proper treatment of the non-negligible pion momenta is required here as performed, e.g., in Refs. 65, 66. The result is a broadening of the spectral distribution and in particular the appearance of strength at low invariant masses connected to the Dalitz decay $a_1 \rightarrow \pi + \text{dilepton}$.

We turn to the second term which multiplies $1/M^6$ in (30). It also stems from a non-scalar twist-2 condensate. In contrast to the a_2 term discussed above the contribution of the a_4 term is numerically small. We note in passing that we have not displayed non-scalar twist-4 contributions. They have been estimated to be small.^{67,68}

In (30) we have neglected all condensates which come with $1/M^8$ or higher inverse powers of the Borel mass. The sum rule is formulated for large space-like momenta which translates to large Borel masses. Therefore, it should be justified to neglect terms which are accompanied by higher powers in $1/M$. Nonetheless, the use of QCD sum rules in particular at finite nuclear densities is still a matter of debate.^{69,70,71}

2.3.4. Consequences for the spectral distribution

To summarize, the numerically most important contributions to the OPE side of (30) come from the gluon condensate, the four-quark condensates, and the (purely density dependent) a_2 term. Concerning especially the density dependence, the four-quark condensates and the a_2 term have the dominant influence. This is shown in Fig. 2. The a_2 term stems from a chirally symmetric operator, i.e. does not have a direct relation to chiral restoration. In contrast, the numerically dominant part of the four-quark condensate breaks chiral symmetry. The largest uncertainties come from the four-quark condensates, both concerning their vacuum values and their in-medium modifications. However, since also the a_2 term plays an important role for the in-medium changes, it would be misleading to conclude that the uncertainties in the four-quark condensates are so large that the sum rules are meaningless. Clearly, Fig. 2 contradicts such a pessimistic point of view. One sees that independently of the detailed values for the in-medium change of the four-quark condensates, the OPE side changes significantly at finite density. Therefore, the hadronic side of the sum rule (30) also has to change to account for the changes on the OPE side. Presumably, part of these changes is intimately connected to chiral restoration, while another part is not, corresponding to one four-quark condensate and to the a_2 term, respectively.

We have obtained a firm, yet qualitative result from the QCD sum rule approach: The low-energy spectrum has to change in a medium. It is, however, not so clear which change is demanded by the sum rule. At this stage specific qualitative assumptions about the in-medium shape of the spectral distribution have to enter. If one assumes that the ρ meson remains a quasi-particle, i.e. that its width can be ignored for the sum rule analysis, then the changing OPE side demands for a dropping ρ -meson mass.³ However, this is not the most general in-medium scenario one can think of for a spectral distribution. Indeed, one can explore the more general case where one allows for an in-medium ρ meson which appears as a peak with *a priori* arbitrary mass and arbitrary width in the low-energy spectral distribution of the corresponding current-current correlation function. With such an input, it turns out that the sum rule is not predictive enough to fix mass and width of the in-medium ρ meson.⁶⁰ Instead, a correlation between in-medium mass and width is obtained. Of course, the details of this correlation depend to some extent on the assumptions for the vacuum and in-medium four-quark condensates. An example is shown in Fig. 3. Qualitatively the mass can drop or the width can grow or both. More generally, the in-medium sum rule demands for the appearance of additional strength at lower invariant masses. One possibility to achieve that is a dropping mass. But also a broader distribution even without a mass drop is compatible with this requirement. The point here is that the spectral distribution does not enter the sum rule with equal weight for all invariant masses. Instead, the exponential suppression of the high-energy part in the spectral integral of the sum rule (30) puts a larger weight on the low-energy part of a broad distribution. Finally we note that

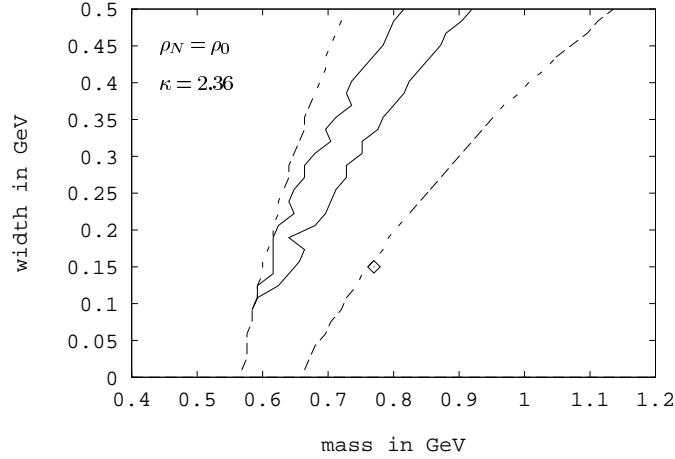


Fig. 3. Correlation between mass and width of a ρ meson placed at rest in cold nuclear matter ($T = 0$, $\rho_N = \rho_0$) as obtained from a QCD sum rule analysis. All mass-width pairs inside the corridor given by the full lines are allowed. It is assumed that the low-energy spectral distribution essentially consists of a single peak with *a priori* arbitrary mass and width. For orientation the vacuum values for the ρ -meson mass and width are given by the diamond. Figure taken from Ref. 60. See this reference for further details.

also other assumptions besides mass and width changes, like the appearance of additional peaks, are explored in the literature.^{72,73} In that respect, the corresponding case of the ω is also very interesting: Also here the OPE side demands for a shift of strength to lower invariant masses. However, there is already a large strength (at space-like momenta) caused by nucleon–nucleon-hole modes (also called Landau damping contribution in the literature).^{3,74} At low densities this contribution to the current-current correlation function can be calculated model independently. It might already overcompensate the demand from the OPE side.^{75,76,77,74}

So far, we have put most of our attention to the ρ meson. One reason was that the sum rule method is better explained with a typical example at hand. In addition, the ρ meson is an interesting probe concerning in-medium modifications. We briefly comment on other hadrons: For hadrons made out of light quarks one typically finds that the OPE side changes sizeably in a medium. Hence, qualitatively there must be a significant change of hadronic properties. Quantitatively, the OPE has to be worked out for each hadron separately. In addition, as already pointed out, the analysis depends on the specific assumptions for the qualitative shape of the spectral distribution. In any case, the sum rule method can be used as a consistency check for a given hadronic model — provided the hadronic model yields a current-current and not only a hadronic correlation function.

Concerning chiral symmetry breaking and restoration we have seen for the ρ meson that part of the numerically important in-medium changes of the OPE side

comes from chirally invariant terms, while another part stems from symmetry breaking terms. Such a finding depends, at least quantitatively, on the considered hadron. For example, for the ω meson the whole four-quark condensate structure is chirally symmetric. This is easy to understand since the ω meson is a chiral singlet.^k Consequently, all condensates appearing in the OPE are either chirally symmetric or break the symmetry explicitly, i.e. contain a quark mass. The latter terms are then numerically small. Hence, from the sum rules one cannot deduce an intimate relation between chiral restoration and in-medium changes of the ω meson. This does not imply that such a relation does not exist. The phenomenon of chiral restoration might also lead to in-medium changes of chirally symmetric condensates. To pin down such more complicated interrelations requires a much better microscopic understanding of non-perturbative QCD.

There are other hadrons where a connection to chiral symmetry breaking is more direct. For example, for the nucleon, but also, e.g., for open-charm D mesons,⁷⁸ the two-quark condensate appears more directly, i.e. is not multiplied by a light-quark mass (which made the contribution rather small for the ρ -meson case). It should be stressed, however, that also here there are other numerically important contributions emerging from chirally symmetric operators.^{79,80} We repeat our firm, but qualitative statement: Since the OPE side sizeably changes in a medium — in part caused by chiral symmetry breaking operators^l — there must be significant changes of the hadronic properties of the considered probe when it is embedded in the medium. To pin down these changes for various probes/hadrons is an important task of in-medium hadron physics. Since part of the in-medium changes of the OPE side are caused by chirally invariant operators, an observed change of hadronic properties does not necessarily imply that a footprint of chiral restoration has been detected.

3. Hadronic Models

In the preceding section we have discussed the “duality” between quark-based models and classical hadronic models. In particular, we have stressed that QCD sum rules, that work in a quark-gluon world, give valuable constraints on hadronic spectral functions, but cannot predict their detailed shape.^{60,68} It is thus necessary to model these spectral functions, based on our present understanding of meson-baryon interactions.

The theoretical challenge is then to calculate the self-energy Π of a meson embedded in a strongly interacting medium. Early calculations for the in-medium self-energy of the ρ meson^{81,82,83,84} started by dressing the decay pions within the framework of the Δ -hole model¹¹. This would obviously change the in-medium width, i.e. the imaginary part of the self-energy. The change of the real part could

^kThis statement concerns the chiral symmetry for two flavors discussed here. Concerning three flavors the ω is not a chiral singlet.

^lExcept for chiral singlets like the ω .

then be obtained from dispersion relations. Later it was realized that the direct ρN coupling could also contribute to the imaginary part of the self-energy and that this contribution was more important than the change of the decay width. Subsequent calculations of the vector-meson–nucleon scattering amplitude combined a chiral model with vector-meson dominance;^{75,85,86} these calculations suffer from the neglect of any nucleon excitations beyond the $\Delta(1232)$ and the use of the heavy-baryon approximation. The latter was later shown to be grossly unreliable.⁸⁷ In addition, there were no experimental constraints on the essential coupling constants contained in the effective Lagrangian. Resonance excitations were first considered in Ref. 40 and then worked out in detail in Refs. 41, 88, 43, 89, 90. These latter papers generated major effects from coupling the vector meson to nucleon–resonance–nucleon-hole loops. For the latter one can draw on a long experience with calculations of the in-medium pion self-energy that are based on the so-called Δ -hole model in which the free pion propagator in the nuclear medium is dressed with Δ -resonance–nucleon-hole excitations.¹¹ In this case the determining quantities are, first, the coupling constant for the $\pi N \Delta$ vertex and, second, the strength of the short-range correlations; the latter are crucial for obtaining the correct self-energies. The same type of model can be used for the vector mesons.

The starting point for these studies is the so-called $t\rho$ approximation in which the self-energy Π of a meson in a medium is determined by the interaction of the hadron with all the surrounding particles. While at temperature $T = 0$ these are only baryons, at higher temperatures mesons, mainly pions, and also antibaryons will fill the space around the hadron in question. The interaction of the hadron with all these particles, baryons and mesons, determines its self-energy.

For the sake of simplicity in the following we write down the relevant expressions only for cold nuclear matter; the self-energy as a function of the energy of the hadron, ω , and its momentum \mathbf{q} is then given by⁴³

$$\Pi_{\text{med}}(\omega, \mathbf{q}) = \int_{\text{F}} \frac{d^3 p_N}{(2\pi)^3 2E_N} t_{\text{tot}}(q, p_N) . \quad (33)$$

Here $t_{\text{tot}}(q, p_N)$ is the meson-nucleon forward scattering amplitude dependent on the hadron's four-momentum q and the nucleon momentum p_N and the integration extends over the Fermi sea of occupied nucleon states. At sufficiently low densities — and correspondingly low Fermi momenta — this expression for the self-energy can be simplified by pulling the scattering amplitude out of the integral if the scattering amplitude varies only smoothly with momentum. This gives

$$\Pi_{\text{med}}(\omega, \mathbf{q}) = \frac{1}{8m_N} \rho t_{\text{tot}}(q, p_N) . \quad (34)$$

where ρ is the baryon density and the nucleon's momentum is simply given by $p_N = (m_N, \mathbf{0})$. A priori it is not clear up to which densities this so-called *low-density* approximation is valid; this depends primarily on the strength of the nucleon-meson coupling. Eq. (34) allows for an easy interpretation: the self-energy is equal to the

meson-nucleon forward scattering amplitude, multiplied with the probability to find a nucleon for an interaction.

For vector mesons there are two distinct polarization directions; the transverse and longitudinal self-energies can be obtained from the self-energy Π by projecting on to the transverse and longitudinal degrees of freedom.⁴³ For simplicity we have not written any spin or isospin factor in (33).

The expressions just given describe the self-energies of vector mesons in the nuclear medium. If these vector mesons couple also to nucleon resonances then the properties of the latter are obviously also changed. This is so because 1. the nucleon resonance can itself collide with a nucleon and 2. the decay legs (in this case vector-meson–nucleon) get modified. The problem to determine the self-energy of the vector meson in a medium is thus intimately coupled to the problem of calculating the self-energy of the nucleon resonances and their decay products in the medium.⁴³

Diagrammatically, the resonance-hole excitation contribution to the meson self-energy can be represented as shown in Fig. 4. This figure contains an important

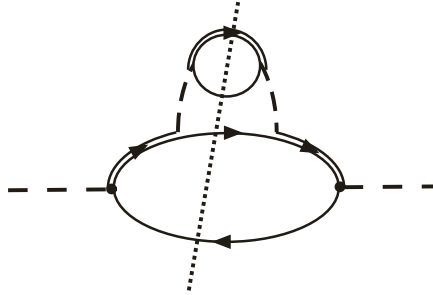


Fig. 4. In-medium self-energy of a meson. The single lines represent nucleon propagators, the double lines nucleon resonance excitations. The internal dashed lines denote the propagators of either the vector meson or other mesons, such as the pion. The straight, dotted line shows the cut leading to the imaginary part of the meson's self-energy.

feature: the upper half shows that the resonance propagator itself is dressed due to interactions with the medium. Thus, the determination of the meson self-energy and the resonance self-energy are coupled. In addition, the internal meson lines in Fig. 4 can either represent a meson of the same type as the incoming meson or other mesons as well that couple to the resonance. For example, for the ρ meson the resonance propagator could be that of the $N(1520) D_{13}$ excitation and the internal dashed lines could be propagators either of the ρ or the π meson.

The dotted line in Fig. 4 illustrates the cut of the diagram that defines the

imaginary part of the self-energy. The latter is given by

$$\Im \Pi(\omega, \mathbf{q}) = I_{\Pi} \left(\frac{f}{m_V} \right)^2 \int \frac{d^3 p}{(2\pi)^3} \frac{\Theta(p_F - |\mathbf{p}|)}{2E_N(\mathbf{p})} \Im \frac{\Omega}{k_0^2 - E_R^2(\mathbf{k}) - \Sigma_{\text{med}}(k)} . \quad (35)$$

Here I_{Π} is an isospin factor. The four-momentum of the resonance is denoted by $k = p + q$, where p is the four-momentum of a nucleon and q that of the meson. The factor $1/(2E_N)$ comes from the hole part of the relativistic nucleon propagator. The numerator Ω contains the vertex factors as well as the traces over the internal polarization degrees of freedom. Details can be found in Ref. 43.

The real part of the meson self-energy is then obtained by using a dispersion relation which guarantees that the spectral function of the meson remains normalized

$$\Re \Pi(q_0, \mathbf{q}) = \mathcal{P} \int_0^{\infty} \frac{d\omega^2}{\pi} \frac{\Im \Pi(\omega, \mathbf{q})}{\omega^2 - q_0^2} . \quad (36)$$

The effects of the self-energies are usually discussed in terms of *spectral functions* which are defined as the imaginary part of the retarded propagator (cf. Eq. (25))

$$\mathcal{A}(q_0, \mathbf{q}) = -\frac{1}{\pi} \frac{\Im \Pi(q_0, \mathbf{q})}{(q^2 - m_V^2 - \Re \Pi(q_0, \mathbf{q}))^2 + (\Im \Pi(q_0, \mathbf{q}))^2} \quad (37)$$

with the self-energy denoted by

$$\Pi(q_0, \mathbf{q}) = \Pi_{\text{vac}}(q^2) + \Pi_{\text{med}}(q_0, \mathbf{q}) . \quad (38)$$

While the spectral function in vacuum depends only on the invariant mass q^2 of the hadron, in a medium it does depend separately on its energy and three-momentum.

In the low-density approximation the imaginary part of the forward scattering amplitude t_{tot} in (34) can be related to the total cross sections by means of the optical theorem and the self-energy becomes

$$\Im \Pi_{\text{med}}(q_0, \mathbf{q}) = -\rho \sigma_{VN} |\mathbf{q}| = -q_0 \Gamma , \quad (39)$$

and thus the width Γ assumes the classical value for a collisional width⁶

$$\Gamma = \rho \sigma_{VN} v , \quad (40)$$

where v is the relative velocity of nucleon and meson and σ_{VN} is the meson-nucleon cross section. Thus in this low-density case the in-medium cross section is directly related to the imaginary part of the in-medium self-energy.

One of the determining factors in all these calculations is the strength of the resonance-nucleon-meson vertex. In principle, this quantity can be derived from nucleon resonance studies such as $\gamma N \rightarrow N\rho$. Several nucleon resonances, such as the N(1520) D_{13} , the N(1650) S_{11} and the N(1700) D_{13} are known²¹ to have sizeable decay branches into ρN which can be used to extract the relevant coupling constants.

The situation is more difficult for the ω and the ϕ mesons; the listings of the Particle Data Group (PDG)²¹ do not contain any nucleon resonances that decay

into nucleon plus these vector mesons so that the coupling constant cannot be easily obtained. We will discuss this further in Sects. 3.2 and 3.3.

Besides the resonance-hole excitations there are other contributions to the in-medium self-energy. An obvious candidate are nucleon-hole excitations which are driven by the nucleon-meson cross section going to channels that do not (dominantly) involve resonance excitations. In addition, the dressing of any decay products of the vectors mesons affects directly their width and thus also — through dispersion relations — the mass. However, even if the in-medium width Γ is large this alone does not necessarily imply also a large shift of the pole mass; the latter is sensitive only to the mass dependence of the width and not to its absolute size as such.

Another, less certain contribution may also come from in-medium higher-order interactions, i.e. from interactions of the meson with two (and more) nucleons. In this case the low-density approximation ((34), (40)) no longer holds and, in particular, the meson-nucleon cross section cannot be obtained from the self-energy. Taking this argument around it is also clear that — in the presence of sizeable many-particle interactions — a small meson-nucleon cross section cannot be used to argue that the meson-nucleus interaction is small as well. There is no general rule up to which density the low-density approximation is valid. Post et al. have shown⁴³ that e.g. for the eta meson the scaling of the self-energy with density is quite good, but it fails already at rather low density for the ρ meson.

3.1. ρ meson

3.1.1. ρ meson in cold matter

Fig. 5 gives the results of a calculation⁴³ in the resonance–nucleon-hole model for the ρ meson. Both the transverse and the longitudinal spectral functions are given there for various values of the three-momentum \mathbf{q} . It is seen that the spectral function can have a quite complicated structure that cannot be parametrized in terms of a Breit-Wigner shape. Instead, the spectral function for a ρ meson at rest in nuclear matter exhibits a distinct lower peak, at a mass of about 500 MeV whereas the main, dominant peak appears at about 800 MeV. This complicated structure is a direct consequence of the coupling of the ρ meson to resonance-hole excitations with the same quantum numbers leading to level-repulsion. In this particular case, the lower-mass peak is generated by the coupling to the N(1520) D_{13} resonance, so that the resonance-hole excitation has quantum numbers $J^\pi = 1^-$, i.e. the same as the ρ meson at rest. This structure moves to lower q^2 and becomes weaker with increasing three-momentum of the ρ meson. This is due to the special coupling of the meson to nucleon resonances. The latter also explains that at high momenta the transverse ρ is considerably broadened compared to the spectral function of a free ρ meson while the longitudinal ρ resembles at high momenta the free meson, with hardly any broadening; for a detailed discussion and explanation of these effects see Ref. 43. The result obtained by Cabrera et al.⁹¹ is qualitatively very similar to the

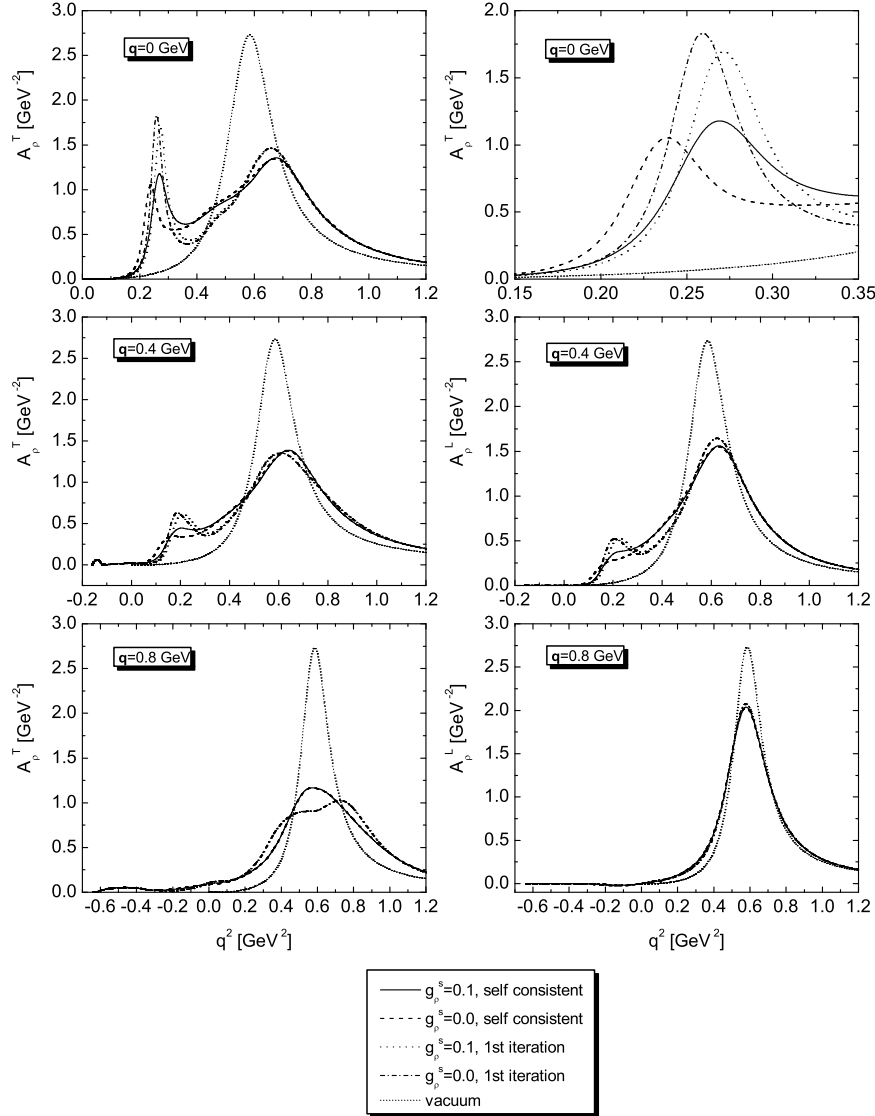


Fig. 5. Spectral function of the ρ meson at normal nuclear matter density. Shown are the transverse and the longitudinal spectral functions, A_ρ^T and A_ρ^L , which are degenerate at $\mathbf{q} = 0$. Also shown are the effects of iterating the spectral functions and of varying the short-range correlation parameter g_ρ^s . The uppermost picture on the right shows a zoom on the low-mass peak in the spectral function. The inset explains the various curves, obtained for different values of the short-range correlation strength g_ρ^s as well as in the low-density approximation (“1st iteration”) and in the full calculation (“self consistent”) (from Ref. 43).

ρ spectral function shown here; in particular, it also exhibits the lower peak due to the resonance coupling (see also Lutz et al.⁴²). The results of the calculations in Refs. 40,41 are similar, but they did not contain the essential $D_{13}N(1520)$ nucleon resonance.

The lower peak in the ρ spectral function leads to a downward shift of the first moment of the spectral function, but it is also evident from this figure that this downward shift appears only at low meson momenta. It should also be recalled that while the QCD sum rules require additional strength of the ρ meson's spectral functions at lower masses (see Fig. 3) there is nothing in them that forces a downward shift of peak masses or first moments. This then limits any attempts³⁶ to justify the Brown-Rho scaling².

The actual strength of this low-mass peak depends sensitively on the $NN^*\rho$ coupling strength. The PDG value of a partial decay width of the $N(1520)$ resonance into ρN of 15-25% is remarkably strong considering that the decay can proceed only through the tails of the ρ spectral function since for the peak mass of the ρ the resonance lies about 200 MeV below threshold. This large decay width then translates directly into a very large coupling constant. It is, therefore, important to realize that the ρN decay channel of this resonance has never been directly observed, but has been indirectly inferred from an analysis of πN scattering.⁹² While the DAPHNE experiment⁹³ and the TAPS experiment⁹⁴, both at MAMI, seem to indicate a ρ decay branch of the $N(1520)$ resonance there is so far no reliable quantitative determination of this coupling strength available. For a detailed understanding of the in-medium ρ spectral function a precise determination of the $N(1520) \rightarrow N\rho$ decay width is necessary and of high importance.

As discussed above any in-medium change of the vector-meson's spectral function will also lead to a change of the resonance spectral function. For the ρ meson which couples "subthreshold" to the $N(1520)$ this is particularly evident: any shift of strength down to lower masses will increase the phase space for this decay and thus broaden the resonance. The result of a coupled-channel calculation⁴³ is shown in Fig. 6. The figure illustrates nicely the effect just discussed. At the peak mass the decay width into $N\rho$ increases dramatically compared to the free case (dotted curve). This increase in the partial decay width translates into an increase of the full width of the resonance. While this increase of the resonance width cannot be directly seen in exclusive particle-production experiments (see Ref. 95 and Sect. 4.4 below) it may play a major role in the experimentally observed disappearance of resonances in the second and third resonance region in the total photoabsorption cross sections.⁹⁶

In summary, the ρ meson becomes significantly broader in a medium, at low momenta (≤ 1 GeV) picking up mainly strength at lower masses due to the coupling to the nucleon resonances. The first moment of the mass distribution is thus shifted downward at low ρ momenta, but for momenta larger than about 1 GeV only a nearly symmetric broadening survives with little shift of the pole mass; this is in line with early predictions in Ref. 4.

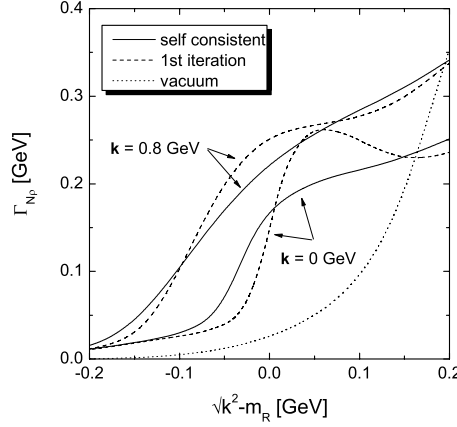


Fig. 6. Decay width of the $N(1520) D_{13}$ resonance to the $N\rho$ channel as a function of the invariant mass of the resonance. The thin dotted curve gives the width for the free resonance. The dashed lines show a first-order result without selfconsistency for the two momenta indicated, the solid curves give the results of a selfconsistent calculation (from Ref. 43).

3.1.2. ρ meson at finite temperatures

In heavy-ion reactions higher densities than in cold nuclei can be reached. However, such a compression is always connected with an increase of temperature; at very high, ultrarelativistic, energies a very hot fireball with nearly zero net baryon density is created. At this point a transition from hot hadronic matter to the quark-gluon plasma is expected, in which chiral symmetry is restored. It is, therefore, of considerable interest to also study the temperature dependence of the ρ meson's spectral function.

In a hot hadronic environment ρ mesons pick up in-medium changes of their spectral functions from three different interactions: first, the external decay legs, the pions, get modified in a hot hadronic environment, second there is a contribution from direct ρ scattering off thermal pions and third, there is ρN scattering, where the nucleons are thermally distributed in momentum space. Such a model has been worked out by Rapp and Wambach.^{97,9} Fig. 7, taken from their work, shows that the spectral function becomes very broad when the density and temperature approach the expected transition into the quark-gluon plasma phase. Overall the T -dependence broadens the spectral function; raising the temperature thus has an effect similar to that seen when raising the ρ -meson momentum in cold matter (cf. Fig. 5).

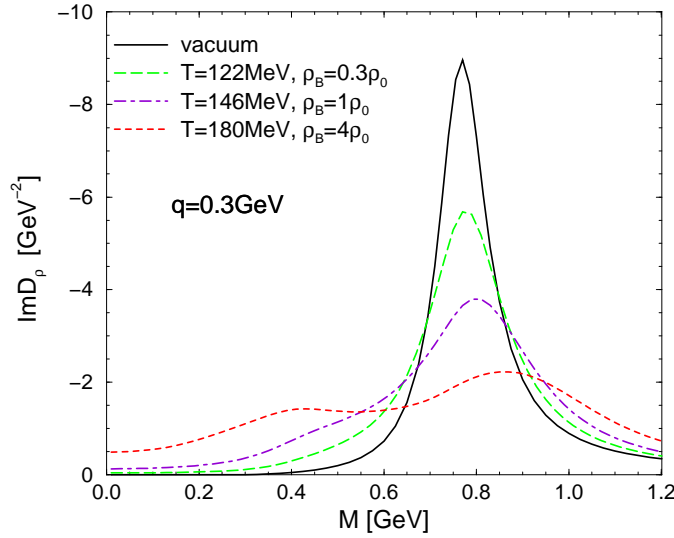


Fig. 7. Polarization-averaged ρ -meson spectral function at fixed three-momentum $q = 0.3$ GeV in hot and dense hadronic matter at the temperatures and densities indicated in the figure (from Ref. 9).

3.2. ω meson

For the ω meson the theoretical situation is more complicated than for the ρ . This is due to the fact that the elementary ω production cross section close to threshold is still a problem of ongoing research and that, correspondingly, there is much less known about the coupling of ω mesons to nucleons. Indeed, the PDG does not list any nucleon resonance with an $N\omega$ decay branch. Thus a simple application of a resonance-hole model is not possible in this case.

The uncertainties in extracting the resonance contributions from measured cross sections can be illustrated for the ω meson where recent $\gamma + N \rightarrow N + \omega$ data have been analyzed in the framework of a coupled channel K -matrix calculation, see Fig. 8. The figure shows that various resonances, plus t - and u -channel background terms, all contribute coherently to the observed production cross section. There is thus no obvious resonance that sticks out through its strength.⁹⁸ The largest contributions at threshold come from the D_{13} and the S_{11} partial waves.

At present, calculations of the ω in-medium self-energy therefore still have to start from theoretical analyses of $\pi N \rightarrow \omega N$ and $\gamma N \rightarrow \omega N$ cross sections. In particular the latter have much smaller experimental errors.^{99,100} In the model of Refs. 42, 101, 102, fitted to photo- and pion-production experiments invoking

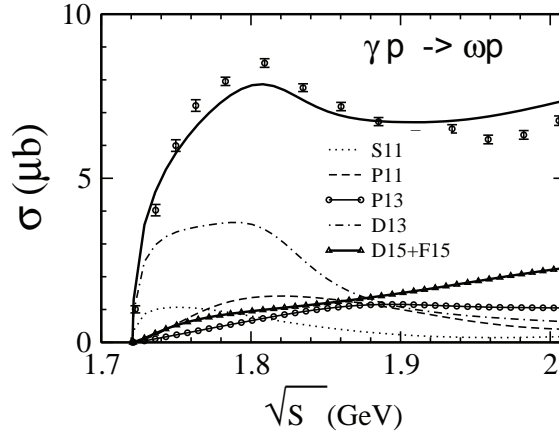


Fig. 8. Total and partial wave contributions to the $\gamma + p \rightarrow p + \omega$ cross section (from Ref. 98).

vector-meson dominance from the start, resonances are generated dynamically. A rather strong coupling of the N(1520) D_{13} and the N(1535) S_{11} to the ωN channel is found. Thus, here the situation is similar to that for the ρ meson, and indeed a second peak appears in the in-medium spectral function at lower masses. This calculation was restricted to the ω meson at rest in the nuclear medium, while actual experiments lead to rather large momenta of the ω meson produced. The authors of Ref. 45 have overcome this restriction by using a unitary K -matrix approach to the analysis of πN and γN data using the same Lagrangian and the same parameters for both types of reactions.^{103,104} The K -matrix method is a unitary coupled-channel approach and gives cross sections for the reaction under study. Resonance parameters and coupling constants are obtained by a fit to measured cross sections. Thus all the couplings are constrained by data.

The results of these studies show — as for the ρ meson — again a strong influence of couplings to nucleon resonances; t -channel graphs alone give a much too small contribution to the cross section at backward angles.¹⁰⁵ Contrary to the ρ meson case, however, there is much more interference between resonance and t -channel amplitudes and contributions from several overlapping nucleon resonances. Fig. 9 shows the result for the ω spectral function, both in vacuum and at densities of ρ_0 and $2\rho_0$. The in-medium spectral function of the ω meson is again double-humped, but the lower-mass hump is much less developed than for the ρ meson, reflecting the lower coupling strength to the resonances around 1500 MeV; qualitatively the result is similar to that obtained by the authors of Refs. 42, 101, 102 in a related study. The lower mass peak is due to the excitation of the N(1535) S_{11} and the N(1520) D_{13} resonances. These resonances couple in a relative s -wave to the $N\omega$ channel and dominate the spectrum at low ω momenta. The in-medium spectral

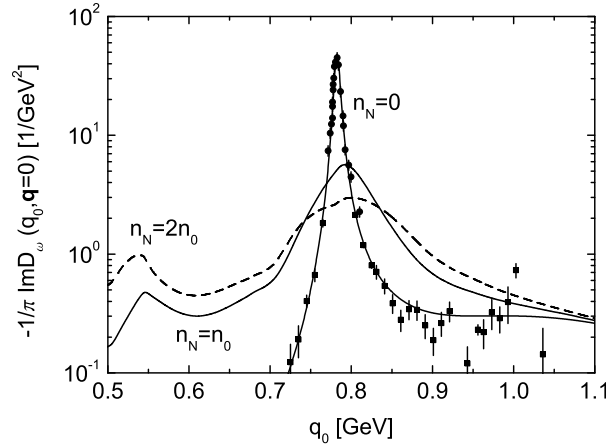


Fig. 9. The ω spectral function for an ω meson at rest. The solid curve through the data describes the spectral function of a free ω meson. The solid and dashed curves show the spectral function for density $\rho_0 = 0.16 \text{ fm}^{-3}$ and $2\rho_0$, respectively (from Ref. 45).

function shows only a very small upwards shift of the main peak, but the spectral function at the free mass is considerably broadened to roughly 60 MeV at saturation density ρ_0 and vanishing ω momentum. It has also been shown in sum rule analyses that a downward shift of the ω mass requires rather extreme assumptions about the in-medium changes of the four-quark condensate.^{106,74} The near constancy of the peak mass shown in Fig. 9 indicates that such a strong in-medium change of the four-quark condensate is not required to be in line with hadronic interactions.

With increasing ω momentum the width grows due to collisions with the nucleons of the surrounding medium. Again, it is the transverse degree of freedom that gets significantly collision-broadened, the longitudinal width stays nearly constant with ω momentum.⁴⁵ While these calculations are done only in the low-density approximation we expect that taking into account higher-order meson-baryon interactions will not change the picture qualitatively. Selfconsistency at higher densities tends to smoothen structures in the spectral functions; we thus expect even slightly larger broadening.

Among the more recent calculations there is now general agreement that the ω mass is only very weakly changed in a medium.^{45,42,101,102,44} Earlier calculations that gave a sizeable downward shift of the mass^{75,85,86} are either unreliable in the methods used⁸⁷ or neglect the essential dispersive corrections¹⁰⁷. As a consequence of the more recent hadronic calculations also the sign of the ωN scattering length is not expected to change much from its free value which comes out to be negative in these calculations. This indicates that contrary to other earlier calculations a bound ω -nucleus state does not exist. The newer calculations agree in their prediction of

a width of about 60 MeV at saturation density ρ_0 for an ω meson at rest. This width can directly be accessed through nuclear transparency measurements (see Sect. 5.4.2 below).

3.3. ϕ meson

For the ϕ meson the situation is different from that for the lighter vector mesons. Because of the pure strange quark composition $\bar{s}s$ of the ϕ there are no nucleon resonances that couple to ϕN in the s -channel. Also the ϕN cross section is theoretically expected to be quite small (7-13 mb). As a consequence the main change of the spectral function is due to the dressing of the kaons in the $K\bar{K}$ decay channel of the ϕ . This implies that the main in-medium change here is in the width since the vacuum width of the ϕ is very small; its mass shift should be negligible. Indeed, one of the latest calculations gives a mass shift of -6 MeV and a broadening of about 28 MeV at saturation density^{108,109} for a ϕ meson at rest. The calculation indeed gets its effects mainly from a dressing of the kaon loops in the ϕ self-energy.

In summary, the mass of the ϕ meson should hardly change in a medium. Instead the main effect is that of a collisional broadening. The latter affects directly the imaginary part of the self-energy and can thus be extracted from nuclear transparency measurements.

3.4. Scalar-meson (σ) production on nuclei

The restoration of chiral symmetry is connected with an equality of the spectral properties of the π and σ mesons which are chiral partners. Hatsuda et al. and Bernard et al. have pointed out that chiral symmetry restoration in hot and dense matter should then lead to a lowering of the σ spectral function.^{110,111,112} As a further consequence the — in vacuum dominant — 2π decay channel of the σ meson should become suppressed because of phase-space limitations. This in turn leads to an increase of the life time of the σ meson. This conjecture that a partial restoration of chiral symmetry in “normal” nuclear matter should cause a softening and narrowing of the σ meson has indeed been worked out by Hatsuda et al.¹¹³ and in Refs. 114, 115 and has triggered experiments to measure the 2π invariant mass distribution near threshold in pion and photon induced reactions on nuclei^{116,117,118}. Even though the particle character of the σ in vacuum is questionable, it might develop a much narrower peak at finite baryon density due to phase-space suppression for the $\sigma \rightarrow \pi\pi$ decay and, in particular, a shift of strength towards lower masses.

This suggestion has led to further theoretical studies of the in-medium 2π propagator. Models with chiral constraints and realistic pion interactions in nuclei indeed show effects on the π - π interaction and thus on the propagator with a resulting shift of the invariant mass distribution to lower masses.^{119,120,121} The main effect here is caused by the coupling of the pion to Δ -nucleon-hole excitations.

4. Hadronic Spectral Functions and Observables

In the preceding section we have discussed the theoretical approaches to calculate in-medium self-energies of vector and scalar mesons. We now discuss the problem how to relate these self-energies and in-medium spectral functions to actual observables.

4.1. Non-equilibrium effects

All the calculations of self-energies that we discussed in the preceding section start from the basic assumption of complete equilibrium: a hadron is embedded into nuclear matter at fixed, constant density ρ , without any surface effects, and temperature T . This yields the self-energy $\Pi(\rho, T)$ as a function of density and temperature and this self-energy is then — in a local-density approximation — used to describe the hadron also in finite nuclei at higher excitation. This procedure is not without problems in the case of heavy-ion reactions where the dynamics of the collision involves also non-equilibrium phases and where the properties of the equilibrium phase change with time. This question has so far hardly been tackled (see, however, Ref. 122). On the other hand, this may be a reasonable approximation to hadron production reactions on cold, static nuclear targets where the whole reactions proceed close to equilibrium.

4.2. Nuclear transparency

The imaginary part of the in-medium self-energy $\Im \Pi_{\text{med}}$ of a vector meson can be determined from nuclear transparency measurements where the total hadron yield produced in a reaction of an elementary projectile (γ, π, p) on a nuclear target is compared with that on a free nucleon. The nucleus then acts both as a target and as an attenuator. For the specific case of photoproduction, the total vector-meson production cross section on a nuclear target then reads in a simple Glauber approximation¹²³

$$\sigma_{\gamma A} = \int d\Omega \int d^3r \rho(\vec{r}) \frac{d\sigma_{\gamma N}}{d\Omega} \exp \left(\frac{1}{|\vec{q}|} \int_0^{\delta r} dl \Im \Pi_{\text{med}}(q, \rho(\vec{r}')) \right) P(\vec{r} + \delta \vec{r}) \quad (41)$$

with

$$\vec{r}' = \vec{r} + l \frac{\vec{r}}{r}, \quad \delta \vec{r} = v \frac{\gamma}{\Gamma_{\text{vac}}} \frac{\vec{q}}{|\vec{q}|}, \quad (42)$$

and the (local) nucleon density $\rho(\vec{r})$; here Γ_{vac} is the free decay width of the hadron in its restframe. Finally, $P(\vec{r})$ is the probability for the final-state hadrons to be absorbed. The imaginary part of the in-medium self-energy that determines the attenuation in (41) is connected to the collision width of the vector meson by

$$\Gamma_{\text{coll}} = -\frac{1}{\omega} \Im \Pi_{\text{med}} \approx \rho \sigma v, \quad (43)$$

where the last (classical) expression follows only in the low-density approximation. In all these equations \vec{q} is the three-momentum of the vector meson and ω its

energy. If one now assumes that the low-density limit holds, i.e. that the collisional width is determined by two-body collisions of the vector meson with a nucleon, then Γ is connected to the effective in-medium two-body cross section by (43). However, it is worthwhile to remember that already for the pion only one half of the absorption is due to two-body collisions whereas the other half involves three-body interactions.¹²⁴

Eq. (41) contains only absorption effects and no sidefeeding (regeneration) of the channel under study which in principle might affect the measured transparency ratios.¹²⁵ However, detailed comparisons with full transport calculations that contain such effects show that the Glauber approximation works very well for the cases studied here.^{123,105} Regeneration of meson channels through secondary interactions plays a role only for weakly absorbed mesons, such as e.g. the K^+ (Ref. 126) or low-energy pions (cf. also the remark on uncharged pions in Sect. 4.5 and the corresponding discussion on the results for 2π production in Sect. 5.8).

4.3. Influence of branching ratios

Experimental determinations of the full in-medium spectral function that involves imaginary *and* real parts of the self-energy always rely on a reconstruction of the spectral function from the measured four-momenta of two decay products (e.g., $\rho \rightarrow 2\pi$; $\omega \rightarrow \pi^0\gamma$; $\phi \rightarrow K^+K^-$; $\rho, \omega, \phi \rightarrow e^+e^-$). In a direct reaction of a microscopic probe, such as a photon, with a nucleon N at a center-of-mass energy \sqrt{s} the production cross section for a vector meson V with invariant mass μ is given by^{105,127}

$$\frac{d\sigma_{\gamma N \rightarrow V N}}{d\mu} = 2\mu \frac{1}{16\pi s |\mathbf{k}_{cm}|} |\mathcal{M}_{\gamma N \rightarrow V N}|^2 \mathcal{A}(\mu) |\mathbf{q}_{cm}| \quad (44)$$

Here \mathcal{M} is the transition matrix element, \mathbf{k} and \mathbf{q} are the momenta of the incoming photon and the outgoing vector meson, respectively, in the cm system and $\mathcal{A}(\mu)$ is the spectral function of the vector meson^m. Assuming a decay of the vector meson into two final particles p_1 and p_2 the cross section for the production of the final state, again with invariant mass μ , is given by:

$$\frac{d\sigma_{\gamma N \rightarrow N(p_1, p_2)}}{d\mu} = \frac{d\sigma_{\gamma N \rightarrow V N}}{d\mu} \times \frac{\Gamma_{V \rightarrow p_1 + p_2}(\mu)}{\Gamma_{\text{tot}}} \times P_1 P_2 . \quad (45)$$

Here Γ_{tot} is the total width of the meson V , obtained as a sum of the vacuum decay width, Γ_{vac} , and an in-medium contribution:

$$\Gamma_{\text{tot}} = \Gamma_{\text{vac}} + \Gamma_{\text{med}} . \quad (46)$$

The ratio $\Gamma_{V \rightarrow p_1 + p_2} / \Gamma_{\text{tot}}$ represents the branching ratio into the final state p_1, p_2 and P_i gives the probability that the particle p_i survives absorption or rescattering

^mIn the nuclear medium Lorentz invariance is not manifest and thus the spectral function depends both on μ and on the vector meson's three-momentum \mathbf{q} .

in the final state (we neglect here possible channel couplings). In the nuclear medium Γ_{tot} increases; it is essential that this increase is contained both in the spectral function \mathcal{A} and the branching ratio.

Eq. (45) shows that the invariant-mass distribution reconstructed from the four-vectors of the final particles always contains effects not only from the spectral function, but also from the branching ratio and from the final-state interactions (fsi) which also depend on μ . For the case of dilepton final states the latter two are known:¹⁰⁵ the decay width goes like $1/\mu^3$ and the branching ratio like $1/(\mu^3\Gamma_{\text{tot}})$; the dilepton fsi can be neglected. The strongly μ -dependent branching ratio shifts the observed mass distribution significantly to lower masses. For hadronic ($\pi\pi$, KK) or semi-hadronic ($\pi^0\gamma$) final states the mass dependence of the decay branching ratio is often not very well known and has to be modeled. While there are theoretical studies available¹⁰⁵ experimental determinations of hadronic spectral functions for the ω meson have so far not taken this into account. This is particularly critical if new particle thresholds open in the mass region of interest. This increases the total width and leads to a strong fall-off of the branching ratio with increasing mass. For example, the branching ratio for the decay $\omega \rightarrow \pi^0\gamma$ is strongly influenced by the opening of the $\rho\pi$ channel just in the ω mass region.¹⁰⁵ In this special case a further complication arises from the fact that the ρ meson gets broadened in a medium so that as a consequence the total decay width of the ω meson may change in the nuclear medium.

In summary, any extraction of the spectral function that relies on the determination of the invariant mass distribution $\mathcal{P}(\mu)$ from the four-momenta of the final particles

$$\mu = \sqrt{(p_1 + p_2)^2} \quad (47)$$

requires that the partial decay width is divided out

$$\mathcal{A}(\mu) = \mathcal{P}(\mu) \frac{\Gamma_{\text{tot}}}{\Gamma_{V \rightarrow p_1 + p_2}} . \quad (48)$$

This complication is independent of any final-state interactions that the decay products may experience.

4.4. *Observability of collisional broadening*

Even if theory predicts a significant broadening of hadronic spectral functions in the nuclear medium it is not clear if this broadening can be directly observed.^a First of all, the in-medium hadrons do not all experience one given density. Instead, because of the nuclear density profile, the relevant densities range from saturation (ρ_0) down to zero in the nuclear surface. Most nucleons are embedded in densities of about 1/2 to 2/3 of normal nuclear density ρ_0 . Thus it is immediately clear that hadrons

^aThe in-medium width which leads to this broadening can be obtained from transparency measurements as discussed in Sect. 4.2.

in nuclei will not exhibit properties corresponding to saturation density, but instead to a lower one. Even more important is, however, another not so straightforward effect that suppresses contributions from higher densities. We briefly outline this effect here; more details can be found in Refs. 95 and 105.

The semi-inclusive cross section for the production of final states, e.g., via a vector-meson resonance in a photon-nucleus reaction, is obtained by integrating Eq. (45) over all nucleons. The result involves a factor

$$\mathcal{A}(\mu) \frac{\Gamma_{V \rightarrow \text{final state}}}{\Gamma_{\text{tot}}} = \frac{\mu \Gamma_{\text{tot}}}{(\mu^2 - m_V^2)^2 + \mu^2 \Gamma_{\text{tot}}^2} \frac{\Gamma_{V \rightarrow \text{final state}}}{\Gamma_{\text{tot}}} \quad (49)$$

with

$$\Gamma_{\text{tot}} = \Gamma_{\text{vac}} + \Gamma_{\text{med}} . \quad (50)$$

The in-medium width Γ_{med} depends on density; in the low-density approximation it is linearly proportional to the density ρ (cf. Eq. (40)),

$$\Gamma_{\text{med}}(\rho(r)) = \Gamma_{\text{med}}(\rho_0) \frac{\rho(r)}{\rho_0} . \quad (51)$$

If $\Gamma_{\text{med}} \gg \Gamma_{\text{vac}}$, as it is the case at least for ω and ϕ mesons, the density dependence of the in-medium width drives the sensitivity of a meson-production experiment towards the surface. Contributions from higher densities are suppressed by order $1/\rho^2$; they are significantly broader and lower in their maximum. Inspecting Eq. (49) one sees that at the peak position, $\mu = m_V$, one suppression factor $1/\rho$ comes from the spectral function and one from the branching ratio. The effect can be seen in Fig. 10 where simply two Breit-Wigner spectral functions for the ω meson with widths differing by about a factor of 10 and equal integrated strengths have been superimposed. Since the significantly broader distribution is suppressed $\sim 1/(\Gamma_{\text{vac}} + \Gamma_{\text{med}})$ it changes the summed distribution only in the outer tails. In an experiment this change is difficult to separate from a background contribution. This comparison contains only the effects of the density dependence of the spectral function. The effects of the additional density dependence of the branching ratio will only enhance the observed behavior, contributing an additional suppression factor $1/\rho$. In the example shown only the width was increased, but it is clear that the same suppression will also take place if – in addition – there is a shift in the peak mass. The final-state interactions, not taken into account in this argument, will actually lead to an even further suppression of signals from higher densities, if the decay channel involves strongly interacting particles.

Fig. 11 shows the results of a full simulation for the reaction $\gamma + {}^{40}\text{Ca}$ at $E_\gamma = 1.5$ GeV. Plotted is the width of the $\pi^0\gamma$ spectrum as a function of a K factor that multiplies the in-medium width in Eq. (51) to account for a possible increase of the in-medium ωN cross section. While the total observed width stays nearly constant when K is increased by a factor of 3, the width of the in-medium decay events (solid line) indeed increases with K , but its relative contribution (dashed line) decreases at the same time.

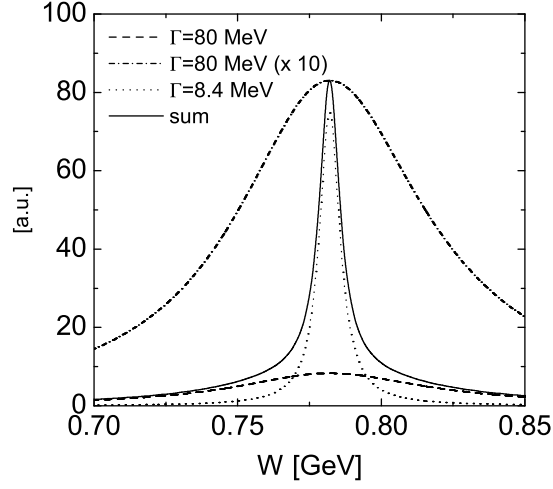


Fig. 10. Relativistic Breit-Wigner distributions with equal integrated strength. Their widths are 8.4 and 80 MeV, as given in the figure. The summed spectrum has a fitted Breit-Wigner width of about 12 MeV (from Ref. ¹⁰⁵).

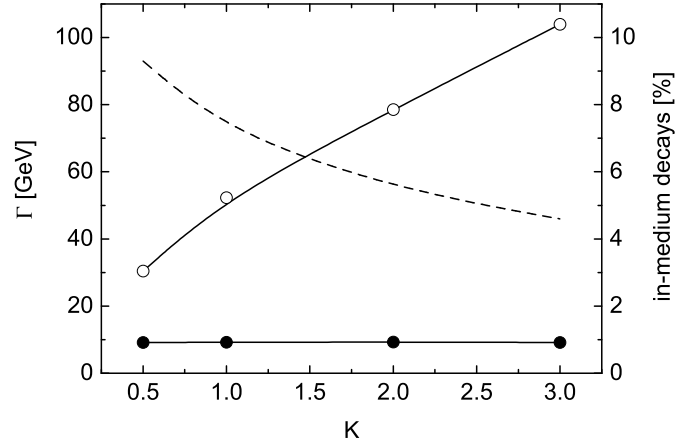


Fig. 11. Fitted Breit-Wigner (BW) width of the $\pi^0\gamma$ spectrum from transport simulations for the reaction $\gamma + {}^{40}\text{Ca} \rightarrow \omega + X$ at 1.5 GeV photon energy. The full symbols show the BW width of the full spectrum, the open symbols that from events with in-medium decays ($\rho > 0.1\rho_0$) only. The dashed line (right axis) shows the percentage of in-medium decays; here no cut on low momentum ω mesons has been applied (from Ref. ¹⁰⁵).

The suppression of higher-density contributions is less pronounced if total cross sections are considered instead of semi-inclusive or exclusive ones. In this case $\Gamma_{V \rightarrow \text{final state}}$ in (49) has to be replaced by the total width Γ_{tot} , effectively removing one power of $1/\rho$ so that there is less suppression for higher densities. If in addition the in-medium width is comparable to the vacuum width and not, e.g., an order of magnitude higher, then the broadening can be observable. Concerning baryon resonances, this explains why the total photoabsorption cross section on nuclei exhibits a clear broadening in the second-resonance region.⁹⁶ A similar situation prevails in heavy-ion collisions where Γ_{tot} in the denominator of the branching ratio is canceled by Γ_{in} , the width for producing the hadron in the entrance channel: While in an elementary nuclear reaction Γ_{in} is selected by the specific experiment, the thermal production of the considered hadron in a heavy-ion collision involves all possible production channels, i.e. $\Gamma_{\text{in}} \sim \Gamma_{\text{tot}}$.

4.5. Final-state interactions

In addition, the spectral functions observed in experiments by reconstructing them from hadronic decay products can be quite different from those of the original decaying meson. Final-state interactions can affect — through rescattering — the momenta and angles of the final-state hadrons, thus affecting also the spectral information reconstructed from the four-momenta of these hadrons. For example, the rescattering always leads to energy loss of the scattered outgoing hadron. This necessarily shifts the strength distribution towards smaller masses. In addition, hadrons can get absorbed or even reemitted (fsi); the former process will reduce the cross sections whereas the latter spoils any connection between the final observed momenta and the original spectral function.

While fsi do affect the actual observables in a significant way, if hadrons are among the decay products, their theoretical treatment is in most cases not up to the same degree of sophistication. Usually otherwise quite sophisticated in-medium calculations, which use state-of-the-art theoretical methods, do apply much more simplified methods to the treatment of fsi. Among the latter are the eikonal approximation or even a simple, absorption-only Glauber treatment. An obvious shortcoming of both of these methods is that it is ad hoc assumed that the particle that is initially hit in the very first interaction is the same as the one that ultimately leaves the nucleus on its way to the detector. However, detailed analyses have shown that there can be significant contributions from coupled-channel effects, in which a sidefeeding from an initially different channel into the final channel takes place. An example is charge transfer for pions where the more copiously produced charged pions can — due to fsi — be converted into uncharged ones. Such an effect plays a major role in particular in reactions with elementary probes in the incoming channel.

In addition, both the eikonal and the simple Glauber method take only flux out of a given channel; they do not yield any information on what happens with these

particles. This is a major shortcoming for inclusive and semi-inclusive reactions.

An up-to-date method to treat fsi that is free of these shortcomings is provided by transport calculations. These transport calculations do take all the coupled channel effects into account, they allow for elastic and inelastic interactions and for sidefeeding and absorption. They are limited to inclusive, incoherent processes, so that exclusive particle production, for example, in coherent interactions cannot be described. However, for inclusive and semi-inclusive (or even semi-exclusive) reactions they are applicable and yield the desired results. They also provide a full dynamical simulation of the reaction and thus help to understand the reaction mechanism. State-of-the-art methods all rely on the Boltzmann-Uehling-Uhlenbeck (BUU) equation.¹²⁸ A modern example of such an approach is provided by the GiBUU model.¹²⁹

5. Experimental Approaches and Results

The theoretically predicted medium modifications, discussed in the previous sections, can be studied experimentally by measuring the mass distribution of short-lived hadrons. The life times of these hadrons have to be so short that, after being produced in some nuclear reaction, they decay with sizeable probability within the nuclear environment, i.e. within the atomic nucleus or in the collision zone of a heavy-ion reaction. Information on the in-medium mass μ of a hadron can be deduced from the four-momentum vectors p_1, p_2 of its decay products for different three-momenta \vec{p} of the hadron with respect to the nuclear medium. In general, the mass depends on the baryon density ρ and temperature T of the medium:

$$\mu(\vec{p}, \rho, T) = \sqrt{(p_1 + p_2)^2}. \quad (52)$$

The light vector mesons ρ, ω , and ϕ are particularly suited for these investigations. Produced in a nuclear reaction at energies in the GeV regime, their decay lengths in the laboratory $\beta \cdot \gamma \cdot c \cdot \tau \approx 1.3$ fm, 23 fm and 46 fm, respectively, are of the order of magnitude of nuclear dimensions ($\beta \cdot \gamma$ is of the order of 1 for the reactions of interest). For experimental investigations of in-medium properties of the longer lived ω and ϕ mesons severe cuts on their momentum will nevertheless have to be applied to ensure a sizeable fraction of decays in the nuclear medium.

In principle, all decay modes of a meson can be used to reconstruct its in-medium mass according to Eq. (52). As discussed in Sect. 4.5 a problem, however, arises when hadrons are involved as final states since these hadrons may interact strongly with the surrounding nuclear medium. As a consequence, their four-momentum vectors may be distorted leading to an erroneous result for the invariant mass of the decaying meson. In special cases, which have to be investigated individually, these effects can, however, be reduced by specific cuts on kinematic variables like in the $\omega \rightarrow \pi^0 \gamma$ decay (see Sect. 5.4.2). Alternatively, these final-state effects can be modeled with good accuracy as outlined above.

Leptons are the preferred decay channel because they escape even a compressed collision zone of a heavy-ion reaction without strong final-state interactions. Vector

mesons have such a decay branch into lepton pairs (e^+e^- or $\mu^+\mu^-$). Unfortunately, the branching ratios are only of the order of 10^{-5} - 10^{-4} which make these measurements very difficult and sensitive to background subtraction.

Medium modifications of hadrons have been investigated experimentally in nuclear reactions with elementary probes as well as in heavy-ion collisions. Both approaches have their advantages and disadvantages. First observations of a change of the vector meson spectral function in dense matter were obtained in heavy-ion experiments. These experiments do reach high densities and temperatures but they suffer from an intrinsic limitation: every experimental signal is time-integrated over the whole collision history and thus also over very different states of strongly interacting matter. While the initial hard nucleon-nucleon (parton-parton) collisions in relativistic heavy-ion reactions are highly out of equilibrium, the system then develops to a thermalized quark-gluon plasma or hadronic phase with a temperature that decreases with time until freeze-out is reached. Any theoretical analysis of heavy-ion data with a focus on reconstructing the vector meson's spectral function thus also involves modeling the time-development of the reaction. Indeed, the latest analysis of dilepton data shows a significant dependence of the momentum spectra and of the overall yield on the model parameters describing the time development of the reaction.¹³⁰ Usually, the time development is not obtained from dynamical simulations, but instead is parametrized in terms of the times which the system spends in the various phases. This parametrization is then constrained by other observables, such as flow.

The advantage of heavy-ion collisions is that the regeneration of mesons in the collision zone helps to enhance the in-medium effects: The dilepton yield from meson decays in the hot and dense medium is determined by the partial decay width Γ_{l+l^-} and the life time of the fireball τ_F , i.e. $N_{l+l^-} \sim \Gamma_{l+l^-} \cdot \tau_F$, independent of the life time of the meson. In elementary reactions on nuclei the yield from meson decays within the nuclear medium is again given by the partial decay width Γ_{l+l^-} and — in contrast to heavy-ion collisions — proportional to the in-medium life time of the meson $\tau = 1/\Gamma_{\text{tot}}$, i.e. $N_{l+l^-} \sim \Gamma_{l+l^-} / \Gamma_{\text{tot}}$. Since the total width Γ_{tot} is increased in a medium — and as we will discuss below this increase may be large — the yield of the particles of interest can sizeably drop as compared to the vacuum case, as discussed in Sect. 4.4. Nevertheless, and even though the densities probed in the elementary nuclear reactions are lower, the medium effects may still be comparable to those in heavy-ion reactions.¹³¹ In addition, there is no time dependence of the density and temperature which makes the theoretical analysis of the results more transparent.¹³² Since the determination of in-medium hadron masses and life times requires rather demanding experiments corresponding results have only recently been published.

5.1. Experimental challenges

The detection and identification of electron or muon pairs in heavy-ion collisions but also in photon and proton induced reactions represents a severe experimental challenge. The main problem is the discrimination against $\pi^+\pi^-$ pairs which are produced in these reactions with about 4-5 orders of magnitude higher yields. All experimental setups working in this field use Cherenkov detectors for electron/pion discrimination. In addition, information from shower detectors or shower sizes in calorimeters is used. Pion-pair suppression factors of the order of 10^{-7} have been reported.¹³³ Furthermore, conversion of photons into electron pairs represents a

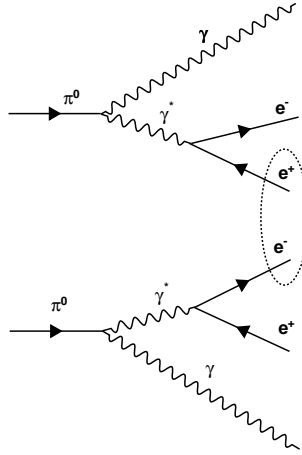


Fig. 12. Feynman diagram illustrating the generation of unlike-sign combinatorial background through the Dalitz decay of two π^0 mesons produced in the same event.¹³³

huge background. To suppress this contribution the detectors have to be built with minimum material budget. Thin multi-layer target slices rather than bulk targets have to be used to suppress conversion already in the target. These processes are characterized by small opening angles of the lepton pairs and can thus be reduced by cuts on the angle between the two leptons.

A central problem in lepton spectroscopy are electrons and positrons of low energy (≤ 50 MeV). They curl up in the magnetic field or may be deflected into an angular range not covered by the detector, leading to limited track reconstruction efficiencies, a reduced conversion-pair rejection, and acceptance problems.

There are additional dilepton (e^+e^- , $\mu^+\mu^-$) sources like Dalitz decays of hadrons, e.g., $\pi^0, \eta \rightarrow e^+e^-\gamma$; $\eta \rightarrow \mu^+\mu^-\gamma$, or decays of charged pions and kaons like $\pi^+, K^+ \rightarrow \mu^+\nu$; $\pi^-, K^- \rightarrow \mu^-\bar{\nu}$ which contribute to the dilepton invariant-mass spectrum. They also give rise to a combinatorial background when a positron (μ^+)

from one source is erroneously paired in the analysis with an electron (μ^-) from another source within the same event, as illustrated in Fig. 12 for combinatorial e^+e^- pairs.

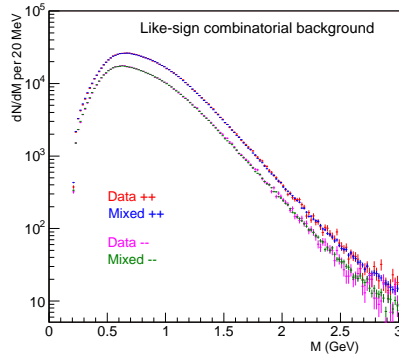


Fig. 13. Dilepton background generated by event mixing for In-In collisions at 158 AGeV in comparison to like-sign $\mu^+\mu^+$ and $\mu^-\mu^-$ invariant-mass spectra.^{134,135}

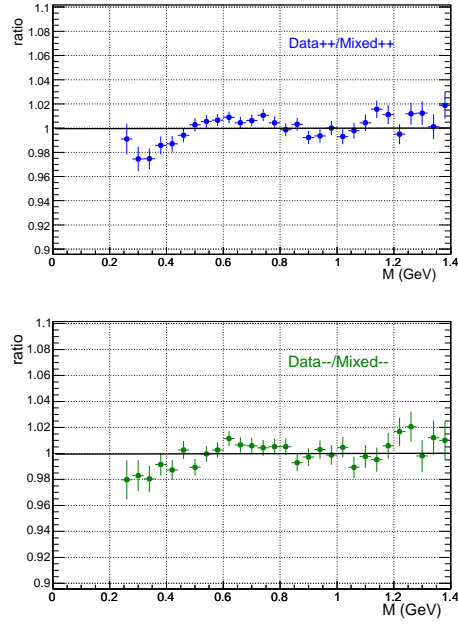


Fig. 14. Ratio of like-sign invariant-mass distribution over mixed-event distributions.¹³⁵

In a procedure followed by most collaborations this combinatorial background is determined by measuring like-sign dileptons. Assuming that the like-sign pairs are uncorrelated and have the same acceptance as unlike-sign pairs the combinatorial background B and the signal S are then given by

$$B = 2 \cdot \sqrt{N^{++} \cdot N^{--}} \quad , \quad S = N^{+-} - B \quad (53)$$

where N^{++} , N^{--} , and N^{+-} are the number of measured l^+l^+ , l^-l^- , and l^+l^- lepton pairs. This approach has the disadvantage that for most detector systems the acceptances for like-sign and unlike-sign pairs are not completely identical and that the background is only determined with about the same statistical significance as the signal. A high-statistics background can be obtained by the event-mixing technique: like-sign tracks from different events are paired whereby extreme care has to be applied in selecting events of similar topology. The method is checked by comparing the mixed-event background to the like-sign invariant-mass distribution. The procedure is illustrated in Fig. 13 with data from the NA60 collaboration who

studied dimuon production in ultra-relativistic heavy-ion collisions (see Sect. 5.3.1). Like-sign and mixed-event distributions agree over nearly 3 1/2 orders of magnitude on the level of less than 2% as shown by the ratios of the distributions in Fig. 14.

In general, the mixed-event distribution is used for background subtraction after normalization to the like-sign background. Mixed-event and like-sign pair subtraction techniques have been developed to a high degree of sophistication and have even been applied in cases with signal-to-background ratios in the percent range.¹³⁶

5.2. Pioneering Experiments

Pioneering experiments on dilepton emission in heavy-ion and elementary nuclear reactions started in the late 1980's at the Lawrence Berkeley Laboratory with the Dilepton Spectrometer (DLS)^{137,138,139} and at the CERN SPS with the CERES¹⁴⁰

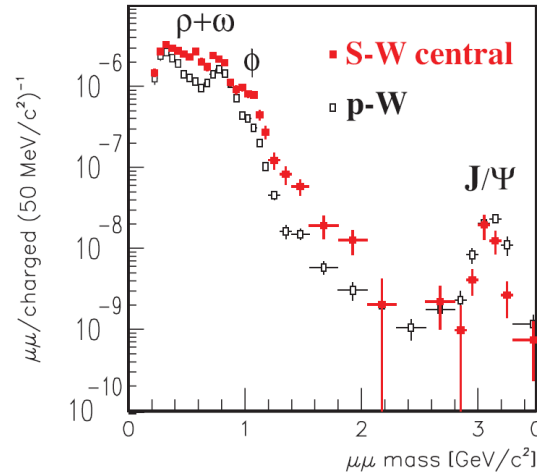


Fig. 15. $\mu^+\mu^-$ invariant-mass distribution for S+W (filled squares) and p+W (open squares) collisions at 200 GeV measured by the HELIOS-3 collaboration.¹⁴¹

and HELIOS¹⁴¹ detector systems in the energy ranges of $\sqrt{s_{NN}} = 2\text{--}3$ GeV and 17 GeV, respectively.

The DLS data showed an unexpectedly high dielectron yield in C+C and Ca+Ca collisions at 1 AGeV which was much larger than could be explained in transport calculations¹⁴² at that time. Also introducing medium effects as discussed in the previous sections did not remove this discrepancy which was then called the *DLS-puzzle*. Other calculations which also failed to reproduce the observed dielectron yields are summarized in Ref. 8. The DLS data will be discussed together with recent results obtained with the HADES detector at GSI in Sect. 5.6.2.

The HELIOS-3 collaboration¹⁴¹ reported an enhanced $\mu^+\mu^-$ yield throughout

the whole invariant-mass range up to $3.5 \text{ GeV}/c^2$ in central S+W collisions compared to proton-induced reactions on Tungsten at $200 \text{ GeV}/c^2$ (see Fig. 15).

The CERES collaboration¹⁴⁰ focused on the low-mass part of the dilepton spectrum below the ϕ mass, motivated by discussions of possible medium modifications of the ρ meson which were initiated by Pisarski¹. In particular the CERES results discussed below initiated widespread further experimental and theoretical activities. New dedicated experiments were designed, optimized for the detection of lepton pairs and theoretical tools were developed for studying in-medium modifications of hadrons.

In the following sections the wealth of data obtained in a series of experiments will be confronted with the current status of our theoretical understanding developed in the previous sections. The results on the ρ , ω , and ϕ meson and on 2π production will be presented in separate subsections.

5.3. In-medium properties of the ρ meson

5.3.1. Heavy-ion experiments

First information on medium modifications of vector mesons was derived from ultra-relativistic heavy-ion reactions with the CERES detector.

The setup of the CERES experiment is shown in Fig. 16. It was initially designed as a hadron blind detector consisting of two ring imaging Cherenkov detectors. With a high Cherenkov threshold of $\gamma_{thr} \approx 32$ it was only sensitive to dileptons. The centrality of the heavy-ion collisions was characterized by measuring the particle multiplicity in a Si drift detector near the target. Later on a cylindrical time-projection chamber was added to improve the invariant-mass resolution to $\frac{\delta m}{m} = 3.8\%$. Fig. 16 (bottom) shows the acceptance of CERES for dileptons relative to the full phase space.^{143,135}

Fig. 17 shows a comparison of e^+e^- invariant-mass spectra measured in p+Be at 450 GeV ¹⁴⁴ and Pb+Au collisions at 158 AGeV ¹⁴⁵, respectively, after subtracting the combinatorial background. For p+Be, the measured dilepton yield is reproduced by the sum of contributions from Dalitz and direct decays of neutral mesons with known production cross sections in p+p reactions. In contrast, the Pb+Au collisions reveal an enhancement relative to this cocktail in the mass range below the ϕ mass. Here, the cocktail is constructed from meson yields predicted in statistical model calculations (see Ref. 143). Similar di-electron excess yields had been observed in earlier CERES experiments on S+Au and Pb+Au collisions, published in Refs. 140, 144, 143. The enhancement was attributed to the annihilation of charged pions which are produced in the fireball of the heavy-ion collision with high multiplicity.

The annihilation proceeds via an intermediate ρ meson, $\pi^+\pi^- \rightarrow \rho \rightarrow e^+e^-$, and thereby provides access to the properties of the ρ meson at high densities and temperatures reached in heavy-ion collisions.⁸ As shown below (see Figs. 18, 23), however, not only pion annihilation but also formation and decays of baryon resonances like $\pi N \rightarrow N^*, \Delta, \Delta^* \rightarrow N\rho \rightarrow Ne^+e^-$ contribute to the observed

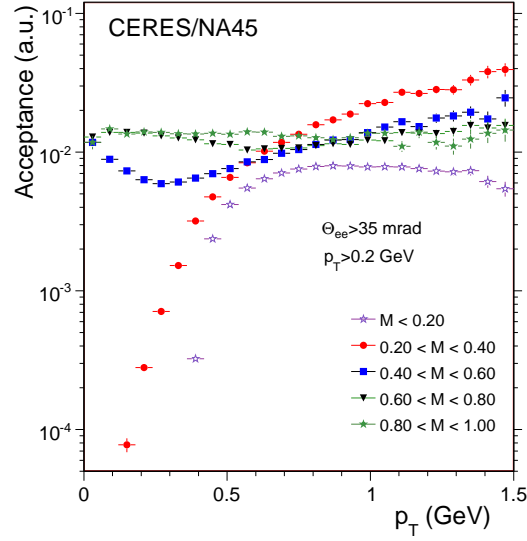
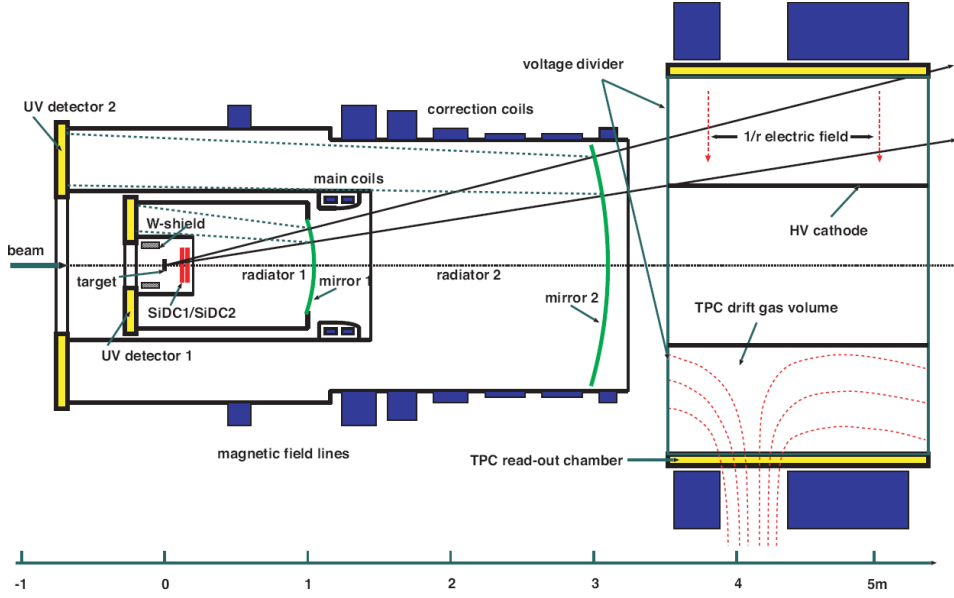
50 *S. Leupold, U. Mosel, V. Metag*

Fig. 16. Top: Schematic view of the CERES spectrometer, comprising two ring imaging Cherenkov detectors and a radial time projection chamber.¹⁴⁶ Bottom: CERES acceptance (upper limit) for dileptons relative to the full phase space as a function of transverse momentum for different invariant-mass bins.^{143,135}

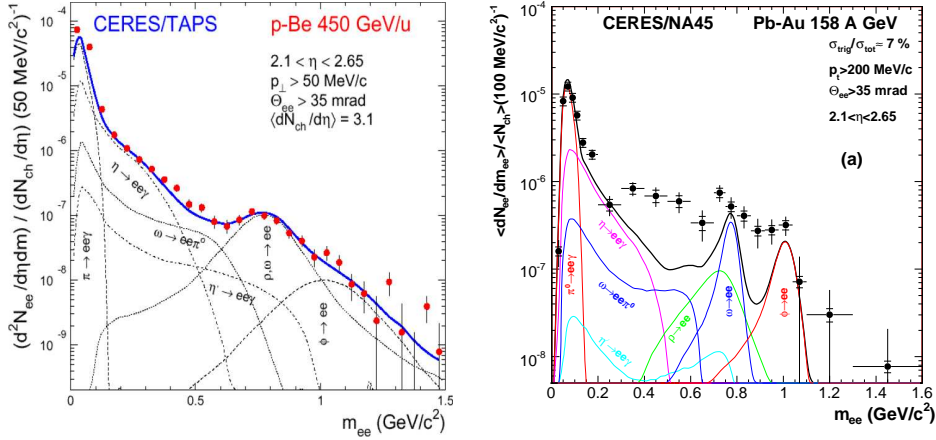


Fig. 17. Inclusive e^+e^- invariant-mass spectra for p+Be reactions at 450 GeV/c (left) and Pb+Au collisions at 158 AGeV (right) measured with the CERES detector. Contributions from different hadronic decays expected for p+p collisions are indicated. The sum of these contributions (*post-freeze-out cocktail*) reproduces the observed dilepton yield in p+Be reactions¹⁴⁴ but leaves an excess unaccounted for in the Pb+Au collisions¹⁴⁵. The figure on the right hand side represents the most recent CERES result making use of the additional radial time projection chamber as shown in Fig. 16.

dilepton invariant-mass spectra, in particular at low masses. For a more detailed study of the ρ meson, the post-freeze-out dilepton cocktail has been subtracted in Fig. 18 except for the ρ contribution. The data are compared to two theoretically proposed scenarios, a mass shift² or an in-medium broadening⁹ of the ρ meson, respectively. With the limited statistics it is difficult to clearly differentiate between the two cases. The authors of Ref. 145 conclude that the excess is smeared out over a wider mass range than expected for a dropping mass scenario and therefore favor the interpretation of the data in terms of an in-medium broadening of the ρ meson over a density dependent ρ mass shift. The relevance of high baryon densities for the observed medium modifications indicated in Fig. 18 (right) has also been noted in a measurement of Pb+Au collisions at a lower incident energy of 40 AGeV.¹⁴⁷

A breakthrough in statistics and resolution in dilepton spectroscopy of nucleus-nucleus collisions has been achieved by the NA60 collaboration¹⁴⁸ who studied the $\mu^+\mu^-$ decay channel in the In+In reaction at 158 AGeV. The experimental setup and the dilepton acceptance of the detector relative to the full phase space are shown in Fig. 19. A radiation-hard Si-pixel detector was installed between the target and the hadron absorber of the former NA50 dimuon spectrometer. By matching the tracks before and after the absorber in angle and momentum a mass resolution of 2.5% was achieved for vector mesons. As shown in Fig. 20, peaks from the ω and ϕ decays are cleanly resolved in the $\mu^+\mu^-$ invariant-mass spectrum after

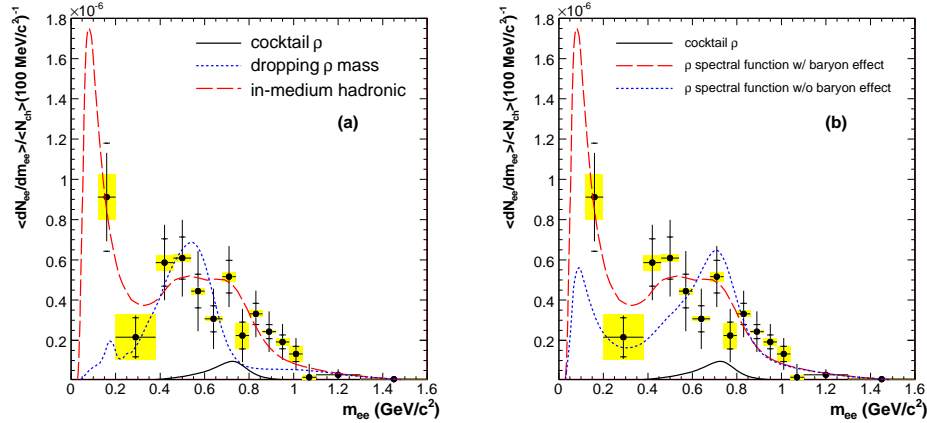


Fig. 18. e^+e^- invariant-mass distribution after subtraction of the post-freeze-out hadronic cocktail. Statistical errors, systematic errors (horizontal ticks) and the systematic uncertainty due to the cocktail subtraction (shaded boxes) are indicated. The broadening scenario⁹⁷ (long-dashed curve) is compared to a calculation assuming a density dependent dropping ρ mass² (dotted line in (a)) and to a broadening scenario excluding baryonic effects (dotted line in (b))¹⁴⁵.

subtraction of the combinatorial background. The quality of the data has allowed to subtract the *measured* post-freeze-out dilepton cocktail separately for different centrality bins and therefore does not rely on meson yields from statistical model predictions. The remaining dimuon invariant-mass spectrum is attributed mainly to the $\rho \rightarrow \mu^+\mu^-$ decay. A monotonic broadening of the excess and a more than linear rise is observed with increasing centrality of the heavy-ion reaction (see Fig. 21). The ratio of the dimuon-excess yield to the cocktail ρ intensity is a measure for the ρ multiplicity which is found to be up to 6 times larger in central In+In collisions than in elementary nucleon-nucleon reactions at the same energy. As discussed in Refs. 150, 149 this ratio is related to the number of ρ generations created by formation and decay during the fireball evolution. Applying this “ ρ -clock”,¹⁵¹ information on the life time of the fireball can be deduced and is estimated to be of the order of ≈ 6 fm/c in central In+In collisions.⁴⁶

For the most central collisions, Fig. 20 indicates a strong in-medium broadening of the ρ meson while the centroid of the distribution remains at the nominal ρ mass of 770 MeV/c². This observation has been interpreted by the authors of Ref. 148 as a melting of the ρ meson indicative of a restoration of chiral symmetry in the fireball of the collision zone which may be associated with the phase transition into the quark-gluon plasma.

The measured $\mu^+\mu^-$ invariant-mass spectrum is compared in Fig. 22 with two theoretical predictions, a scenario taking the broadening of the ρ meson⁹ into account and another one assuming only a dropping of the ρ mass in the medium

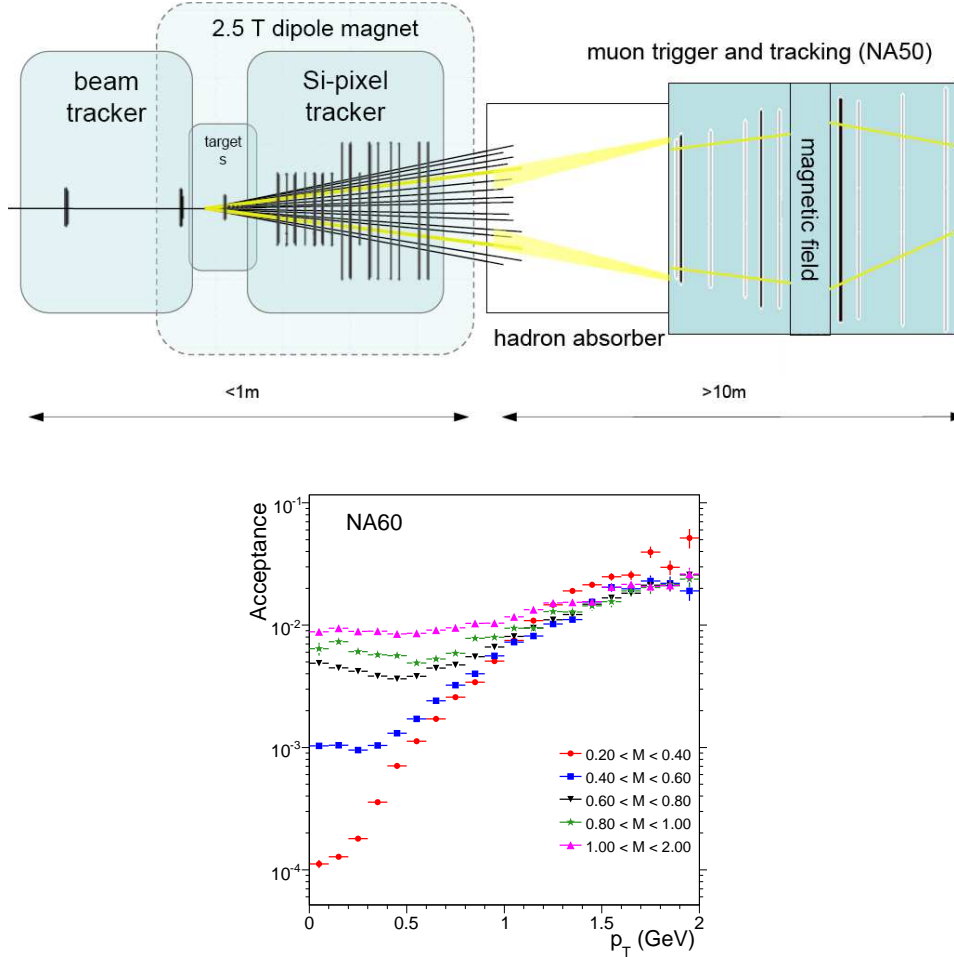


Fig. 19. Layout of the NA60 experiment: The radiation-hard Si-pixel detector before the hadron absorber was the essential addition to the former NA50 muon spectrometer to achieve a mass resolution of $\frac{\delta m}{m} = 2.5\%$. The bottom part of the figure shows the acceptance for dimuons relative to the full phase space as a function of transverse momentum for different invariant-mass bins.¹⁵⁵

as proposed by Brown and Rho². Both scenarios are calculated for the same parameter set of the fireball evolution¹⁵². We note, however, that several aspects of the decomposition of the dilepton spectrum (primordial, thermal and freeze-out components) and of the fireball evolution are still a matter of debate.^{46,135,154} The dropping mass scenario is found to be incompatible with the NA60 data.^{148,153}

The decisive role of high baryon densities for the observed medium modifications is convincingly demonstrated in Fig. 23 by comparing the NA60 data to model calculations by van Hees and Rapp¹⁵⁰ including and neglecting the contribution of

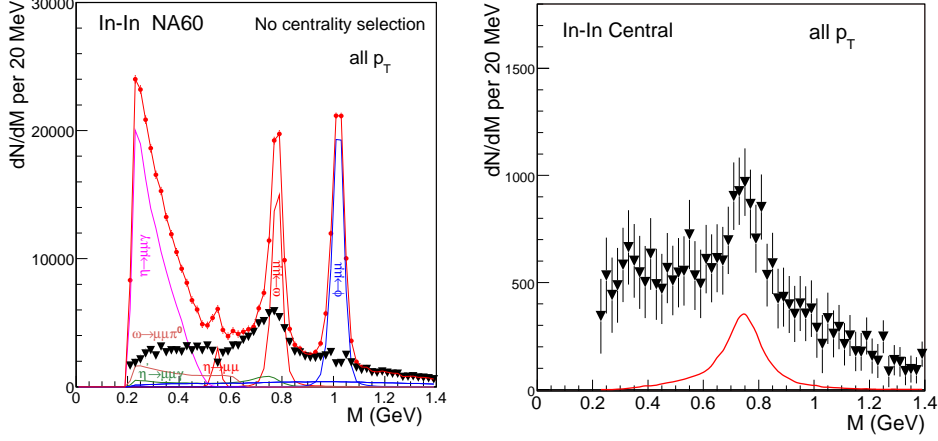


Fig. 20. Left: Background-subtracted $\mu^+\mu^-$ invariant-mass spectrum before (dots) and after subtraction (triangles) of the known hadronic decay sources for In+In collisions at 158 AGeV. Right: $\mu^+\mu^-$ invariant-mass spectrum for central collisions in comparison to the spectral function of a free (“cocktail”) ρ meson.^{148,135}

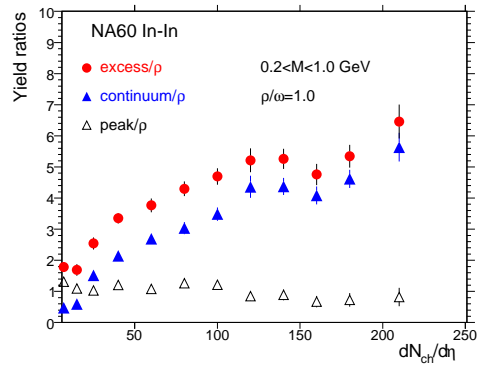


Fig. 21. Ratio of the dimuon-excess yield to the cocktail ρ intensity as a function of centrality, assuming a production ratio $\rho/\omega = 1$. The centrality dependence is separately shown for the mass range 0.2-1.0 GeV/c², the ρ peak and the continuum.¹⁴⁹

(in-medium) baryon-resonance formation and decay processes, $\pi N \rightarrow N^*, \Delta, \Delta^* \rightarrow N\rho \rightarrow N\mu^+\mu^-$, to the dilepton spectrum, respectively.

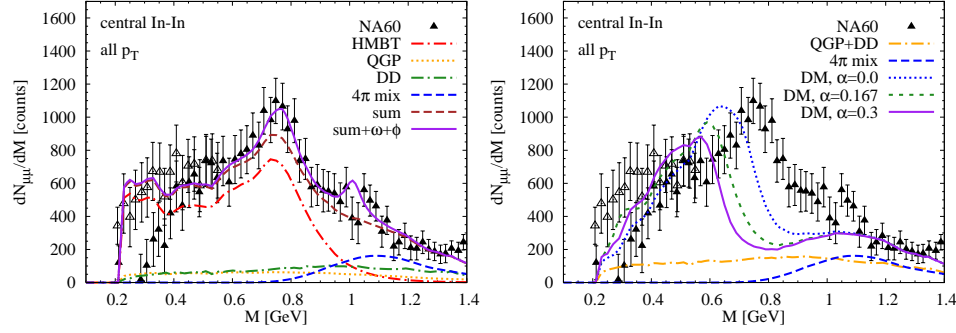


Fig. 22. Comparison of the $\mu^+\mu^-$ excess for central In+In collisions to model predictions, (left) taking an in-medium broadening of the ρ meson into account⁹, and (right) for a dropping mass scenario according to Ref. 2. Both calculations are performed for the same set of the fireball parameters assuming a transverse acceleration of $a_t = 0.085 \text{ c}^2/\text{fm}$. The parameter α controls the temperature dependence of the in-medium mass. The figure is taken from Ref. 152.

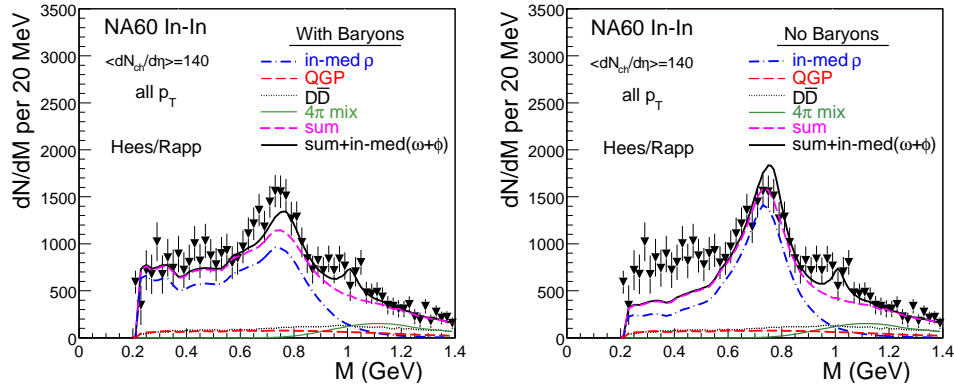


Fig. 23. NA60 data for semi-central In+In collisions in comparison to two model calculations¹⁵⁰ including and neglecting meson-baryon interactions, respectively.

5.3.2. Nuclear reactions with elementary probes

The properties of ρ mesons in nuclei have also been investigated in nuclear reactions using proton and photon beams. In early experiments at DESY¹⁵⁶ ρ production from nuclei was studied in bremsstrahlung induced reactions. The ρ mesons were detected via their $\rho \rightarrow \pi^+\pi^-$ decays (the same group also did detect dileptons¹⁵⁷ from the light target *Be*) and had recoil momenta in the range of 3.5-7 GeV/c. For these high recoil momenta the in-medium width of the ρ mesons is very large.⁶ As discussed in Sect. 4.4 such ρ mesons are outshined by the ones which decay in vacuum: Although a sizeable fraction of ρ mesons decays within the nuclear medium

even at these high recoil momenta, no strong deviation from the free ρ line shape can be expected since the contributions to the ρ signal from higher nuclear densities are suppressed. It is therefore not surprising that the experiment did not exhibit any change of the ρ line shape with increasing nuclear mass.

For ρ mesons with lower recoil momenta this problem is reduced. A nearly ideal experiment for the investigation of in-medium changes of vector mesons has been proposed in Ref. 158. In that reference all the cross sections as well as the expected sensitivities to in-medium changes had been worked out. Recently this proposed experiment has indeed been performed by the CLAS collaboration at JLAB in a $\gamma + A \rightarrow e^+e^- + X$ reaction^{159,133}. This is – as the earlier exploratory studies of Ref. 157 – an experiment where electromagnetic interactions are exploited in the entrance as well as in the exit channel, thereby avoiding initial as well as final state interactions. An additional advantage is that the partial decay width is known so that the spectral function itself can be extracted from the measured dilepton spectra.

Compared to the DESY experiment the CLAS collaboration has studied the photoproduction of vector mesons at lower incident energies ($E_\gamma = 0.6\text{--}3.8$ GeV) on a series of nuclear targets. Vector mesons were identified via their e^+e^- decay. The detector system and the acceptance for dileptons are shown in Fig. 24. The detector

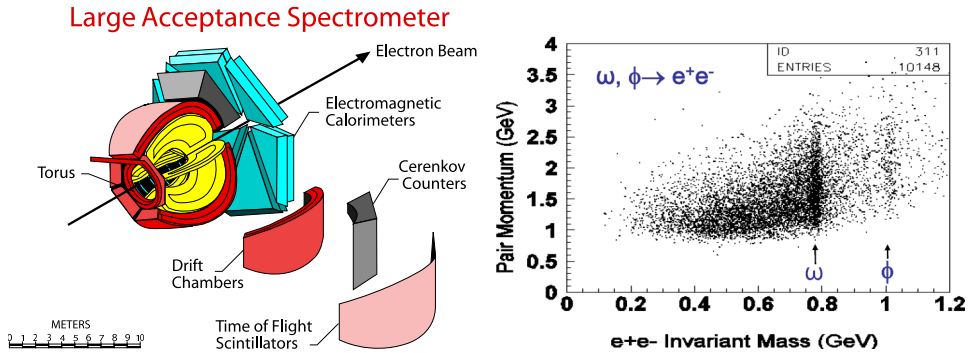


Fig. 24. Layout of the CLAS detector comprising a superconducting toroidal magnet, drift chambers, time-of-flight hodoscopes, an electromagnetic calorimeter and gas Cherenkov counters.¹⁶⁰ The plot on the right hand side illustrates that there is only acceptance for e^+e^- pairs with momenta above about 800 MeV/c.

covers almost the full solid angle and comprises six identical sectors embedded in a six-coil superconducting toroidal magnet. Each sector consists of drift chambers, time-of-flight scintillators, Cherenkov counters and an electromagnetic calorimeter. Low-energy e^+e^- background from pair production in the target is suppressed by a “mini-torus” magnet. Suitable trigger conditions were chosen to suppress coherent photoproduction of vector mesons.

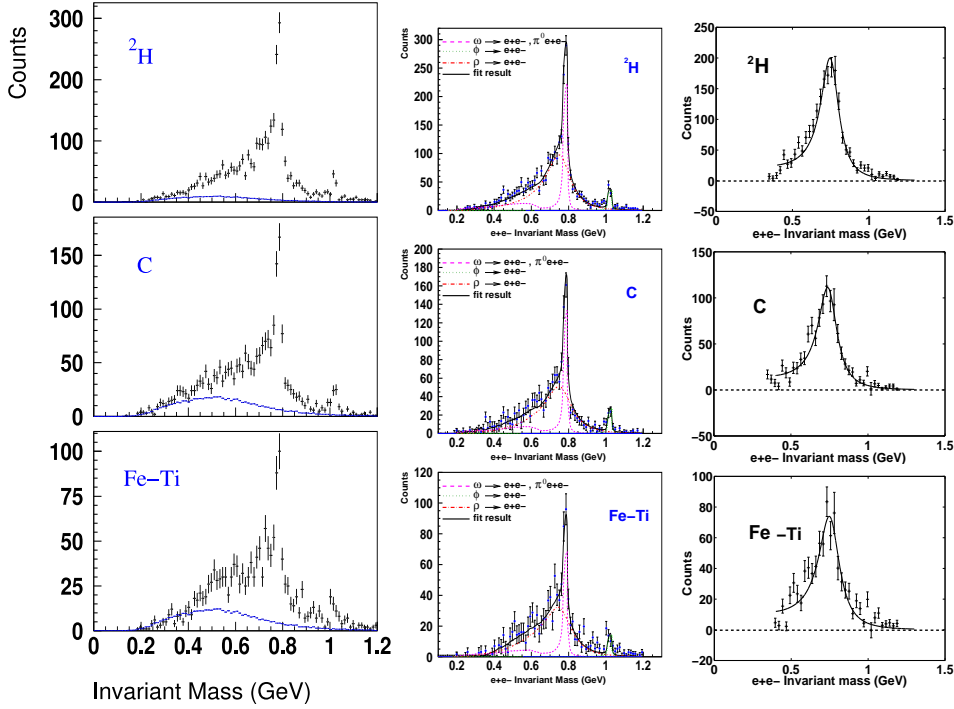


Fig. 25. Left panels: e^+e^- spectra with combinatorial background normalized to like-sign pairs for different target nuclei. Middle panels: Same spectra after subtracting the combinatorial background, decomposed into contributions from different vector meson decays.^{159,133} The curves are transport model calculations with the GiBUU code.¹²⁹ Right panels: Same spectra with contributions from ρ mesons only.

Resulting dilepton spectra are shown in Fig. 25. The spectra on the left hand side include the combinatorial background which was determined by the event-mixing technique and normalized to the number of observed like-sign pairs, as described in Sect. 5.1. After subtracting the combinatorial background the spectra were decomposed into the ω , ϕ , and ρ contributions (see Fig. 25). The e^+e^- invariant-mass distributions attributed to the ρ meson decay are shown separately on the right hand side of the figure.

The experiment — because of acceptance limitations — sees only vector mesons with rather high momenta beyond about 1 GeV (cf. Fig. 24). The longer-lived vector mesons, i.e. the ω and the ϕ meson, decay mostly outside the nuclear target. However, the shorter-lived ρ experiences a significant fraction of its decays inside the medium so that its in-medium properties can be extracted. For this region the results of Ref. 43 have predicted a slightly broadened ρ spectral function, without any significant shift of the peak position (see Fig. 5).

All measured spectra are indeed consistent with a collisional broadening of the

58 *S. Leupold, U. Mosel, V. Metag*

ρ meson without mass shift. The width increases by about 70 MeV in medium size nuclei, as expected in BUU simulations⁴⁵ for densities of $\rho \approx \rho_0/2$ and typical recoil momenta of 1-2 GeV/c.

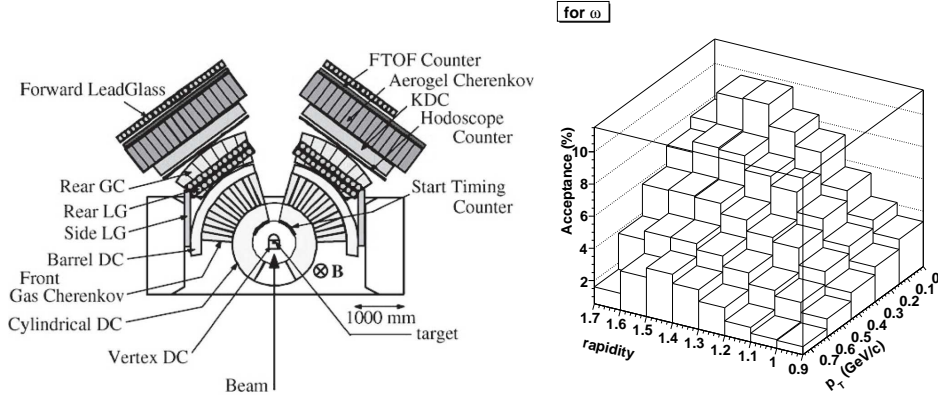


Fig. 26. Schematic view of the KEK-E325 experimental setup. The two-arm spectrometer comprises drift chambers, Cherenkov detectors, leadglass calorimeters, and time-of-flight hodoscopes.¹⁶¹ The right hand side shows the acceptance for lepton pairs from $\omega \rightarrow e^+e^-$ decays as a function of the rapidity and transverse momentum of the ω meson.¹⁶²

A quite different result has been obtained in the KEK-E325 experiment. Here, protons of 12 GeV were used to produce vector mesons on different targets. This experiment was the first to measure dileptons in nuclear reactions with elementary projectiles in the search for medium modifications of vector mesons. The experimental arrangement is shown in Fig. 26. It is a two arm configuration, each spectrometer arm being equipped with Cherenkov detectors, drift chambers, time-of-flight counters, and an electromagnetic calorimeter. The right hand side of Fig. 26 shows the acceptance of the detector setup for lepton pairs from ω decay as a function of their invariant mass.¹⁶³

The dilepton spectra obtained for Carbon and Copper targets are shown in Fig. 27. The shape of the combinatorial background was determined by event mixing and its absolute magnitude by fitting the spectra together with contributions from ω, ρ and $\phi \rightarrow e^+e^-$ and the Dalitz decays $\eta \rightarrow e^+e^-\gamma$ and $\omega \rightarrow e^+e^-\pi^0$. A normalization of the combinatorial background to the like-sign dilepton yield was not possible because of the trigger condition, requiring unlike-sign particles in the two arms of the spectrometer. After subtraction of the combinatorial background a significant excess on the low-mass side of the ω peak is seen (see Fig. 27). For C and Cu, a best fit to the spectra is obtained for a ρ/ω ratio of 0.7 ± 0.1 and 0.9 ± 0.2 and a drop of the ρ and ω mass by $9.2 \pm 0.2\%$ at normal nuclear matter density without any in-medium broadening of the mesons. This result is surprising as hadrons in the

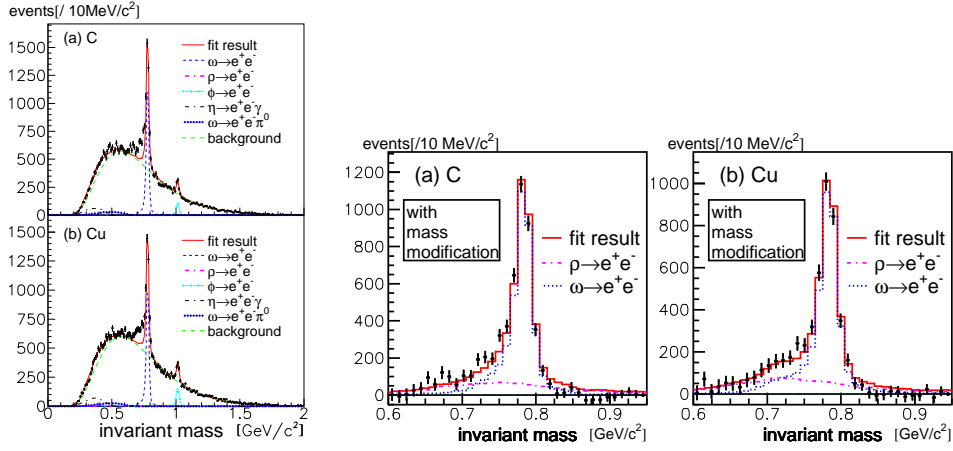


Fig. 27. Invariant-mass spectra of e^+e^- pairs for C and Cu nuclei. The fit shows the decomposition of the spectrum into the combinatorial background (long-dashed curve) and signals from the ρ , ω , and ϕ decays into e^+e^- and the Dalitz decay modes $\eta \rightarrow e^+e^-\gamma$, and $\omega \rightarrow e^+e^-\pi^0$. The right hand side of the figure shows the same spectra for the ρ , ω mass range after subtraction of the combinatorial background. The shapes of the $\rho \rightarrow e^+e^-$ (dash-dotted) and $\omega \rightarrow e^+e^-$ (dotted curve) contributions are fitted by the formula $m_V(\rho)/m_V(0) = 1 - k \cdot (\rho/\rho_0)$ with $k = 0.092$.¹⁶⁴

medium have additional “decay” options through inelastic channels and as a consequence their width is expected to increase in the nuclear environment. Inspection of Fig. 27 shows that most of the data points above an e^+e^- mass of 820 MeV are systematically below the fit curve which indicates uncertainties in the background subtraction; a possible oversubtraction of the background would remove ρ strength in this mass range and could lead to an apparent downward shift of the ρ mass distribution.

It should be noted that the CLAS experiment is more sensitive to a possible in-medium modification of the ρ meson as the production of the ρ meson relative to the ω meson is about 3 times higher in the photonuclear reaction.^{165,99} Furthermore, it should be kept in mind that also the KEK-E325 experiment — just like the CLAS experiment — has acceptance only for mesons with three-momenta of almost 1 GeV/c and higher and is thus not sensitive to these prominent in-medium modifications theoretically expected at momenta less than 600 MeV/c, as discussed in Sect. 3.1.1.

Summarizing the experimental information on the ρ meson, the majority of experiments, using heavy-ion collisions as well as nuclear reactions with elementary probes, observes a broadening of the ρ meson which depends in magnitude on the density and temperature of the nuclear environment. A mass shift of the ρ meson is reported by one experiment while all other measurements find that the centroid of the mass distribution remains at the pole mass of the free ρ meson.

5.4. In-medium properties of the ω meson

The in-medium properties of the ω meson have also been studied in heavy-ion collisions as well as in elementary nuclear reactions.

5.4.1. Heavy-ion reactions

As shown in Fig. 20 a clean ω signal is observed by the NA60 collaboration in In+In collisions at 158 AGeV. Many of the ω mesons live longer than the fireball and decay in vacuum after thermal freeze-out. Medium effects can only be expected for low momentum ω mesons. In a search for possible medium effects, the NA60 collaboration studied the intensity of the ω and ϕ peaks in Fig. 20 as a function of the transverse momentum of the mesons. Both distributions are plotted in Fig. 28 as a function of the transverse kinetic energy $m_t - m = \sqrt{p_t^2 + m^2} - m$ and fitted with an exponential $1/m_t \cdot dN/dm_t = N_0 \cdot \exp(-m_t/T_{\text{eff}})$.

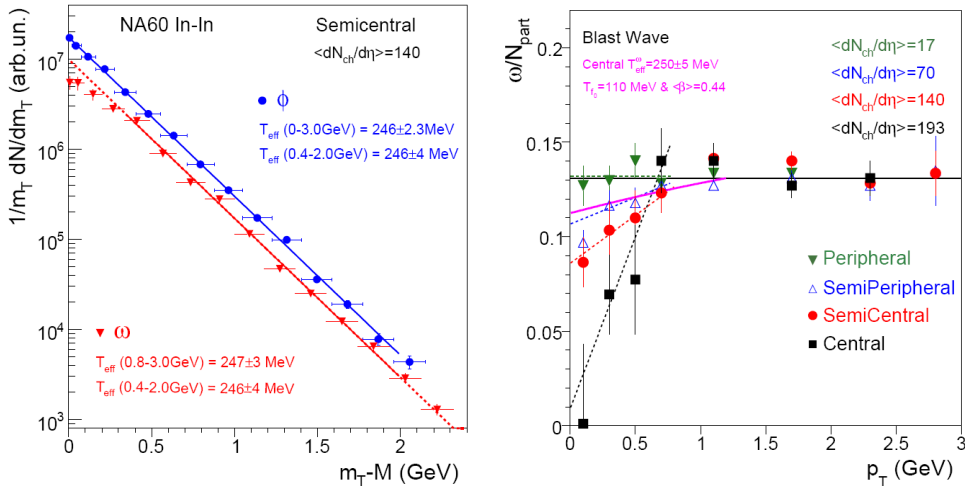


Fig. 28. Left: Acceptance-corrected transverse-mass spectra of the ω and ϕ meson for semi-central In+In collisions at 158 AGeV. A depletion of the ω yield relative to the exponential fit is observed at low transverse masses. Right: p_t dependence of the ω yield relative to the fit line for different centralities, absolutely normalized for the full phase space. The solid curve for $p_t \leq 1$ GeV/c shows the result of a blast wave fit¹⁵³ to the ω data for central collisions (from Ref. 166).

While the ϕ meson follows a straight exponential fall off a deviation from the corresponding reference line is observed for the ω meson at transverse momenta below 1 GeV/c. This suppression of the ω line intensity at low momenta indicates that slow ω mesons may either be broadened or shifted in mass in the environment of the heavy-ion collision. This effect is more pronounced for the more central collisions where the highest baryon densities and temperatures and therefore also

the largest medium modifications are expected. This is illustrated on the right hand side of Fig. 28 which shows the ω yield divided by the respective exponential fit curve for different centrality bins.

While the experiment is sensitive to the disappearance of the ω yield at low momenta the appearance of the intensity elsewhere in the $\mu^+\mu^-$ invariant-mass spectrum is practically unmeasurable since it is masked by the dominating $\pi^+\pi^- \rightarrow \mu^+\mu^-$ and $\pi N \rightarrow N^* \rightarrow N\mu^+\mu^-$ contributions. The measurement shows that slow ω mesons undergo medium modifications but it cannot be concluded whether this is due to a mass shift, a broadening, or both.

5.4.2. Nuclear reactions with elementary probes

In-medium properties of the ω meson have been deduced simultaneously with information on the ρ meson in the KEK-E325 experiment. Fitting the spectrum in Fig. 27, Naruki et al.¹⁶⁴ conclude that not only the ρ meson but also the ω meson drops in mass by 9% at normal nuclear density, although — according to their model — only 9% of the ω mesons decay within a Cu nucleus, the heavier nucleus studied.

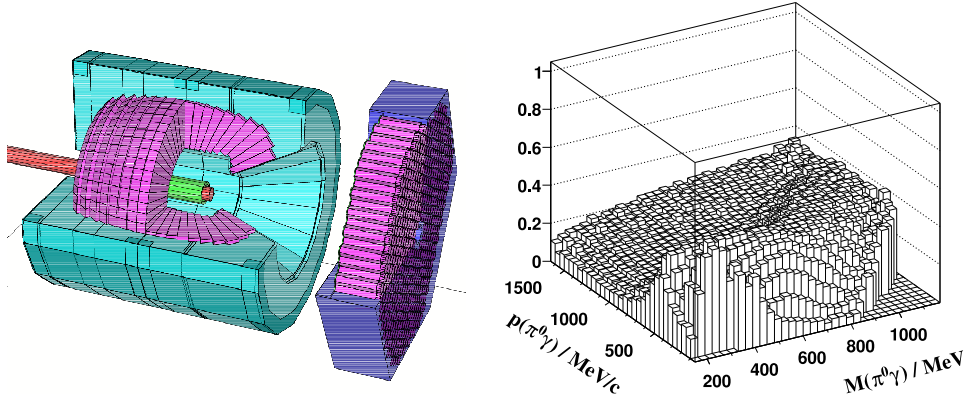


Fig. 29. Left: Experimental setup of the CBELSA/TAPS detector system, comprising the Crystal Barrel (1290 CsI crystals), the TAPS forward wall (528 BaF₂ scintillators) and a scintillating fiber array for charged particle detection.¹⁷¹ Right: CBELSA/TAPS acceptance for $p\pi^0\gamma$ events.¹⁷²

In-medium modifications of the ω meson have also been studied by the CBELSA/TAPS collaboration. In this experiment, photon beams of 0.9-2.2 GeV were used to produce ω mesons on LH₂, C, Ca, Nb, and Pb target nuclei. In contrast to all other experiments which studied the dilepton decay of vector mesons this measurement exploited the $\omega \rightarrow \pi^0\gamma$ decay branch. This decay mode has the advantage of a high branching ratio of 9% which gains about three orders of mag-

nitude in intensity compared to the dilepton decay; furthermore this decay mode is insensitive to possible in-medium effects of the ρ meson as the $\rho \rightarrow \pi^0\gamma$ branch is only $7 \cdot 10^{-4}$. A medium effect seen in the $\pi^0\gamma$ channel can thus be attributed to the ω meson. A serious disadvantage of this exit channel, however, is a possible strong final-state interaction of the π^0 meson after the ω decay within the nuclear medium which may distort the extracted invariant-mass distribution. Detailed Monte Carlo simulations¹⁶⁷ show that this effect is small in the mass range of interest ($600 \text{ MeV}/c^2 \leq m_{\pi^0\gamma} \leq 800 \text{ MeV}/c^2$) and that it can be further reduced by removing low-energy pions with kinetic energies less than 150 MeV, typical of rescattered pions, as also found in Refs. 168, 169.

Since the π^0 meson decays into two photons, a 3-photon final-state has to be detected. The CBELSA/TAPS experiment is ideally suited for this measurement as it is an almost hermetic photon detector (see Fig. 29). The acceptance for the $p\pi^0\gamma$ channel as a function of mass and momentum of the $\pi^0\gamma$ pair varies in the range of 10-40% and is particularly large for $\pi^0\gamma$ momenta below 500 MeV/c.

A comparative study of photo production¹⁷⁰ on the proton and on Nb showed a difference in the ω line shape for the two targets which was considered by the authors of Ref. 170 to be consistent with a lowering of the ω mass by 14% at normal nuclear matter density. In order to enhance the fraction of in-medium ω decays a cut on the momentum of the $\pi^0\gamma$ pair of less than 500 MeV/c had been applied. Subsequently, the background subtraction used in this analysis was criticized in the literature.¹⁶⁹ Meanwhile, a new method has been developed which allows a model-independent background determination in shape and absolute magnitude directly from the data. Applying this method, a re-analysis of the data is being performed. Preliminary results¹⁷² do not seem to confirm the earlier claim by Trnka et al.¹⁷⁰ It has been questioned^{105,127} whether an experiment including incident photon energies up to 2.2 GeV is at all sensitive to medium modifications of the ω meson because of the high fraction of decays outside of the nuclear medium; a search for medium effects would be much more promising for incident photon energies near the production threshold of $E_\gamma \approx 1100 \text{ MeV}$. This is similar to the enhancement of subthreshold particle production in heavy-ion collisions.^{128,132} At threshold a change in the mass and/or width leads to drastic changes of the cross section. On the other hand, if the incoming photon energies are too large the slow ω mesons that experience most of the in-medium interactions become relatively less abundant so that more and more stringent momentum cuts become necessary for any sensitivity to in-medium properties. A new measurement in this lower-energy regime with much higher statistics has been performed which will hopefully clarify the situation. At present, the experimental results are consistent with current theoretical predictions of no mass shift.

Additional information will hopefully soon be provided by the HADES collaboration who have recently studied the in-medium properties of the ω meson in the e^+e^- channel in p+Nb reactions. At present, the analysis of the data is still ongoing.

Because of the detector resolution and uncertainties in the decomposition of the ω signal into in-medium and in-vacuum decay contributions it is difficult to extract an in-medium ω width from the ω signal reported in Ref. 170. An access to the in-medium width, i.e. the imaginary part of the self-energy, of the ω is provided by measuring the transparency ratio^{169,173}

$$T = \frac{\sigma_{\gamma A \rightarrow \omega X}}{A \cdot \sigma_{\gamma N \rightarrow \omega X}}, \quad (54)$$

i.e. the ratio of the ω production cross section on a nucleus divided by the number of nucleons A times the ω production cross section on a free nucleon. As the ω photoproduction cross section on the neutron is not yet known the transparency ratio is here normalized to Carbon. If nuclei were completely transparent to ω

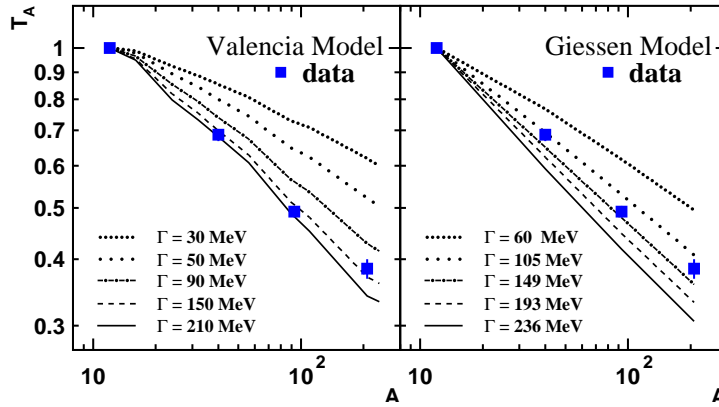


Fig. 30. Experimentally determined transparency ratio for ω mesons normalized to the Carbon data in comparison with a Monte-Carlo calculation¹⁶⁹ (left) and a BUU transport calculation⁴⁵ (right). The width values are given in the nuclear rest frame.¹⁷⁴

mesons, the transparency ratio would be $T = 1$. Consequently, T is a measure for the loss of ω flux via inelastic processes in nuclei and can be determined in attenuation experiments on nuclei of different mass number A . Within the low-density approximation the ω absorption cross section is related to the inelastic ω width by $\Gamma_\omega = v\rho\sigma$. A comparison of CBELSA/TAPS data¹⁷⁴ with calculations of the Valencia¹⁶⁹ and Giessen¹⁷³ theory groups (cf. Figs. 30, 31) yields an in-medium ω width in the nuclear reference frame of about 130-150 MeV at normal nuclear matter density and at an average ω momentum of 1100 MeV/c. This implies an in-medium broadening of the ω meson by a factor ≈ 16 , i.e., the ω meson in the nuclear medium is about as broad as the ρ meson in free space. Transport calculations, which involve only two-body collisions, can reproduce this result only if the ωN cross section is significantly enhanced up to 60 mb which is a factor of 2.5-3 over previous estimates^{173,105} and larger than measurements at ω momenta

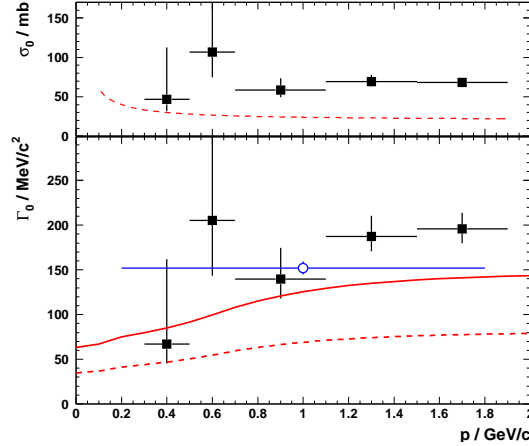


Fig. 31. Top: Inelastic ω N cross section deduced in a Glauber analysis of the data in comparison to the inelastic cross section used in BUU simulations. Bottom: Extracted width of the ω meson (squares) in the nuclear rest frame as a function of the ω momentum in comparison to theoretical predictions by Refs. 169 (blue circle) and 45 (dashed curve) as well as to a BUU calculation after a fit of the measured transparency ratio data (solid curve)¹⁷⁴.

of 7-10 GeV/c ¹⁷⁶. Assuming the momentum dependence of the ω width given in Ref. 173 a width of 130-150 MeV at $\langle p_\omega \rangle \approx 1.1 \text{ GeV}/c$ would correspond to a total width of the ω meson at rest in the medium of about 70 MeV, in line with theoretical expectations (cf. Sect. 3.2). As discussed earlier the large width could, however, also imply that the in-medium collisional width is generated by collisions of the ω meson with more than one nucleon. In any case, this large collisional width makes the determination of any in-medium change of the ω spectral function very difficult as we have discussed in Sect. 4.4.

Summarizing the experimental information on the ω meson, one has to concede that a clear picture has not emerged as yet. Claims of an in-medium mass shift are not confirmed. The large in-medium width deduced from a transparency ratio measurement is in line with the depletion of ω strength at low momenta observed in a heavy-ion experiment.

5.5. *In-medium properties of the ϕ meson*

Information on in-medium modifications of the ϕ meson has only been reported from nuclear reactions with elementary probes. While γA reactions may seem to be attractive because of the absence of any initial-state interactions Muehlich et al. have shown¹⁷⁵ that in the dominant $K^+ K^-$ decay channel final-state interactions hide any genuine in-medium changes of the ϕ meson. In particular no measurable effect caused by a shift of the ϕ -meson pole mass was found in these calculations which take the kaon self-energies as well as the effects of the Coulomb force on the

outgoing kaons into account.

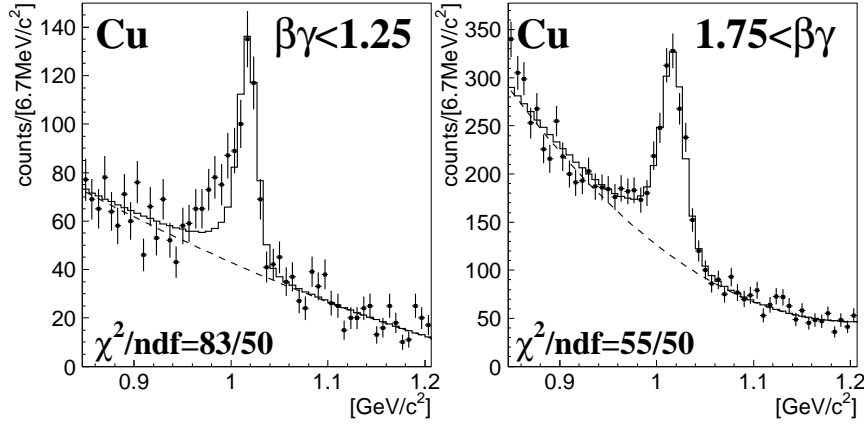


Fig. 32. e^+e^- invariant-mass distributions near the ϕ mass obtained in p+Cu for slow ($\beta\gamma \leq 1.25$) and fast ($\beta\gamma \geq 1.25$) recoiling ϕ mesons. No difference in line shape is observed for the corresponding measurement on a C target.¹⁷⁷

In pA reactions the KEK-E325 experiment has also investigated possible in-medium modifications of the ϕ meson by looking both at the K^+K^- channel as well as at the dilepton decays (see Fig. 32).¹⁷⁷ The production of ϕ mesons in proton-induced reactions at 12 GeV on a heavy (Cu) and a light nucleus (C) have been measured and compared. In case of the light C target no difference in line shape is observed for ϕ mesons recoiling with different velocities. For the heavier Cu nucleus Fig. 32 shows a significant excess on the low-mass side of the ϕ meson peak for slow ϕ mesons ($\beta \cdot \gamma < 1.25$) which have a higher probability to decay within the nucleus than fast ones. From a careful analysis of the structure in the Cu spectrum Muto et al.¹⁷⁷ extracted a drop of the ϕ mass by 3.4% and an increase of the ϕ width by a factor 3.6 at normal nuclear matter density ρ_0 .

The in-medium width of the ϕ meson has also been determined in a transparency ratio measurement.¹⁷⁸ At SPring8 the photoproduction of the ϕ meson has been measured on a series of nuclei. The transparency ratio, introduced in the previous section, was measured for Li, C, Ca, and Pb and is shown in Fig. 33.

As in the case of the ω meson, the transparency ratio — here normalized to Li — is much smaller than theoretically expected. If — in a low-density approximation — the collisional width is attributed to two-body collisions alone then a ϕN cross section of ≈ 30 mb is needed to explain the observed attenuation.^{178,179,173} (see right hand side of Fig. 33). As discussed earlier this can either signal a significantly different in-medium cross section for the ϕN interaction or the presence of strong n -body ($n > 2$) interactions. A cross section of 30 mb corresponds to an in-medium

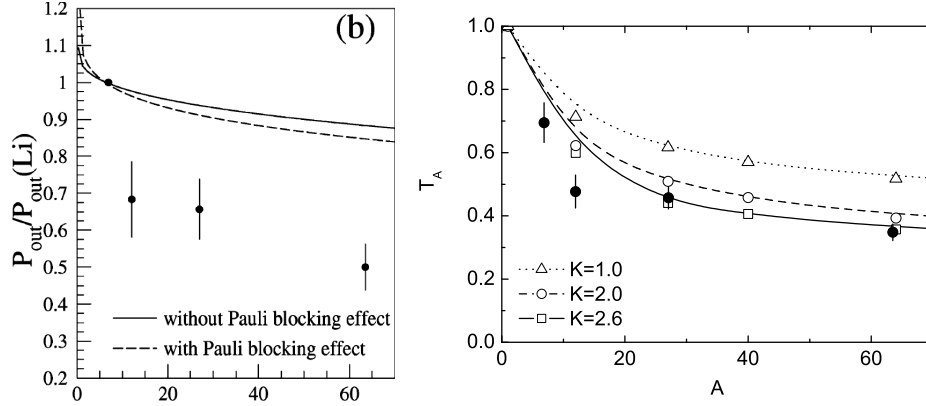


Fig. 33. Left: Transparency ratio for ϕ mesons as a function of mass, normalized to the Li data in comparison to a calculation¹⁸⁰ with (dashed curve) and without (solid curve) Pauli-blocking¹⁷⁸. Right: The same data (normalized to hydrogen) in comparison to a BUU calculations.¹²³ The K-factor indicates the increase in the ϕN cross section needed to reproduce the experimentally determined transparency ratio.

width of the ϕ meson of ≈ 70 MeV which again is much larger than the width deduced by the KEK-E325 experiment from the e^+e^- invariant-mass spectrum in Fig. 32. One has to take into account, however, that the value reported in Ref. 178 refers to a higher average recoil momentum than for the events selected in Fig. 32.

Summarizing the experimental information on the ϕ meson, a lowering of the ϕ mass in the medium and an increase in width has been reported. The amount of broadening, however, is different in the two analyses performed so far.

5.6. Ongoing dielectron spectroscopy experiments

There are ongoing dielectron-spectroscopy experiments at RHIC and GSI which also aim at extracting information on medium modifications of vector mesons. In both cases clean vector-meson signals have been observed in p+p reactions which serve as a reference. Corresponding measurements involving nuclei are currently being analyzed. No information on specific properties of ρ , ω , and ϕ mesons is as yet available. The current status of these experiments is summarized in the following subsections.

5.6.1. Vector-meson production at RHIC

Vector-meson production and dielectron continua have been studied in p+p reactions and ultra-relativistic heavy-ion collisions with the PHENIX detector at the Relativistic Heavy-Ion Collider RHIC shown in Fig. 34. Electrons and positrons are detected in the two central arm spectrometers; the leptons are identified and

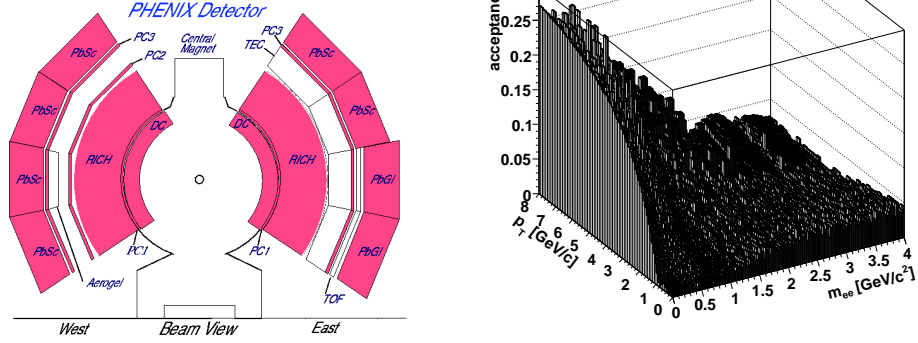


Fig. 34. Left: The PHENIX experiment at RHIC,¹⁸¹ comprising drift chambers (DC), ring-imaging Cherenkov detectors (RICH), and electromagnetic calorimeters (PbSc,PbGl). Right: Acceptance for a thermal-like dilepton source.¹⁸²

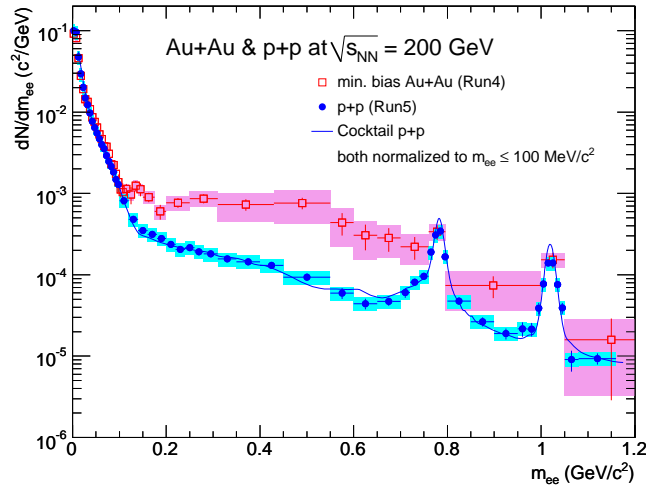


Fig. 35. Invariant e^+e^- mass distributions measured in p+p reactions and in Au+Au minimum-bias collisions at $\sqrt{s_{NN}} = 200$ GeV. The combinatorial background has been subtracted using mixed event distributions after normalizing to the like-sign pair yields.^{183,184,136}

distinguished from other particles by ring imaging Cherenkov detectors and electromagnetic calorimeters; drift chambers measure their deflection angles in an axial magnetic field to determine their momenta. Fig. 35 shows a comparison of the dielectron invariant-mass distributions measured in p+p reactions and Au+Au col-

lisions at $\sqrt{s_{NN}} = 200$ GeV. In the mass range between 150 and 750 MeV/ c^2 a significant enhancement in the dilepton yield is observed for the heavy-ion reaction. However, all theoretical models which successfully explain the phenomena at SIS energies fail to reproduce this enhancement. Peaks from the decay of the vector mesons ω and ϕ are clearly resolved in the $p + p$ experiment. A detailed analysis of the dilepton continuum and possible in-medium modifications of the vector mesons is ongoing¹⁸⁵.

5.6.2. Dilepton emission in the 1 AGeV range

The *DLS-puzzle* discussed in Sect. 5.2 was a prime motivation for building the **H**igh **A**cceptance **D**i-**E**lectron **S**pectrometer (HADES) which is shown in Fig. 36. As a second-generation experiment it was planned to cover a much larger solid

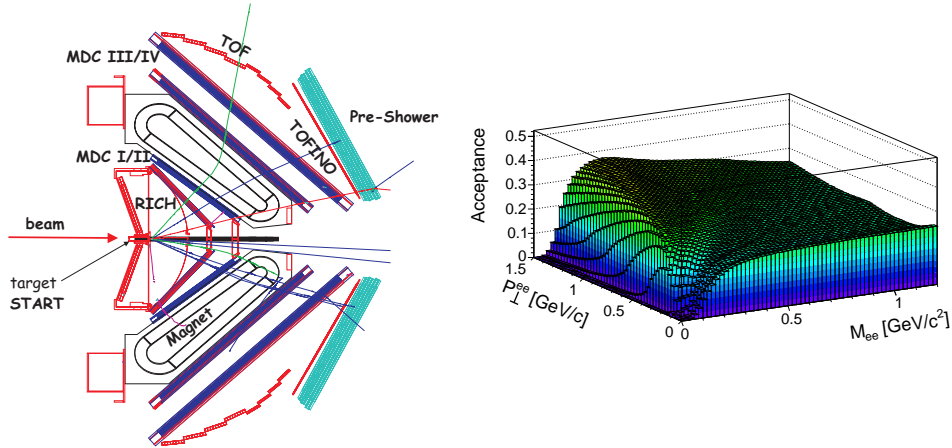


Fig. 36. Left: Cross section of the HADES experiment at GSI.¹⁸⁷ It consists of 6 identical detection systems subtending polar angles between 18° - 85° . Each sector comprises a ring-imaging Cherenkov detector (RICH), 4 planes of drift chambers (MDC I-IV), a time-of-flight detector (TOF/TOFINO) and a shower detector. Right: Acceptance for lepton pairs.¹⁸⁷

angle than the DLS spectrometer. The design of the detector is similar to that of the CLAS detector (cf. Fig. 24). It is azimuthally symmetric and consists of a 6-coil toroidal magnet centered on the beam axis and 6 identical azimuthal detector sections mounted in between the coils. Electron/pion discrimination is provided by the ring-imaging Cherenkov detector and the shower detector combined with a matching of tracks in the drift chambers. The resulting very flat acceptance for lepton pairs in the relevant kinematic range is shown on the right hand side in Fig. 36.

The most important result obtained so far with HADES is the confirmation of

the DLS data. This is demonstrated in Fig. 37 which shows a comparison of the pair-mass distributions in the DLS acceptance. Within statistical and systematic uncertainties, the HADES and DLS data are in good agreement. Recent theoretical

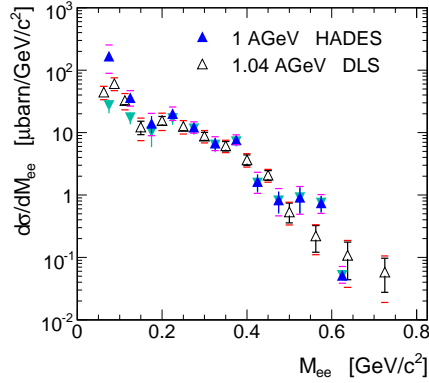


Fig. 37. Comparison within the DLS acceptance of the dilepton cross sections measured in C+C at 1 AGeV by HADES¹⁸⁶ and at 1.04 AGeV by DLS¹³⁹.

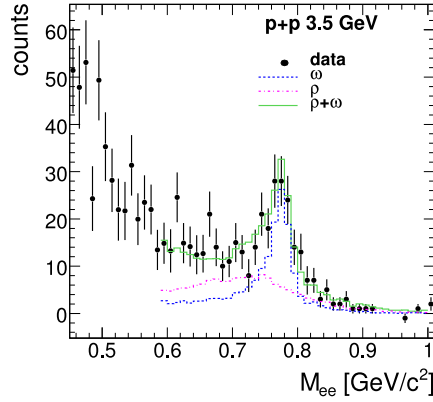


Fig. 38. Dielectron invariant-mass spectrum near the ω peak measured with the HADES detector in p+p reactions at 3.5 GeV. The spectrum is decomposed into an $\omega \rightarrow e^+e^-$ signal and a $\rho \rightarrow e^+e^-$ contribution.¹⁸⁷

calculations^{188,189} indicate that dilepton production due to bremsstrahlung may have been underestimated in previous studies. Indeed, it is found that implementing a larger bremsstrahlung contribution may account for most of the observed high dielectron yield.¹⁹⁰

Experiments at HADES will also contribute to the search for in-medium modifications of vector mesons. Fig. 38 shows the $\omega \rightarrow e^+e^-$ signal on top of the $\rho \rightarrow e^+e^-$ contribution measured in proton-proton reactions at 3.5 GeV. This spectrum will be compared to the measurement of the p+Nb reaction at 3.5 GeV which is currently being analyzed. Furthermore, in an attempt to search for in-medium effects, ω production has also been studied in Ar+KCl reaction at 1.756 AGeV. Corresponding results are eagerly awaited.

5.7. Summary of vector-meson experiments

The experimental results on medium modifications of vector mesons reported in the previous sections are compiled in Table 3. The table lists the reactions, momentum ranges and results for ρ, ω , and ϕ mesons obtained in the different experiments discussed in this review. A fully consistent picture has so far not been achieved. For

experiment	momentum acceptance	ρ	ω	ϕ
KEK-E325 pA 12 GeV	$p > 0.6$ GeV/c	$\frac{\Delta m}{m} = -9\%$ $\Delta\Gamma \approx 0$	$\frac{\Delta m}{m} = -9\%$ $\Delta\Gamma \approx 0$	$\frac{\Delta m}{m} = -3.4\%$ $\frac{\Gamma_\phi(\rho_0)}{\Gamma_\phi} = 3.6$
CLAS γ A 0.6-3.8 GeV	$p > 0.8$ GeV/c	$\Delta m \approx 0$ $\Delta\Gamma \approx 70$ MeV ($\rho \approx \rho_0/2$)		
CBELSA /TAPS γ A 0.9-2.2 GeV	$p > 0$ MeV/c		$\Delta m \approx ?$ $p_\omega < 0.5$ GeV/c $\Delta\Gamma(\rho_0) \approx 130$ MeV $\langle p_\omega \rangle = 1.1$ GeV/c	
SPRING8 γ A 1.5-2.4 GeV	$p > 1.0$ GeV/c			$\Delta\Gamma(\rho_0) \approx 70$ MeV $\langle p_\phi \rangle = 1.8$ GeV/c
CERES Pb+Au 158 AGeV	$p_t > 0$ GeV/c	broadening favored over mass shift		
NA60 In+In 158 AGeV	$p_t > 0$ GeV/c	$\Delta m \approx 0$ strong broadening		

Table 3. Experimental results on in-medium modifications of ρ , ω and ϕ mesons reported by different experiments. The reactions, incident energy ranges, and momentum acceptances of the detector systems are also given (adapted from Ref. 191).

the ρ meson, the majority of experiments observes a broadening but no mass shift in the nuclear medium. Conflicting results reported by the KEK experiment will have to be confirmed. Earlier claims from one experiment¹⁷⁰ of a dropping ω mass could not be reproduced in a re-analysis of the data. A broadening of the ω meson has been observed in elementary nuclear reactions which is in line with a depletion of the ω yield at low momenta observed in ultra-relativistic heavy-ion reactions but which is again in conflict with the KEK-E325 result. For the ϕ meson an in-medium mass shift and a broadening has been reported.

When comparing the experimental results it should be noted that some detector systems have no or little acceptance for low meson momenta for which the strongest medium modifications are expected. In view of the existing inconsistencies further experiments are needed to clarify the situation. Corresponding experiments are planned at CLAS, HADES, PHENIX, and the JPARC facility.

5.8. 2π correlations in nuclei: the σ meson

In Sect. 3.4 it was pointed out that as a consequence of a conjectured partial restoration of chiral symmetry in normal nuclear matter the mass of the σ meson would be expected to drop in the nuclear medium, combined with a reduction in width for the $\sigma \rightarrow \pi^+\pi^-$ and $\sigma \rightarrow \pi^0\pi^0$ decay channels as a result of the reduced phase space. Indeed, $\pi^+\pi^-$ production experiments with pion beams on nuclear targets did show

a striking shift of the 2π invariant-mass distributions towards lower masses.^{192,116} Corresponding shifts were not observed in the $\pi^+\pi^+$ channel, not accessible in the decay of the neutral σ meson. These experiments, however, suffered from a very small acceptance and correspondingly large corrections. A π beam experiment using the Crystal Ball as a large-acceptance detector system also showed a shift in the $2\pi^0$ invariant-mass distributions with increasing nuclear mass number.¹¹⁷ It was pointed out, however, that in both experiments the pion initial-state interactions led to a dominance of surface production thus complicating the interpretation of the data.¹⁹³

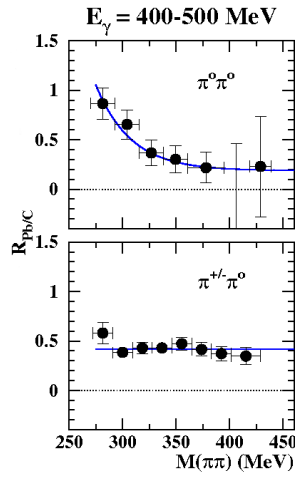


Fig. 39. Ratio of 2π invariant-mass distributions for Pb and C targets in the $2\pi^0$ and $\pi^\pm\pi^0$ channel.^{167,196}

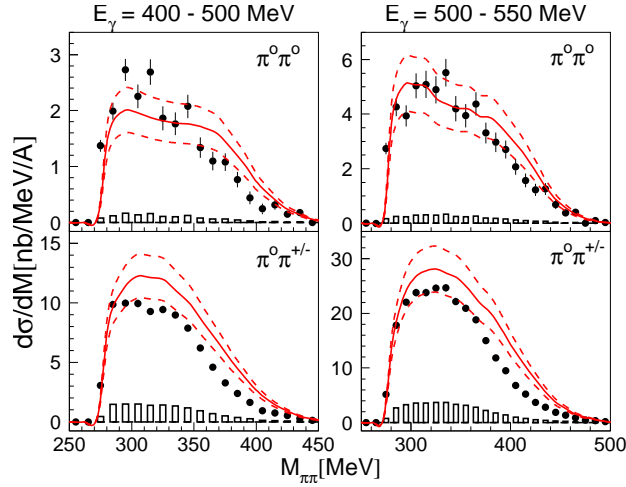


Fig. 40. Pion-pion invariant-mass distributions compared to results of the GiBUU calculation.⁴⁵ The bars at the bottom represent systematic uncertainties of the data. The dashed lines represent the error band in the BUU calculations arising from uncertainties in the elementary 2π production cross sections (from Ref. 197).

A later photoproduction experiment,¹¹⁸ where no initial-state interactions are expected, did again show a striking shift of the $2\pi^0$ mass distributions with increasing nuclear target mass while the $\pi^\pm\pi^0$ channel, not possible in σ decay, appeared to be less affected. This result is demonstrated in Fig. 39 which shows the ratio of 2π mass distributions for Pb and C targets in the $2\pi^0$ and $\pi^\pm\pi^0$ channels, respectively. For the $\pi^\pm\pi^0$ channel this ratio is almost constant as a function of the 2π mass, indicating no change in the shape of the invariant-mass spectra when going from C to Pb. In contrast, the ratio for the $2\pi^0$ channel indicates an accumulation of strength near the 2π threshold for the heavier Pb target.

While the theoretical models cited earlier^{114,115,119,120,121} represent state-of-the-

art treatments of pion-pion interactions and thus of the in-medium σ , they were much less sophisticated in their treatment of the actual observables, i.e. pions after final-state interactions, which were described in a simple eikonal approximation without allowance for charge transfer. As discussed in Sect. 4.5 and investigated in transport calculations,^{194,195} the different behavior for both channels may, however, also arise from charge-exchange reactions which shuffle strength from the dominant $\pi^\pm\pi^0$ to the $2\pi^0$ channel. This reaction mechanism is associated with an energy loss of the pions and consequently leads to a shift of strength towards lower invariant masses which is more pronounced for the $2\pi^0$ than for the $\pi^\pm\pi^0$ channel. Fig. 40 shows that these calculations provide a good description of the data for a Ca target; remaining differences reflect uncertainties in the elementary 2π photoproduction cross sections on the nucleon.

In order to establish differences in the $2\pi^0$ and $\pi^\pm\pi^0$ channels beyond the charge-exchange effect data of much higher statistics are needed. Corresponding data have been taken but are still under analysis.¹⁹⁸ In addition, any interpretation of the data must involve state-of-the-art descriptions of the final-state interactions which tend to generate effects in the same direction as the predicted in-medium changes.

6. Conclusions

The study of in-medium modifications of hadrons is in the focus of many ongoing theoretical and experimental investigations. This is a vibrant field which has recently made a lot of progress as outlined in this review. Eventually, these investigations will provide a deeper and more quantitative understanding of quantum chromodynamics in the non-perturbative regime. In this review we have described the necessary steps one needs to go from aspects of non-perturbative QCD via hadronic-model building towards actual observables. Some of the links between these corner stones are much more involved than initially expected.

Starting from the symmetries of QCD we have first discussed the connection between non-perturbative properties of the vacuum and the spectral functions of hadrons; here QCD sum rules provide the link between the two worlds, the quark-gluon and the hadronic one. We have discussed the changes of condensates in strongly interacting hadronic matter and have pointed out that they correspond to changes in “standard” hadronic models. There is thus a duality between these two descriptions of in-medium effects. We have also found, and we stress this again here, that QCD sum rules do not fix the properties of hadrons inside the nuclear medium, but they do provide important constraints for hadronic models. Such models offer the only explicit access to hadronic in-medium properties and, in particular, their in-medium self-energies; the latter are often summarized in spectral functions. As for the well-known example of pion-nucleon-Delta interactions in nuclei, which have been studied since the 70’s, also for vector mesons the coupling to nucleon resonances plays a major role. Foremost essential is the strength of the meson-nucleon-resonance coupling, which determines the importance of resonance

loops for the in-medium self-energies; this is where resonance physics on nucleons, preferentially studied at electron machines, meets heavy-ion physics with nuclei, which studies the dense and hot environment so interesting for in-medium effects.

We have pointed out that there is a clear consensus now that the ρ -meson properties should indeed change in a medium. This change is, however, subtle: the pole mass is not expected to shift significantly and the shape of the spectral function is strongly momentum dependent. Only for momenta (in the nuclear restframe) between 0 and about 800 MeV/c the spectral function of the ρ meson is predicted to become significantly skewed towards lower masses. Unfortunately this interesting regime has so far not yet been studied in nuclear reactions with elementary probes. For momenta above 1 GeV/c, on the other hand, the spectral function resembles that of a free ρ meson with some broadening and again no mass shift. For the ω meson, the situation is more complicated since there are no distinct resonances known at present that couple significantly to the ωN decay channel. Here, the basic ωN scattering problem still has to be investigated and resonance couplings have to be uniquely identified. Calculations aiming at such a description again yield hardly any mass change, but predict a considerable broadening of the ω in cold nuclear matter. A similar situation prevails for the ϕ meson. Finally, we have discussed theoretical expectations for the in-medium changes of the σ meson, which is the chiral partner of the pion and is thus particularly sensitive to precursor phenomena of chiral symmetry restoration. For this meson, theories predict a significant shift and narrowing of the spectral function towards lower masses; this is a consequence of the closing of the 2π decay channel when σ and π spectral functions approach each other, caused by (partial) chiral symmetry restoration in nuclei.

Linking these theoretical in-medium properties with actual observables is a challenging task and involves some assumptions. Foremost one has to be aware of the fact that all hadronic in-medium properties are being calculated for mesons embedded in hadronic matter in equilibrium, i.e. infinitely long-lived without spatial boundaries and with equilibrated momentum distributions. This is clearly an idealization which, however, is probably more justified for the case of cold nuclear ground state targets than for heavy-ion collisions where the reaction proceeds through non-equilibrium and equilibrium phases, the latter possibly of different nature, and where all the experimental signals involve an integration in time over the collision history. In any case, profound transport calculations are needed that allow to link the fundamental hadronic properties with observables, in particular when the final decay products of the vector meson under study are hadrons. But even for dileptons in the final state a state-of-the-art coupled-channel description is necessary since the radiating mesons may be absorbed or recreated on their way through the nuclear medium. As outlined in this review, in-medium properties of mesons are strongly linked to the properties of baryon resonances due to the excitation of the latter in collisions of the considered meson with the nucleons of the medium. The future of the field is therefore closely linked to a better theoretical understanding and experimental determination of baryon resonance parameters which reflect their

underlying quark-gluon structure. Theoretical and experimental advancements in resonance spectroscopy are thus essential for progress in the field of in-medium physics.

On the experimental side the following picture has emerged: For the ρ , ω , and ϕ meson a broadening in the nuclear medium has been reported by almost all experiments in heavy-ion collisions as well as in nuclear reactions with elementary probes. This is in line with theoretical predictions. For the ρ meson even quantitative agreement between theory and experiment has been achieved while for the ω and ϕ meson the broadening deduced from transparency-ratio measurements is a factor 2-3 larger than theoretically expected. With regard to possible in-medium mass shifts the experimental situation is less clear. The majority of experiments does not find evidence for mass changes in the medium. For the ρ meson the centroid of the mass distribution is reported by two experiments to remain at the pole mass of the free ρ meson, while in one experiment a drop in mass is claimed. The search for in-medium mass shifts in elementary nuclear reactions turns out to be more complicated than initially thought because of the observed large in-medium broadening. While the ρ meson is only broadened by a factor of about 1.5-3, for the ω and ϕ meson this factor is found to be in the range of 6 - 15. As a consequence, the branching ratio for in-medium decays into the channels of interest is reduced accordingly and makes these experiments less sensitive. Experiments with much higher statistics will be needed to obtain reliable results. Furthermore, the acceptance of some detector systems for low-momentum mesons will have to be increased because the dominant in-medium modifications are expected at recoil momenta of less than 1 GeV/c. Initiatives for corresponding new experiments have been taken and experimental results are eagerly awaited.

7. Acknowledgments

We gratefully acknowledge many stimulating discussions and very helpful comments on the manuscript from Sanja Damjanovic, Hideto En'yo, Bengt Friman, Tetsuo Hatsuda, Hendrik van Hees, Burkhard Kämpfer, Eulogio Oset, Ralf Rapp, Piotr Salabura and Hans Specht. We also thank Chaden Djalali, Megumi Naruki and Alberica Toia for providing figures for this review. This work has been supported by BMBF, DFG (SFB/TR16) and GSI.

References

1. R. D. Pisarski, Phys. Lett. B **110** (1982) 155.
2. G. E. Brown and M. Rho, Phys. Rev. Lett. **66** (1991) 2720.
3. T. Hatsuda and S. H. Lee, Phys. Rev. C **46** (1992) 34.
4. V. Bernard and U. G. Meissner, Nucl. Phys. A **489** (1988) 647.
5. H. Leutwyler and A. V. Smilga, Nucl. Phys. B **342** (1990) 302.
6. D. V. Bugg, Nucl. Phys. B **88** (1975) 381.
7. R. S. Hayano and T. Hatsuda, arXiv:0812.1702 [nucl-ex].
8. W. Cassing and E. L. Bratkovskaya, Phys. Rept. **308** (1999) 65.

9. R. Rapp and J. Wambach, *Adv. Nucl. Phys.* **25** (2000) 1 [arXiv:hep-ph/9909229].
10. R. Rapp, J. Wambach and H. van Hees, arXiv:0901.3289 [hep-ph].
11. E. Oset, H. Toki and W. Weise, *Phys. Rept.* **83** (1982) 281.
12. M. E. Peskin and D. V. Schroeder, “An Introduction To Quantum Field Theory,” *Reading, USA: Addison-Wesley (1995)*.
13. G. ’t Hooft, *Nucl. Phys. B* **138** (1978) 1.
14. G. ’t Hooft, *Nucl. Phys. B* **153** (1979) 141.
15. A. M. Polyakov, *Phys. Lett. B* **72** (1978) 477.
16. T. Matsubara, *Prog. Theor. Phys.* **14** (1955) 351.
17. F. Karsch, *Lect. Notes Phys.* **583** (2002) 209 [arXiv:hep-lat/0106019].
18. K. Holland and U. J. Wiese, arXiv:hep-ph/0011193.
19. S. Scherer, *Adv. Nucl. Phys.* **27** (2003) 277 [arXiv:hep-ph/0210398].
20. U. Mosel, “Fields, Symmetries, and Quarks”, *Berlin: Springer (1999)*
21. C. Amsler *et al.* [Particle Data Group], *Phys. Lett. B* **667** (2008) 1.
22. M. Gell-Mann, R. J. Oakes and B. Renner, *Phys. Rev.* **175** (1968) 2195.
23. Y. Aoki, G. Endrodi, Z. Fodor, S. D. Katz and K. K. Szabo, *Nature* **443** (2006) 675 [arXiv:hep-lat/0611014].
24. S. Leupold, M. F. M. Lutz and M. Wagner, arXiv:0811.2398 [nucl-th].
25. R. Rapp, T. Schafer, E. V. Shuryak and M. Velkovsky, *Phys. Rev. Lett.* **81** (1998) 53 [arXiv:hep-ph/9711396].
26. M. G. Alford, K. Rajagopal and F. Wilczek, *Phys. Lett. B* **422** (1998) 247 [arXiv:hep-ph/9711395].
27. M. G. Alford, K. Rajagopal and F. Wilczek, *Nucl. Phys. B* **537** (1999) 443 [arXiv:hep-ph/9804403].
28. T. Schafer and F. Wilczek, *Phys. Rev. Lett.* **82** (1999) 3956 [arXiv:hep-ph/9811473].
29. L. McLerran and R. D. Pisarski, *Nucl. Phys. A* **796** (2007) 83 [arXiv:0706.2191 [hep-ph]].
30. P. Gerber and H. Leutwyler, *Nucl. Phys. B* **321** (1989) 387.
31. U. G. Meissner, J. A. Oller and A. Wirzba, *Annals Phys.* **297** (2002) 27 [arXiv:nucl-th/0109026].
32. J. Gasser and H. Leutwyler, *Phys. Lett. B* **184** (1987) 83.
33. J. Gasser and H. Leutwyler, *Nucl. Phys. B* **307** (1988) 763.
34. E. G. Drukarev and E. M. Levin, *Prog. Part. Nucl. Phys.* **27** (1991) 77.
35. J. Gasser, H. Leutwyler and M. E. Sainio, *Phys. Lett. B* **253** (1991) 252.
36. Y. Kwon, M. Procura and W. Weise, *Phys. Rev. C* **78** (2008) 055203 [arXiv:0803.3262 [nucl-th]].
37. P. Danielewicz, *Annals Phys.* **152** (1984) 239.
38. G. Ecker, J. Gasser, H. Leutwyler, A. Pich and E. de Rafael, *Phys. Lett. B* **223** (1989) 425.
39. H. W. Fearing and S. Scherer, *Phys. Rev. C* **62** (2000) 034003 [arXiv:nucl-th/9909076].
40. B. Friman and H. J. Pirner, *Nucl. Phys. A* **617** (1997) 496 [arXiv:nucl-th/9701016].
41. R. Rapp, G. Chanfray and J. Wambach, *Nucl. Phys. A* **617** (1997) 472 [arXiv:hep-ph/9702210].
42. M. F. M. Lutz, G. Wolf and B. Friman, *Nucl. Phys. A* **706** (2002) 431 [Erratum-ibid. **A 765** (2006) 431] [arXiv:nucl-th/0112052].
43. M. Post, S. Leupold and U. Mosel, *Nucl. Phys. A* **741** (2004) 81 [arXiv:nucl-th/0309085].
44. F. Riek and J. Knoll, *Nucl. Phys. A* **740** (2004) 287 [arXiv:nucl-th/0402090].
45. P. Muehlich, V. Shklyar, S. Leupold, U. Mosel and M. Post, *Nucl. Phys. A* **780**

- (2006) 187 [arXiv:nucl-th/0607061].
46. H. van Hees and R. Rapp, Nucl. Phys. A **806** (2008) 339 [arXiv:0711.3444 [hep-ph]].
 47. E. V. Shuryak, Rev. Mod. Phys. **65** (1993) 1.
 48. M. A. Shifman, A. I. Vainshtein and V. I. Zakharov, Nucl. Phys. B **147** (1979) 385.
 49. M. A. Shifman, A. I. Vainshtein and V. I. Zakharov, Nucl. Phys. B **147** (1979) 448.
 50. M. Asakawa, T. Hatsuda and Y. Nakahara, Prog. Part. Nucl. Phys. **46** (2001) 459 [arXiv:hep-lat/0011040].
 51. T. Hatsuda, Int. J. Mod. Phys. A **21** (2006) 688 [arXiv:hep-ph/0509306].
 52. S. Durr *et al.*, Science **322** (2008) 1224.
 53. S. Schael *et al.* [ALEPH Collaboration], Phys. Rept. **421** (2005) 191 [arXiv:hep-ex/0506072].
 54. D. G. Caldi and H. Pagels, Phys. Rev. D **14** (1976) 809.
 55. C. A. Dominguez, M. Loewe and J. C. Rojas, Z. Phys. C **59** (1993) 63.
 56. Y. Nambu and G. Jona-Lasinio, Phys. Rev. **122** (1961) 345.
 57. A. I. Bochkarov and M. E. Shaposhnikov, Nucl. Phys. B **268** (1986) 220.
 58. K. G. Wilson, Phys. Rev. **179** (1969) 1499.
 59. M. Asakawa and C. M. Ko, Phys. Rev. C **48** (1993) 526.
 60. S. Leupold, W. Peters and U. Mosel, Nucl. Phys. A **628** (1998) 311 [arXiv:nucl-th/9708016].
 61. S. Leupold, Nucl. Phys. A **743** (2004) 283 [arXiv:hep-ph/0303020].
 62. T. Hatsuda, Y. Koike and S. H. Lee, Nucl. Phys. B **394** (1993) 221.
 63. S. Leupold, Phys. Lett. B **616** (2005) 203 [arXiv:hep-ph/0502061].
 64. M. Dey, V. L. Eletsky and B. L. Ioffe, Phys. Lett. B **252** (1990) 620.
 65. J. V. Steele, H. Yamagishi and I. Zahed, Phys. Lett. B **384** (1996) 255 [arXiv:hep-ph/9603290].
 66. M. Urban, M. Buballa and J. Wambach, Phys. Rev. Lett. **88** (2002) 042002 [arXiv:nucl-th/0110005].
 67. T. Hatsuda, S. H. Lee and H. Shiomi, Phys. Rev. C **52** (1995) 3364 [arXiv:nucl-th/9505005].
 68. S. Leupold and U. Mosel, Phys. Rev. C **58** (1998) 2939 [arXiv:nucl-th/9805024].
 69. V. L. Eletsky and B. L. Ioffe, Phys. Rev. Lett. **78** (1997) 1010 [arXiv:hep-ph/9609229].
 70. T. Hatsuda and S. H. Lee, arXiv:nucl-th/9703022.
 71. V. L. Eletsky and B. L. Ioffe, arXiv:hep-ph/9704236.
 72. S. Leupold, Phys. Rev. C **64** (2001) 015202 [arXiv:nucl-th/0101013].
 73. S. Leupold and M. Post, Nucl. Phys. A **747** (2005) 425 [arXiv:nucl-th/0402048].
 74. B. Steinmueller and S. Leupold, Nucl. Phys. A **778** (2006) 195 [arXiv:hep-ph/0604054].
 75. F. Klingl, N. Kaiser and W. Weise, Nucl. Phys. A **624** (1997) 527 [arXiv:hep-ph/9704398].
 76. A. K. Dutt-Mazumder, R. Hofmann and M. Pospelov, Phys. Rev. C **63** (2001) 015204 [arXiv:hep-ph/0005100].
 77. R. Thomas, S. Zschocke and B. Kampfer, Phys. Rev. Lett. **95** (2005) 232301 [arXiv:hep-ph/0510156].
 78. T. Hilger, R. Thomas and B. Kampfer, Phys. Rev. C **79** (2009) 025202 [arXiv:0809.4996 [nucl-th]].
 79. M. C. Birse and B. Krippa, Phys. Lett. B **381** (1996) 397 [arXiv:hep-ph/9603387].
 80. R. Thomas, T. Hilger and B. Kampfer, Nucl. Phys. A **795** (2007) 19 [arXiv:0704.3004 [hep-ph]].
 81. M. Asakawa, C. M. Ko, P. Levai and X. J. Qiu, Phys. Rev. C **46**, 1159 (1992).

82. M. Herrmann, B. L. Friman and W. Noerenberg, Nucl. Phys. A **545** (1992) 267C.
83. R. Rapp, G. Chanfray and J. Wambach, Phys. Rev. Lett. **76** (1996) 368 [arXiv:hep-ph/9508353].
84. R. Rapp, M. Urban, M. Buballa and J. Wambach, Phys. Lett. B **417** (1998) 1 [arXiv:nucl-th/9709008].
85. F. Klingl, T. Waas and W. Weise, Phys. Lett. B **431** (1998) 254 [arXiv:hep-ph/9709210].
86. F. Klingl and W. Weise, Nucl. Phys. A **606** (1996) 329.
87. F. Eichstaedt, S. Leupold, U. Mosel and P. Muehlich, Prog. Theor. Phys. Suppl. **168** (2007) 495 [arXiv:0704.0154 [nucl-th]].
88. W. Peters, M. Post, H. Lenske, S. Leupold and U. Mosel, Nucl. Phys. A **632** (1998) 109 [arXiv:nucl-th/9708004].
89. M. Post, S. Leupold and U. Mosel, Nucl. Phys. A **689** (2001) 753 [arXiv:nucl-th/0008027].
90. M. Post and U. Mosel, Nucl. Phys. A **699** (2002) 169 [arXiv:nucl-th/0108017].
91. D. Cabrera, E. Oset and M. J. Vicente Vacas, Nucl. Phys. A **705** (2002) 90 [arXiv:nucl-th/0011037].
92. D. M. Manley and E. M. Saleski, Phys. Rev. D **45** (1992) 4002.
93. A. Zabrodin *et al.*, Phys. Rev. C **60** (1999) 055201.
94. W. Langgartner *et al.*, Phys. Rev. Lett. **87** (2001) 052001.
95. J. Lehr and U. Mosel, Phys. Rev. C **64** (2001) 042202 [arXiv:nucl-th/0105054].
96. N. Bianchi *et al.*, Phys. Rev. C **54** (1996) 1688.
97. R. Rapp and J. Wambach, Eur. Phys. J. A **6** (1999) 415 [arXiv:hep-ph/9907502].
98. V. Shklyar, H. Lenske, U. Mosel and G. Penner, Phys. Rev. C **71** (2005) 055206 [Erratum-ibid. C **72** (2005) 019903] [arXiv:nucl-th/0412029].
99. J. Barth *et al.*, Eur. Phys. J. A **18** (2003) 117.
100. F. Klein *et al.* [The CBELSA/TAPS Collaboration], Phys. Rev. D **78** (2008) 117101 [arXiv:0807.0594 [hep-ex]].
101. M. Lutz, B. Friman and G. Wolf, Nucl. Phys. A **661** (1999) 526.
102. G. Wolf, M. F. M. Lutz and B. Friman, Acta Phys. Hung. A **19** (2004) 301.
103. G. Penner and U. Mosel, Phys. Rev. C **66** (2002) 055211 [arXiv:nucl-th/0207066].
104. G. Penner and U. Mosel, Phys. Rev. C **66** (2002) 055212 [arXiv:nucl-th/0207069].
105. P. Muehlich, Dissertation, Giessen University, 2007;
http://www.uni-giessen.de/cms/fbz/fb07/fachgebiete/physik/einrichtungen/theorie/theorie1/publications/dissertation/muehlich_diss/at_download/file
106. S. Zschocke, O. P. Pavlenko and B. Kampfer, Phys. Lett. B **562** (2003) 57 [arXiv:hep-ph/0212201].
107. K. Saito, K. Tsushima, A. W. Thomas and A. G. Williams, Phys. Lett. B **433** (1998) 243 [arXiv:nucl-th/9804015].
108. E. Oset and A. Ramos, Nucl. Phys. A **679** (2001) 616 [arXiv:nucl-th/0005046].
109. D. Cabrera and M. J. Vicente Vacas, Phys. Rev. C **67**, 045203 (2003) [arXiv:nucl-th/0205075].
110. T. Hatsuda and T. Kunihiro, Phys. Rev. Lett. **55**, 158 (1985).
111. V. Bernard, U. G. Meissner and I. Zahed, Phys. Rev. Lett. **59**, 966 (1987).
112. V. Bernard and U. G. Meissner, Phys. Rev. D **38** (1988) 1551.
113. T. Hatsuda, T. Kunihiro and H. Shimizu, Phys. Rev. Lett. **82** (1999) 2840.
114. H. C. Chiang, E. Oset and M. J. Vicente-Vacas, Nucl. Phys. A **644**, 77 (1998) [arXiv:nucl-th/9712047].
115. R. Rapp *et al.*, Phys. Rev. C **59**, 1237 (1999) [arXiv:nucl-th/9810007].
116. F. Bonutti *et al.*, Phys. Rev. C **60** (1999) 018201.

117. A. Starostin *et al.* [Crystal Ball Collaboration], Phys. Rev. Lett. **85** (2000) 5539.
118. J. G. Messchendorp *et al.*, Phys. Rev. Lett. **89** (2002) 222302 [arXiv:nucl-ex/0205009].
119. G. Chanfray, D. Davesne, M. Ericson and M. Martini, Eur. Phys. J. A **27** (2006) 191 [arXiv:nucl-th/0406003].
120. M. M. Kaskulov, E. Oset and M. J. Vicente Vacas, Phys. Rev. C **73** (2006) 014004 [arXiv:nucl-th/0506031].
121. D. Cabrera, E. Oset and M. J. Vicente Vacas, Phys. Rev. C **72** (2005) 025207 [arXiv:nucl-th/0503014].
122. B. Schenke and C. Greiner, Phys. Rev. C **73** (2006) 034909 [arXiv:hep-ph/0509026].
123. P. Muhlich and U. Mosel, Nucl. Phys. A **765** (2006) 188 [arXiv:nucl-th/0510078].
124. E. Oset, Y. Futami and H. Toki, Nucl. Phys. A **448** (1986) 597.
125. A. Sibirtsev, H. W. Hammer, U. G. Meissner and A. W. Thomas, Eur. Phys. J. A **29** (2006) 209 [arXiv:nucl-th/0606044].
126. M. Effenberger and U. Mosel, Phys. Rev. C **62** (2000) 014605 [arXiv:nucl-th/9908078].
127. K. Gallmeister, M. Kaskulov, U. Mosel and P. Muhlich, Prog. Part. Nucl. Phys. **61** (2008) 283 [arXiv:0712.2200 [nucl-th]].
128. W. Cassing, V. Metag, U. Mosel and K. Niita, Phys. Rept. **188** (1990) 363.
129. For details on GiBUU see: <http://gibuu.physik.uni-giessen.de/GiBUU>
130. H. van Hees and R. Rapp, arXiv:0901.2316 [nucl-th].
131. U. Mosel, Prog. Part. Nucl. Phys. **42** (1999) 163 [arXiv:nucl-th/9812067].
132. U. Mosel, Ann. Rev. Nucl. Part. Sci. **41** (1991) 29.
133. M. H. Wood *et al.* [CLAS Collaboration], Phys. Rev. C **78** (2008) 015201 [arXiv:0803.0492 [nucl-ex]].
134. R. Arnaldi *et al.* [NA60 Collaboration], Eur. Phys. J. C **59** (2009) 607 [arXiv:0810.3204 [nucl-ex]].
135. S. Damjanovic and H.J. Specht, priv. communication 2009.
136. A. Toia, J. Phys. G **35** (2008) 104037 [arXiv:0805.0153 [nucl-ex]].
137. G. Roche *et al.* [DLS Collaboration], Phys. Rev. Lett. **61** (1988) 1069.
138. C. Naudet *et al.*, Phys. Rev. Lett. **62** (1989) 2652.
139. R. J. Porter *et al.* [DLS Collaboration], Phys. Rev. Lett. **79** (1997) 1229 [arXiv:nucl-ex/9703001].
140. G. Agakishiev *et al.* [CERES Collaboration], Phys. Rev. Lett. **75** (1995) 1272.
141. M. Masera [HELIOS Collaboration], Nucl. Phys. A **590** (1995) 93C.
142. E. L. Bratkovskaya, W. Cassing, R. Rapp and J. Wambach, Nucl. Phys. A **634** (1998) 168 [arXiv:nucl-th/9710043].
143. G. Agakishiev *et al.* [CERES Collaboration], Eur. Phys. J. C **41** (2005) 475 [arXiv:nucl-ex/0506002].
144. G. Agakishiev *et al.*, Eur. Phys. J. C **4** (1998) 231.
145. D. Adamova *et al.*, Phys. Lett. B **666** (2008) 425 [arXiv:nucl-ex/0611022].
146. A. Marin [CERES Collaboration], J. Phys. G **30** (2004) S709 [arXiv:nucl-ex/0406007].
147. D. Adamova *et al.* [CERES/NA45 Collaboration], Phys. Rev. Lett. **91** (2003) 042301 [arXiv:nucl-ex/0209024].
148. R. Arnaldi *et al.* [NA60 Collaboration], Phys. Rev. Lett. **96** (2006) 162302 [arXiv:nucl-ex/0605007].
149. R. Arnaldi *et al.* [NA60 Collaboration], arXiv:0812.3053 [nucl-ex].
150. H. van Hees and R. Rapp, Phys. Rev. Lett. **97** (2006) 102301 [arXiv:hep-ph/0603084].

151. U. W. Heinz and K. S. Lee, Phys. Lett. B **259** (1991) 162.
152. H. van Hees and R. Rapp, arXiv:hep-ph/0604269.
153. S. Damjanovic [NA60 Collaboration], J. Phys. G **35** (2008) 104036 [arXiv:0805.4153 [nucl-ex]].
154. J. Ruppert, C. Gale, T. Renk, P. Lichard and J. I. Kapusta, Phys. Rev. Lett. **100** (2008) 162301 [arXiv:0706.1934 [hep-ph]].
155. S. Damjanovic *et al.* [NA60 Collaboration], Nucl. Phys. A **783** (2007) 327 [arXiv:nucl-ex/0701015].
156. H. Alvensleben *et al.*, Phys. Rev. Lett. **24** (1970) 786.
157. H. Alvensleben *et al.*, Nucl. Phys. B **25** (1971) 342.
158. M. Effenberger, E. L. Bratkovskaya and U. Mosel, Phys. Rev. C **60** (1999) 044614 [arXiv:nucl-th/9903026].
159. R. Nasseripour *et al.* [CLAS Collaboration], Phys. Rev. Lett. **99** (2007) 262302 [arXiv:0707.2324 [nucl-ex]].
160. B. A. Mecking *et al.* [CLAS Collaboration], Nucl. Instrum. Meth. A **503** (2003) 513.
161. K. Ozawa *et al.* [E325 Collaboration], Phys. Rev. Lett. **86** (2001) 5019 [arXiv:nucl-ex/0011013].
162. T. Tabaru *et al.*, Phys. Rev. C **74** (2006) 025201 [arXiv:nucl-ex/0603013].
163. R. Muto, priv. communication 2009.
164. M. Naruki *et al.*, Phys. Rev. Lett. **96** (2006) 092301 [arXiv:nucl-ex/0504016].
165. C. Wu *et al.*, Eur. Phys. J. A **23** (2005) 317.
166. S. Damjanovic, Eur. Phys. J. C **49** (2007) 235 [arXiv:nucl-ex/0609026].
167. J. G. Messchendorp, A. Sibirtsev, W. Cassing, V. Metag and S. Schadmand, Eur. Phys. J. A **11** (2001) 95 [arXiv:hep-ex/0106041].
168. P. Muhlich, T. Falter and U. Mosel, Eur. Phys. J. A **20** (2004) 499 [arXiv:nucl-th/0310067].
169. M. Kaskulov, E. Hernandez and E. Oset, Eur. Phys. J. A **31** (2007) 245 [arXiv:nucl-th/0610067].
170. D. Trnka *et al.* [CBELSA/TAPS Collaboration], Phys. Rev. Lett. **94** (2005) 192303 [arXiv:nucl-ex/0504010].
171. V. Metag, Prog. Theor. Phys. Suppl. **168** (2007) 503.
172. M. Nanova, proceedings Eur. Phys. Soc. Nucl. Phys. conference, Bochum, 2009.
173. P. Muhlich and U. Mosel, Nucl. Phys. A **773** (2006) 156 [arXiv:nucl-th/0602054].
174. M. Kotulla *et al.* [CBELSA/TAPS Collaboration], Phys. Rev. Lett. **100** (2008) 192302 [arXiv:0802.0989 [nucl-ex]].
175. P. Muhlich, T. Falter, C. Greiner, J. Lehr, M. Post and U. Mosel, Phys. Rev. C **67** (2003) 024605 [arXiv:nucl-th/0210079].
176. H.-J. Behrend *et al.*, Phys. Rev. Lett. **24** (1970) 1246.
177. R. Muto *et al.* [KEK-PS-E325 Collaboration], Phys. Rev. Lett. **98** (2007) 042501 [arXiv:nucl-ex/0511019].
178. T. Ishikawa *et al.*, Phys. Lett. B **608** (2005) 215 [arXiv:nucl-ex/0411016].
179. V. K. Magas, L. Roca and E. Oset, Nucl. Phys. A **755** (2005) 495 [arXiv:nucl-th/0412066].
180. D. Cabrera, L. Roca, E. Oset, H. Toki and M. J. Vicente Vacas, Nucl. Phys. A **733** (2004) 130 [arXiv:nucl-th/0310054].
181. K. Adcox *et al.* [PHENIX Collaboration], Nucl. Instrum. Meth. A **499** (2003) 469.
182. A. Toia, priv. communication 2009.
183. A. Adare *et al.* [PHENIX Collaboration], Phys. Lett. B **670**, 313 (2009) [arXiv:0802.0050 [hep-ex]].
184. S. Afanasiev *et al.* [PHENIX Collaboration], arXiv:0706.3034 [nucl-ex].

- 185. A. Milov, arXiv:0809.3880 [nucl-ex].
- 186. G. Agakishiev *et al.* [HADES Collaboration], Phys. Lett. B **663** (2008) 43 [arXiv:0711.4281 [nucl-ex]].
- 187. G. Agakishiev *et al.* [HADES Collaboration], Eur. Phys. J. A **41** (2009) 243 [arXiv:0902.3478 [nucl-ex]].
- 188. R. Shyam and U. Mosel, Phys. Rev. C **67** (2003) 065202 [arXiv:hep-ph/0303035].
- 189. L. P. Kaptari and B. Kampfer, Nucl. Phys. A **764** (2006) 338 [arXiv:nucl-th/0504072].
- 190. E. L. Bratkovskaya and W. Cassing, Nucl. Phys. A **807** (2008) 214 [arXiv:0712.0635 [nucl-th]].
- 191. V. Metag, J. Phys. G **34** (2007) S397.
- 192. F. Bonutti *et al.* [CHAOS Collaboration], Phys. Rev. Lett. **77** (1996) 603.
- 193. M. J. Vicente Vacas and E. Oset, Phys. Rev. C **60** (1999) 064621 [arXiv:nucl-th/9907008].
- 194. P. Muhlich, L. Alvarez-Ruso, O. Buss and U. Mosel, Phys. Lett. B **595** (2004) 216 [arXiv:nucl-th/0401042].
- 195. O. Buss, L. Alvarez-Ruso, P. Muhlich and U. Mosel, Eur. Phys. J. A **29** (2006) 189 [arXiv:nucl-th/0603003].
- 196. B. Krusche, Int. J. Mod. Phys. A **22** (2007) 406 [arXiv:nucl-ex/0608044].
- 197. F. Bloch *et al.*, Eur. Phys. J. A **32** (2007) 219 [arXiv:nucl-ex/0703037].
- 198. R. Gregor, Dissertation, Giessen University, 2007, and priv. communication 2009.